NASA TECHNICAL NOTE

NASA TN D-5208

C.1

NASA TN D-5208

AERODYNAMIC CHARACTERISTICS DETERMINED DURING DEVELOPMENT OF THE APOLLO LAUNCH ESCAPE VEHICLE CONFIGURATION

by William C. Moseley, Jr., and Francis Evans Bowen

Manned Spacecraft Center
Houston, Texas

NATIONAL AERONAUTICS AND SPACE ADMINISTRATION • WASHINGTON, D. C. • JUNE 1969

AERODYNAMIC CHARACTERISTICS DETERMINED DURING DEVELOPMENT OF THE APOLLO LAUNCH ESCAPE VEHICLE CONFIGURATION

By William C. Moseley, Jr., and Francis Evans Bowen

Manned Spacecraft Center
Houston, Texas

NATIONAL AERONAUTICS AND SPACE ADMINISTRATION

For sale by the Clearinghouse for Federal Scientific and Technical Information
Springfield, Virginia 22151 – CFSTI price $3.00

ABSTRACT

Wind-tunnel studies were conducted in the development of the Apollo launch escape vehicle to determine the effect of configuration changes on the aerodynamic characteristics of the vehicle. Results indicate that changes in escape-tower and rocket-body length had only slight effects on the static stability.

CONTENTS

TABLES

FIGURES

AERODYNAMIC CHARACTERISTICS DETERMINED DURING DEVELOPMENT OF THE APOLLO LAUNCH ESCAPE VEHICLE CONFIGURATION

By William C. Moseley, Jr., and Francis Evans Bowen*
Manned Spacecraft Center

SUMMARY

In the development of the Apollo launch escape vehicle, wind-tunnel studies were conducted to determine the effect of various changes in configuration on the aerodynamic stability characteristics. Studies of the static stability characteristics of models representing a variety of launch escape vehicle configurations were made for Mach numbers from 0.5 to 9.0 and for a diagnostic angle-of-attack range. Configuration changes included changes in length of the escape rocket and escape tower, changes in the escape-rocket nose shape and skirt diameter, the addition of flow separators to the escape rocket, and the addition of strakes to the command module. Data obtained from these studies indicated that, within reasonable limits, tower and rocket length had little effect on static stability. Rocket nose and skirt variations and the addition of command module strakes also had negligible effects on the static stability. The addition of flow separators generally resulted in improved static stability and a decrease in the axial-force coefficient at trim angle of attack. However, the flow separators were eliminated from the configuration because the configuration exhibited negative damping, and a similar increment of pitching-moment coefficient could be obtained by adding a ballast (equivalent in mass to the flow separators) at the escape-rocket nose.

INTRODUCTION

The Apollo Spacecraft Program, with the ultimate goal of a lunar landing, was inaugurated by NASA as part of the continuing space-exploration effort following Project Mercury and the Gemini Program. Initial study contracts, NASA Space Task Group studies, and other nonfunded studies established design requirements and specifications for the Apollo configurations, using the separable module concept. Some of the early wind-tunnel studies subsequently used in support and verification of this selection are reported in references 1 to 4.

As part of the design and development program established to support the Apollo Spacecraft Program, the Apollo wind-tunnel test program was initiated. An

*ITT Federal Electric Corp.

introduction to this program and associated studies reported to date are given in references 5 to 8. The associated studies include descriptions of the aerodynamic stability characteristics of the production Apollo launch escape vehicle (LEV), the production Apollo command module (CM), and the Apollo LEV with canard surfaces deployed. Aerodynamic stability characteristics acquired as a result of tests during the development of the Apollo CM are presented in reference 9. The program had to provide the experimental data necessary for efficient spacecraft design through verification of theoretical estimates of the stability characteristics of the basic vehicle. A series of static stability studies were made to determine what effects on the aerodynamic characteristics of the Apollo LEV might be induced by variations in the length of the escape-tower structure. Subsequently, tests were made in which the configuration of the escape rocket was modified. These modifications included variations in the length and shape of the nose, variations in overall length, the addition of toroidal tanks, variations in the diameter of the skirt at the base, and the addition of flow separators (disks). These flow separators — varying in size, shape, and location — were added in an attempt to improve stability of the LEV. The effects on stability caused by the addition of strakes to the CM were also tested. The purpose of this paper is to present the static stability characteristics of a representative group from the many configurations tested in the process of selecting a launch escape vehicle which met design requirements. Static stability data are presented for Mach numbers from 0.5 to 9.0 and for a diagnostic angle-of-attack range.

SYMBOLS

C	scale model of Apollo command module
C_A	axial-force coefficient, $\frac{\text{axial force}}{qS}$
C_m	pitching-moment coefficient, $\frac{\text{pitching moment}}{qSd}$
$C_{m,a}$	pitching-moment coefficient referenced about theoretical apex
C_{m_α}	pitching-moment curve slope parameter $\left(\text{measured at trim angle of attack, } \frac{\partial C_m}{\partial \alpha}\right)$
C_N	normal-force coefficient, $\frac{\text{normal force}}{qS}$
d	maximum body diameter (154-in. full scale)
E	scale model of escape rocket
L	scale model of strake

M	free-stream Mach number
q	free-stream dynamic pressure, lb/ft^2
R	Reynolds number (based on maximum model diameter)
S	maximum cross-sectional area perpendicular to X-body axis, ft^2
T	scale model of escape-tower structure
V	free-stream velocity, ft/sec
X, Y, Z	body reference axes
α	angle of attack of model center line, deg
α_T	total angle of attack, deg
α_t	trim angle of attack, deg
β	angle of sideslip, deg
ϕ	roll angle, deg

Subscripts:

BL	boundary-layer separator
1, 2, . . . , 64	indicative of various models of each component of the LEV

FACILITIES AND MODELS

Test Facilities

The broad range of expected flight conditions (Mach number, Reynolds number, and angle of attack α) and the inability of any single tunnel to simulate all these conditions required the use of a variety of wind-tunnel test facilities. The tunnel size and capabilities of the wind-tunnel facilities used in the acquisition of the data contained in this report are listed in table I.

Test Models

The data selected for the subject study were taken from tests of 0.02-, 0.045-, and 0.105-scale models of various Apollo LEV configurations. These data are presented for 44 combinations of three command modules, 10 escape-tower structures,

27 escape rockets, and one set of stabilizing strakes. The positive direction of forces and moments and the body system of axes are illustrated in figure 1. The data presented are referred to about both the body axis system and the stability axis system. Sketches of these components and a typical LEV are presented in figure 2, and photographs of typical test models are shown in figure 3. The models and ranges over which they were tested are listed in table II.

The basic CM models (C_1, C_2, and C_{39}) used with the LEV configuration discussed herein did not simulate all of the protuberances and cavities that were included on many of the models that were used in later tests. The C_1 and C_2 models are identical except for differences in nose-cone radii. The basic C_{39} configuration differs from C_2 only in that the tower-leg cavities are left open on C_{39} and, inasmuch as the LEV is installed on all subject test-model configurations, this difference is not significant for the purpose of this investigation. However, C_{39} was designed to accommodate the strakes (L_{28}) and was used in the tests in which the strakes were employed. A summary of the CM variables is presented in table III.

The eight escape-tower structures (T_1, T_2, T_5, T_7, T_8, T_9, T_{10}, and T_{11}) used in determining the effect of tower-length variations are of similar design. They are four-legged derrick-type structures that differ primarily in overall length which varies from 249.0 to 79.467 scale inches. Less significant differences are slight variations in overall width, placement and number of longitudinal members and cross bracing, and the addition of stiffener gussets and braces at the base of the legs on some models. Towers T_{26} and T_{27} are basically similar and were designed to approximate the optimum tower length (120 scale inches) and to incorporate a ring in lieu of longitudinal members in the first bay aft of the escape-rocket base. This "hourglass" configuration was designed to preclude impingement upon the support members by the escape-rocket exhaust plume. The sketches presented in figure 2(b) do not represent exact reproductions of the complete model towers (attachment arrangements at each end are not shown), but represent only that portion of a tower which is exposed to the airstream. A summary of the escape-tower structure variables is presented in table IV.

The initial escape-rocket configuration E_1 consisted of a cylindrical rocket body with a cone-shaped nose and a flared skirt at the base. Configuration E_1 has two toroidal tanks located forward of the skirt and an aft jettison motor projecting from the base. Configuration E_2 has the same overall dimensions as E_1, but E_2 uses a double-cone configuration instead of a cylindrical body with external tanks and flared base. The addition of a narrow band of 0.0076-inch grit to the nose cone of E_2 produced the E_{2BL} configuration. Configuration E_3 is identical to E_1 except for the size and shape of the nose cone. The toroidal tanks were abandoned on E_4 and E_5, which are otherwise identical to E_1 and E_3, respectively. The E_6 is the basic E_4 configuration with the aft jettison motor removed. Beginning with E_7 and including

all subsequent models, the basic E_6 configuration was lengthened to incorporate the jettison motor into the forward part of the rocket body. The nozzles of the forward jettison rocket protrude on E_7 and E_8, which are identical except for the diameter of the flared skirt. Configuration E_9 represents a reverse thrust-type escape rocket which attaches directly to the nose of the CM. Beginning with configuration E_{10} and continuing through E_{62}, the jettison rocket nozzles are flush mounted, and no representation of the nozzles was attempted on the models. Configuration E_{10} is identical to E_7 in all other respects. Configurations E_{12} and E_{14} differ from E_{10} in that the diameter of the flared skirt is greater on E_{12}, and the nose angle and length is changed on E_{14}. By the addition of a ring and flow separator forward of the skirt, E_{20} was developed from the E_{14} configuration. Configuration E_{23} was similarly developed from E_{14} by increasing the angle of the skirt flare and by adding a ring forward of the skirt and a disk aft. By changing the size and placement of the flow separator or by removing the ring, models E_{25}, E_{29}, E_{32}, E_{37}, E_{38}, and E_{39} were likewise developed from E_{23}. Configuration E_{48} is a lengthened version of E_{23} less the flow separator, and E_{49} is identical to E_{48} except for the addition of a flow separator forward of the skirt and a ring fairing attachment at the base of the flow separator. Configurations E_{60} and E_{62} are similar to E_{48} and E_{49}, respectively. They are slightly longer, have a slight increase in skirt diameter, and have two raceways added to the rocket body. Configurations E_{63} and E_{64} represent improved versions of E_{60} and E_{62}. The raceways have been eliminated, the two jettison motor nozzles protrude slightly on each side, and four rocket nozzles are angled outward from the rocket center line aft of the skirt. Four fairings are located on the forward portion of the flared skirt on E_{63}. Cutouts in the ring fairing on E_{64} correspond to the skirt fairings on E_{63}. A summary of the escape-rocket variables is presented in table V.

TESTS AND ACCURACY

Tests

Sting-mounted models attached to a strain-gage balance were used to measure the static force and moment data. Testing was conducted over an α range of -15° to $+90^\circ$.

Data Accuracy

Standard statistical analyses of balance-calibration data and data repeatability indicated certain accuracy tolerances of the force and moment coefficients. Available accuracy estimates are presented in table VI.

PRESENTATION OF RESULTS

A summary of the test data used in the subject study is presented in the following table. The effect of the various configuration changes on the static stability of the LEV is presented in the designated figures.

Figure	Mach number range	Angle-of-attack range, deg	Nature of investigation
4	0.7 to 2.4	-15 to 95	Effect of tower length
5	1.65 to 9.0	-20 to 90	Effect of tower length
6	1.57 to 3.27	-10 to 30	Effect of tower length
7	1.57	-10 to 30	Effect of variations in escape-rocket size and shape
8	2.49	-10 to 30	Variations in escape-rocket size and shape
9	3.27	-10 to 30	Variations in escape-rocket size and shape
10	1.57	-10 to 30	Variations in escape-rocket size and shape, assorted escape towers
11	.7 to 1.35	-15 to 75	Effect of variations in escape-rocket nose angle
12	.7 to 1.35	-15 to 50	Variations in escape-rocket size and shape
13	.7 to 1.35	-15 to 35	Effect of disk ahead of escape-rocket skirt

Figure	Mach number range	Angle-of-attack range, deg	Nature of investigation
14	0.7 to 2.4	-15 to 50	Effect of disk at base of escape-rocket skirt
15	.7 to 2.4	-15 to 35	Effect of variations in size, placement, and shape of disk
16	.7 to 2.0	-15 to 50	Effect of variation in size and shape of disk at base of escape-rocket skirt
17	.7 to 3.4	-5 to 55	Effect of flow separator
18	.7 to 2.0	-15 to 95	Effect of variations in skirt-base diameter
19	.5 to 6.0	-15 to 70	Effect of strakes
20	.7 to 6.0	-15 to 70	Effect of strakes

DISCUSSION

The aerodynamic characteristics of the flight LEV configuration have been reported in reference 6. Numerous configurations or modifications were investigated during the development of this flight configuration, and data from a representative sampling of these configurations are presented in this document.

These data are referenced to the system of body axes that is illustrated in figure 1. Tne pitching-moment data are referenced to the CM theoretical apex.

Effect of Tower Length

Aerodynamic characteristics of the effect of tower length are presented in figures 4 to 6. The basic stability of the LEV as indicated by the slope of the pitching-moment curve at α_t ($\alpha \approx 0°$) varied but slightly as a result of changes in tower length (figs. 4 to 6). The major effect of decreasing tower length is an increase in the α range over which negative pitching moments occur. However, this stability gain would

appear less significant if more realistic centers of gravity were used, because a center of gravity (c.g.) transfer along the X-axis and a Z-axis offset in c.g. for the flight configuration would result in a decrease in stability. Inasmuch as shorter tower lengths produce rocket-exhaust plume impingement on the CM with attendant heat-protection problems and inasmuch as longer tower lengths produce structural dynamic problems, the 120-inch tower length originally proposed in the Apollo specifications was selected as being optimum.

Effect of Escape-Rocket Modifications

Some of the preliminary rocket configurations at a Mach number of 1.57 are shown in figure 7. The original tests were run with the escape-rocket jettison motor located inside the tower at the base of the escape rocket. The toroidal tanks shown on configuration E and E_3 (fig. 2(f)) were originally designed as part of the escape-rocket control system. However, early in the LEV design phase the launch escape control system concept was abandoned in favor of a passive-type system. Configuration E_2 has the rocket-motor fairing around the toroidal tanks. It should also be noted that configurations E_3 and E_5 have drooped noses which were proposed to increase stability at low angles of attack. Early in the program, when it became obvious that the rearward location of the jettison motor would introduce heat protection problems in the CM apex region, configurations E_7 and E_8 were proposed with the jettison motor forward of the main escape motor in an integral rocket case. The data presented in figure 7 indicate that the E_2 fairing reduced the stability of the vehicle. The addition of either toroidal tanks or drooped nose had little or no effect on LEV stability over the test α range (-10° to 30°). Configurations E_7 and E_8 had slightly reduced stability primarily due to the jettison rocket design which had nozzles exposed to the free stream. Data for several of the same configurations shown in figure 7 at Mach numbers of 2.49 and 3.27, respectively, are presented in figures 8 and 9. The effects on stability produced at the higher Mach numbers are consistent with those reported for a Mach number of 1.57.

The effects of varying both tower and escape-rocket configurations at a Mach number of 1.57 and a towerless configuration E_9 with a reverse-thrust escape rocket are shown in figure 10. The tower length varied from 85 to 247 inches, and the rocket modifications are basically the ones treated in figures 7 to 9. The reduction in stability caused by the E_2 fairing is reaffirmed by data presented in figures 10(a) and 10(b), but the other modifications have little or no effect. The data presented in figure 10(c) indicate that escape-rocket configurations E_7 and E_8 reduce the stability, as previously shown by the data presented in figure 7. The towerless configuration E_9 is less stable than E_6 and exhibits erratic variations in C_A over the test α range which can probably be attributed to flow interaction phenomena associated with the conical fairing near the nose of the escape rocket.

Data for three escape-rocket configurations, E_{10}, E_{14}, and E_{48}, at transonic speeds are presented in figures 11 and 12. These data and all subsequent data in this document are descriptive of LEV configurations which have nominal 120-inch escape-tower structures and jettison motors forward of the main escape-rocket motor. Configuration E_{10} differs from E_{14} in nose angle only, and configuration E_{48} differs from E_{14} in that it is slightly longer, has a wider angled, flared skirt at the base, and has a structural flange mounted immediately forward of the skirt. These data indicate that the minor changes in the escape-rocket length, nose shape, and skirt diameter have negligible effects on the relative stability of the respective configurations.

Effect of Disks or Flow Separators

The addition of a disk or flow separator at or near the base of the escape rocket was proposed as a means of improving the transonic static-stability characteristics of the Apollo LEV. Generally, these configurations consisted of the addition of a flat plate mounted perpendicular to the airstream and located at or near the base of the escape rocket. Several plate size and shape modifications were investigated, and data for some typical configurations are presented in figures 13 to 17. The $C_{m,a}$ data presented in figure 13 for E_{20} with a disk located at the forward edge of the escape-rocket skirt indicate that the static stability at transonic speeds is improved by the addition. The data presented in figure 14 describe the effect at transonic and low supersonic speeds of a slightly larger diameter disk located at the base of the escape-rocket skirt. These data indicate that the effectiveness of the disk is similar to the previously shown data for a disk in front of the skirt (fig. 13). Data for several configurations of the escape rocket with disks located at various positions near the escape-rocket base are presented in figure 15. Shown for comparison are data for a configuration without the disk (E_{14}) and configurations with disks $(E_{20}$ and $E_{23})$, previously shown in figures 13 and 14. Configuration E_{37} has a disk located in the tower structure which is approximately 85 inches downwind of the skirt base. Configuration E_{38} has a 65-inch disk located at the base of the skirt with a 6-inch-radius segment clipped from the lower edge (fig. 2(g)). Configuration E_{39} has two disks located as noted for configurations E_{23} and E_{27}. As was noted, configurations E_{20} and E_{23} are similarly effective in increasing the static stability. Configuration E_{37} with the disk located in the tower structure rearward of the rocket skirt increases the stability only slightly. The clipped-disk configuration E_{38} and the double-disk configuration E_{39} are very similar in effectiveness to the E_{20} and E_{23} configurations. As indicated in figure 15(e), the addition of disks at the tip or base of the escape-rocket skirt causes a decrease in C_A near $\alpha = 0^\circ$.

Data which represent the effect of a larger disk located at the base of the escape-rocket skirt are shown in figure 16. Configuration E_{25} has a 91-inch disk on the rocket center line; configuration E_{29} is similar, with a 19.5-inch segment clipped from the

lower edge of the disk; and E_{32} has a 91-inch disk centered 10.4 inches above the escape-rocket center line. The data for configuration E_{23} are included for comparison purposes.

The data indicate that the larger flow separator (configuration E_{25}) increases the transonic stability. The clipped disk and offset disk both result in a negative shift in α_t but are less effective in increasing stability. As would be expected, the larger disks increase the C_A, except near $\alpha = 0°$.

The data presented in figure 17 contain a final comparison of the effects of adding a flow separator to the escape rocket. Rocket configuration E_{48} is lengthened to represent a near approach to the length of the final escape-rocket configuration. Escape rocket E_{49} is identical to E_{48} except for the addition of a flow separator at the forward edge of the skirt. The data for escape rocket E_{20} (which is similar to, but shorter than E_{49}) are presented for comparison purposes. The data are presented for a Mach number range of 0.7 to 3.4 at an α range of -5° to 56°. The data indicate that the addition of the flow separator increases the static stability and increases the C_A (except near $\alpha = 0°$) for all Mach numbers tested.

In summary, the flow separators generally increase the static stability of the configuration for the Mach number range studied. However, dynamic stability studies (ref. 10) indicate that the configuration has negative damping at most Mach numbers of 0.3 to 4.63. Also, the addition of ballast (equivalent in mass to the flow separators) at the rocket nose provides a pitching-moment increment of the same general magnitude as that produced by the addition of flow separators. Therefore, the flow separators were eliminated from further consideration.

Effect of Rocket-Skirt Diameter

The effects of an increase in base diameter of the escape-rocket skirt at Mach numbers of 0.7 to 2.0 and an α range of -15° to 95° are indicated by data presented in figure 18. The base diameter of the E_{12} skirt is 5 inches greater than the base diameter of the E_{10} skirt. Little or no effect on the static stability of the LEV results from this change in diameter.

Effect of the Addition of Strakes

The effect on the static stability of the LEV caused by the addition of strakes to the CM is indicated by data presented in figure 19. These data are presented for a Mach number range of 0.5 to 6.0 over an α range of -15° to 70°. A comparison of these data with the data presented in figure 18 indicates that, as expected, the addition of the strakes had only slight effect on the aerodynamic characteristics of the LEV.

Effect of the Addition of Strakes and Flow Separators

The effects of the addition of flow separators to an LEV configuration that has strakes on the CM are indicated by data presented in figure 20. These data are presented for Mach numbers of 0.7 to 6.0 at an α range of -15° to 95°. The data indicate that, as previously noted, the flow separators generally increase the static stability and decrease the C_A near α_t throughout the Mach number range tested.

CONCLUDING REMARKS

Wind-tunnel tests to determine the static stability characteristics of the various Apollo LEV configurations that were studied in the development of the flight configurations were made, using several wind-tunnel facilities. Test data for a representative number of the various LEV configurations tested have been presented in this document. Analyses of these data indicate the following:

1. Within reasonable limits, tower length had little effect on static stability. However, structural problems associated with the longer tower lengths and escape-rocket plume impingement associated with the shorter tower lengths precluded the selection of other than the 120-inch predesign tower length.

2. Rocket-length growth (a result of moving the jettison rocket forward), the addition of the pitch control motor, and the addition of canards had only slight effects on static stability.

3. The effect on static stability of nose and skirt variations, studied in an attempt to determine if optimization of these variables was necessary, was negligible.

4. The addition of flow separators or disks generally resulted in an increase in static stability and a decrease in C_A at α_t ($\alpha \approx 0°$). However, the flow separators were eliminated from the configuration because negative damping was exhibited by the configuration, and a similar increment of pitching-moment coefficient could be obtained by adding a ballast (equivalent in mass to the flow separators) at the escape-rocket nose.

5. The addition of strakes had little or no effect on the static stability of the LEV configuration.

Manned Spacecraft Center
National Aeronautics and Space Administration
Houston, Texas, January 17, 1969
914-50-00-00-72

REFERENCES

1. Morgan, James R.; and Fournier, Roger H.: Static Longitudinal Characteristics of a 0.07-Scale Model of a Proposed Apollo Spacecraft at Mach Numbers of 1.57 to 4.65. NASA TM X-603, 1961.

2. Pearson, Albin O.: Wind-Tunnel Investigation of the Static Longitudinal Aerodynamic Characteristics of Models of Reentry and Atmospheric-Abort Configurations of a Proposed Apollo Spacecraft at Mach Numbers from 0.30 to 1.20. NASA TM X-604, 1961.

3. Pearson, Albin O.: Wind-Tunnel Investigation of the Static Longitudinal Aerodynamic Characteristics of a Modified Model of A Proposed Apollo Atmospheric-Abort Configuration at Mach Numbers from 0.30 to 1.20. NASA TM X-686, 1962.

4. Fournier, Roger H.; and Corlett, William A.: Aerodynamic Characteristics in Pitch of Several Models of the Apollo Abort System from Mach 1.57 to 2.16. NASA TM X-910, 1964.

5. Moseley, William C., Jr.; and Martino, Joseph C.: Apollo Wind Tunnel Program Historical Development of General Configurations. NASA TN D-3748, 1966.

6. Moseley, William C., Jr.; and Hondros, James G.: Aerodynamic Stability Characteristics of the Apollo Launch Escape Vehicle. NASA TN D-3964, 1967.

7. Moseley, William C., Jr.; Moore, Robert H., Jr.; and Hughes, Jack E.: Stability Characteristics of the Apollo Command Module. NASA TN D-3890, 1967.

8. Moseley, William C., Jr.; and Redd, Bass.: Aerodynamic Stability Characteristics of the Apollo Launch Escape Vehicle (LEV) With Canard Surfaces Deployed. NASA TN D-4280, 1967.

9. Moseley, William C., Jr.; Graham, Ralph E.; and Hughes, Jack E.: Aerodynamic Stability Characteristics of the Apollo Command Module. NASA TN D-4688, 1968.

10. Averett, Benjamin T.: Dynamic-Stability Characteristics in Pitch of Models of Proposed Apollo Configurations at Mach Numbers from 0.30 to 4.63. NASA TM X-1127, 1965.

TABLE I.- TEST FACILITIES AND CAPABILITIES

Test facility	Size of test section	Mach number range	Reynolds number range, $\times 10^{-6}$
Continuous tunnels			
Ames Unitary Plan Wind Tunnel (Ames UPWT)	8 by 7 ft 9 by 7 ft 11 by 11 ft	2.4 to 3.5 1.5 to 2.6 .7 to 1.4	0.5 to 5 1 to 7 1 to 10
Arnold Engineering Development Center, Tunnel A (AEDC-A)	40 by 40 in.	1.5 to 6.0	.3 to 9
Jet Propulsion Laboratory 20-Inch Supersonic Wind Tunnel (JPL-20 SWT)	18 by 20 in.	1.3 to 5.0	.4 to 6
Jet Propulsion Laboratory 21-Inch Hypersonic Wind Tunnel (JPL-21 HWT)	21 by 15 to 28 in.	5.0 to 9.5	.25 to 3.6
Intermittent tunnels			
North American Aviation Supersonic Aerophysics Laboratory (NAA-SAL)	16 in^2	0.7 and 1.56 to 3.75	1.16 to 2.49, and .54
North American Aviation Trisonic Wind Tunnel (NAA-TWT)	7 by 7 ft	.2 to 3.5	5 to 14

TABLE II. - MODELS AND TEST RANGES

Model	Scale	Facility	Mach number range	Reynolds number range, $\times 10^{-6}$	α range, deg	Dynamic pressure, lb/ft^2
FS-1	0.02	JPL-20 SWT	1.65 to 3.26	0.724 to 0.924	-20 to 90	573
		JPL-21 HWT	5.0 to 9.0	.29 to .884	-20 to 90	440
		NAA-SAL	1.57 to 3.26	.54 to 1.16	-10 to 30	270 to 984
FS-2	0.105	Ames-UPWT	0.5 to 3.4	0.53 to 14.2	-15 to 96	425 to 540
		NAA-TWT	.7 to 2.0	13.4 to 14.2	-16 to 48	1300 to 2035
FS-3	0.045	AEDC-A	4.0 to 6.0	0.53 to 2.42	-15 to 72	70 to 531

TABLE III. - SUMMARY OF COMMAND MODULE VARIABLES

C number	Nose-cone semiangle, deg	Nose-cone vertex radius, in.	Corner radius, in.	Radius of spherical blunt end, in.	Maximum diameter, in.	Miscellaneous
1	33	15.4	7.7	184.8	154.0	
2	33	9.15	7.7	184.8	154.0	
39	33	9.15	7.7	184.8	154.0	Tower leg cavities are left open

TABLE IV. - SUMMARY OF ESCAPE-TOWER VARIABLES

T, number	Total exposed length,[a] in.	Longitudinal members		Cross-members		Distance between attachment points		Distance of horizontal members from escape-rocket base, in.	Miscellaneous
		Number	Diameter, in.	Number	Diameter, in.	Command module, in.	Escape rocket, in.		
1	169.0	4	2.85	32	2.05	52.00 by 52.00	12.00 by 12.00	36.00, 56.00, 81.00 and 117.00	
2	249.0	4	2.85	48	2.05	52.00 by 52.00	12.00 by 12.00	36.00, 56.00, 81.00, 117.00, 158.00 and 197.00	
5	164.5	4	3.00	48	2.00	46.50 by 46.50	12.00 by 12.00	9.00, 41.90, 75.00, 108.00, 137.00 and 142.90	Braces near base of legs
7	119.0	4	3.20	24	2.50	52.00 by 52.00	12.00 by 12.00	25.00, 50.00 and 75.00	
8	85.0	4	2.85	8	2.85	52.00 by 52.00	30.00 by 30.00	50.75	Stiffener gussets at base
9	114.514	4	3.57	32	2.38	46.75 by 46.75	21.90 by 21.90	9.00, 39.39, 87.05 and 92.89	Braces near base of legs
10	79.467	4	3.57	24	2.38	46.75 by 46.75	21.91 by 21.91	9.00, 52.00 and 57.84	Braces near base of legs
11	119.0	4	3.20	28	2.50	52.00 by 52.00	12.00 by 12.00	25.00, 50.00, 75.00 and 84.75	Stiffener plates at base
26	113.14	4	3.57	37	2.38	46.76 by 46.76	36.07 by 36.07	60.29 and 85.90	Ring 32.10 in. aft of rocket base; stiffener plates, gussets, and feet near base
27	115.35	4	4.00	37	2.67 and 4.00	50.67 by 46.84	36.07 by 36.07	60.24 and 85.89	Ring 32.13 in. aft of rocket base; plate at top

[a]Distance from escape-rocket base to CM with CM having a 33° nose-cone semiangle.

TABLE V. - SUMMARY OF ESCAPE-ROCKET VARIABLES

E number	Rocket diameter, in.	Total length, in.	Nose shape		Skirt shape		Disk diameter, in.	Disk location	Miscellaneous
			Radius, in.	Cone, deg	Diameter, in.	Flare, deg			
1	26.0	248.412	5.2	60	47.00	30	None	None	Aft jettison motor; toroidal tanks
2	Tapered	248.412	5.2	60	None	None	None	None	Aft jettison motor
2BL	Tapered	248.412	5.2	60	None	None	None	None	Aft jettison motor; band of 0.0076-in. grit on nose cone
3	26.0	273.645	2.0	15, offset	47.00	30	None	None	Aft jettison motor; toroidal tanks
4	26.0	248.412	5.2	60	47.00	30	None	None	Aft jettison motor
5	26.0	273.645	2.0	15, offset	47.00	30	None	None	-
6	26.0	178.917	5.2	60	47.00	30	None	None	-
7	26.0	226.92	5.2	60	47.00	30	None	None	Forward jettison motor with protruding nozzles
8	26.0	226.92	5.2	60	50.50	30	None	None	Forward jettison motor with protruding nozzles
9	26.0	239.05	5.2	60	38.00	33	None	None	Reverse flow; 30° forward skirt angle
10[a]	26.0	226.92	5.2	60	47.00	30	None	None	Forward jettison motor; nozzles flush
12	26.0	226.917	5.2	60	52.00	30	None	None	-
14	26.0	252.39	2.0	30	47.00	30	None	None	-
20	26.0	252.39	2.0	30	47.00	30	65.0	Forward of skirt	-
23	26.0	254.88	2.0	30	52.00	30	65.0	Aft of skirt	-
25	26.0	254.88	2.0	30	52.00	30	91.0	Aft of skirt	-
29	26.0	254.88	2.0	30	52.00	30	91.0	Aft of skirt	19.5 in. clipped from bottom of disk

[a]Nozzles of forward jettison motor of escape-rocket motors E_{10} to E_{62} are faired flush with the surface.

TABLE V. - SUMMARY OF ESCAPE-ROCKET VARIABLES - Concluded

E number	Rocket diameter, in.	Total length, in.	Nose shape		Skirt shape		Disk diameter, in.	Disk location	Miscellaneous
			Radius, in.	Cone, deg	Diameter, in.	Flare, deg			
32	26.0	254.88	2.0	30	52.00	30	91.0	Aft of skirt	Center of disk 10.4 in. above rocket center line
37	26.0	252.39	2.0	30	51.85	34	78.0	Aft of skirt	This disk attached near tower base
38	26.0	254.88	2.0	30	51.85	34	65.0	Aft of skirt	6.0 in. clipped from bottom of disk
39	26.0	254.88	2.0	30	51.85	34	65.0	Aft of skirt	A second disk, 78.0 in. diameter, attached near tower base
48	26.0	274.81	2.0	30	51.85	34	None	None	Ring forward of skirt
49	26.0	274.81	2.0	30	51.85	34	65.0	Forward of skirt	Ring forward of skirt; ring fairing from disk to skirt
60	26.0	279.67	2.0	30	52.73	34	None	None	Ring forward of skirt; raceways on body
62	26.0	279.67	2.0	30	52.73	34	65.0	Forward of skirt	Ring forward of skirt; ring fairing from disk to skirt; raceways
63	26.0	279.61	2.0	30	52.73	34	None	None	Ring forward of skirt; four fairings on skirt; aft rocket
64	26.0	279.67	2.0	30	52.73	34	65.0	Forward of skirt	Ring forward of skirt; fairing from disk to skirt with cutouts; aft rocket nozzles; protruding forward jettison nozzles

TABLE VI. - ACCURACY OF DATA

Facility	Mach number	C_m	C_N	C_A
Ames UPWT	0.7 to 0.9	0.0102	0.0058	0.0063
	1.1 to 3.0	.0102	.0059	.0063
	3.4	.0130	.0075	.0080
	.5 to 3.4	.0041	.0071	.0071
AEDC-A	4.0	0.0084	0.026	0.029
	5.0	.0113	.018	.117
	6.0	.0256	.023	.059
JPL-20 SWT	1.65	--	--	--
	2.41	--	--	--
	3.26	--	--	--
JPL-21 HWT	5.0	--	--	--
	7.3	--	--	--
	9.0	--	--	--
NAA-SAL	0.7 and	--	--	--
	1.57 to 3.26	--	--	--
NAA-TWT	0.7 to 3.5	--	--	--

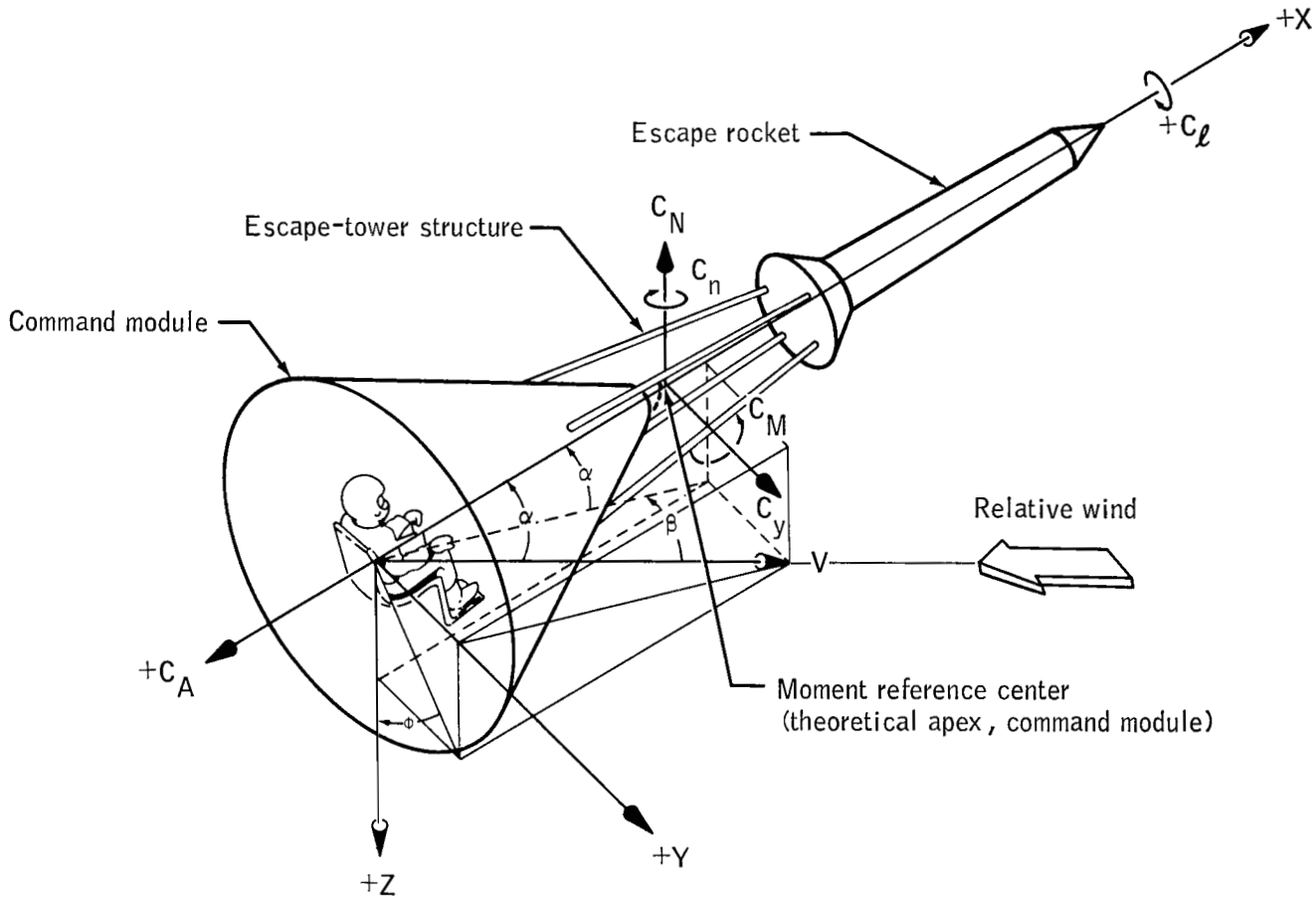

Figure 1. - Sketch showing system of body axes. Arrows indicate positive directions.

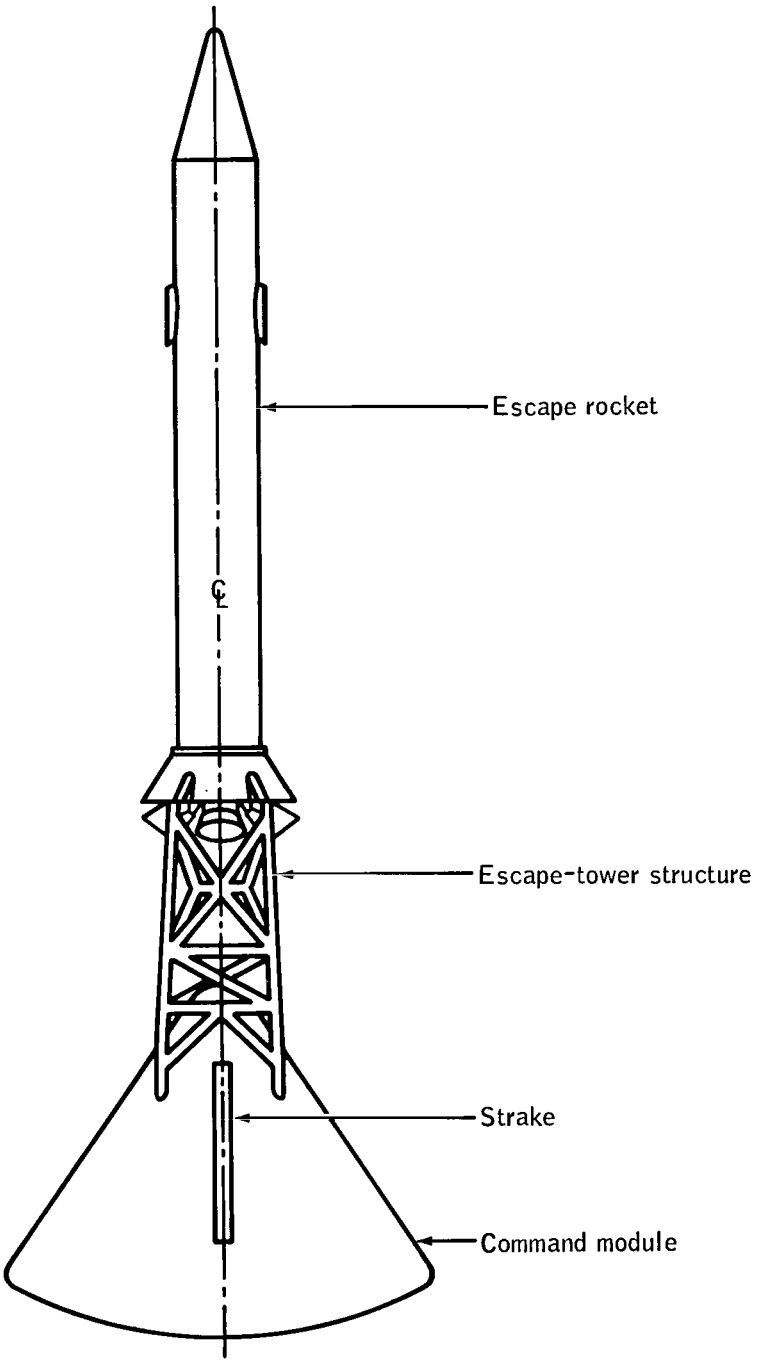

(a) Sketch of typical Apollo launch escape vehicle.

Figure 2. - Configuration of test models.

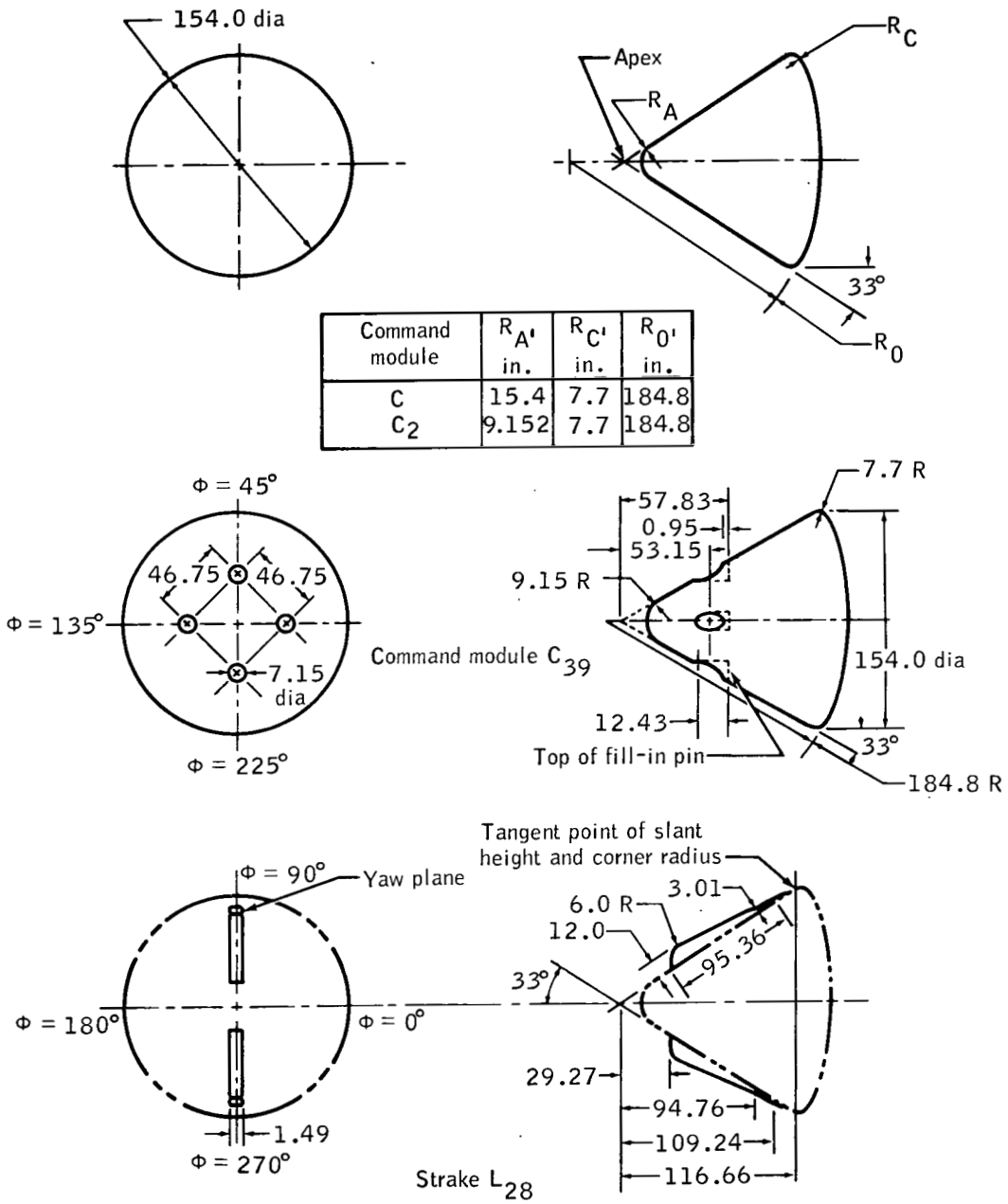

Command module	$R_{A'}$ in.	$R_{C'}$ in.	$R_{0'}$ in.
C	15.4	7.7	184.8
C_2	9.152	7.7	184.8

(b) Command modules and strakes showing full-scale dimensions in inches (drawings not to scale).

Figure 2. - Continued.

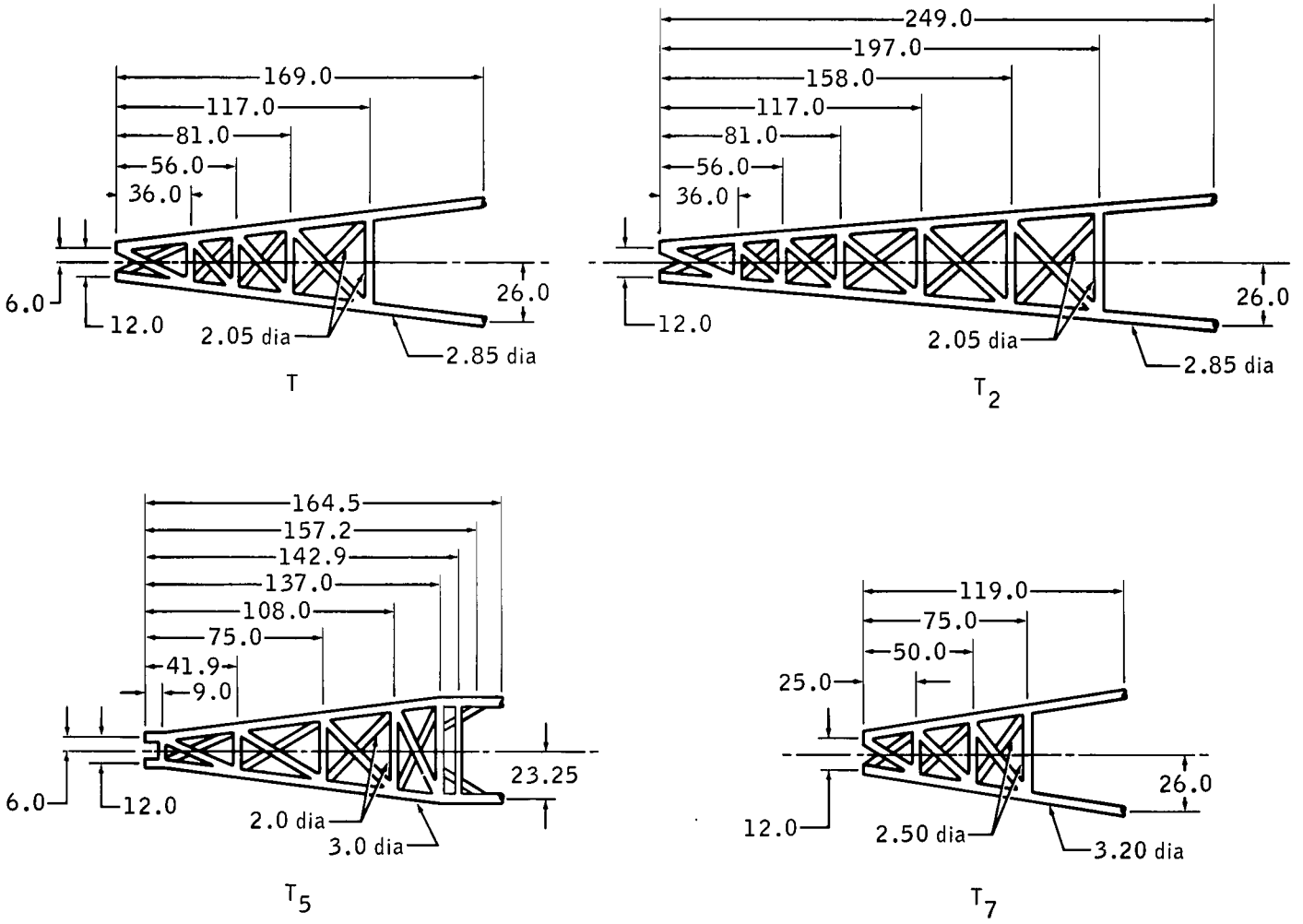

(c) Escape-tower structures T, T_2, T_5, and T_7 showing full-scale dimensions in inches (drawings not to scale).

Figure 2. - Continued.

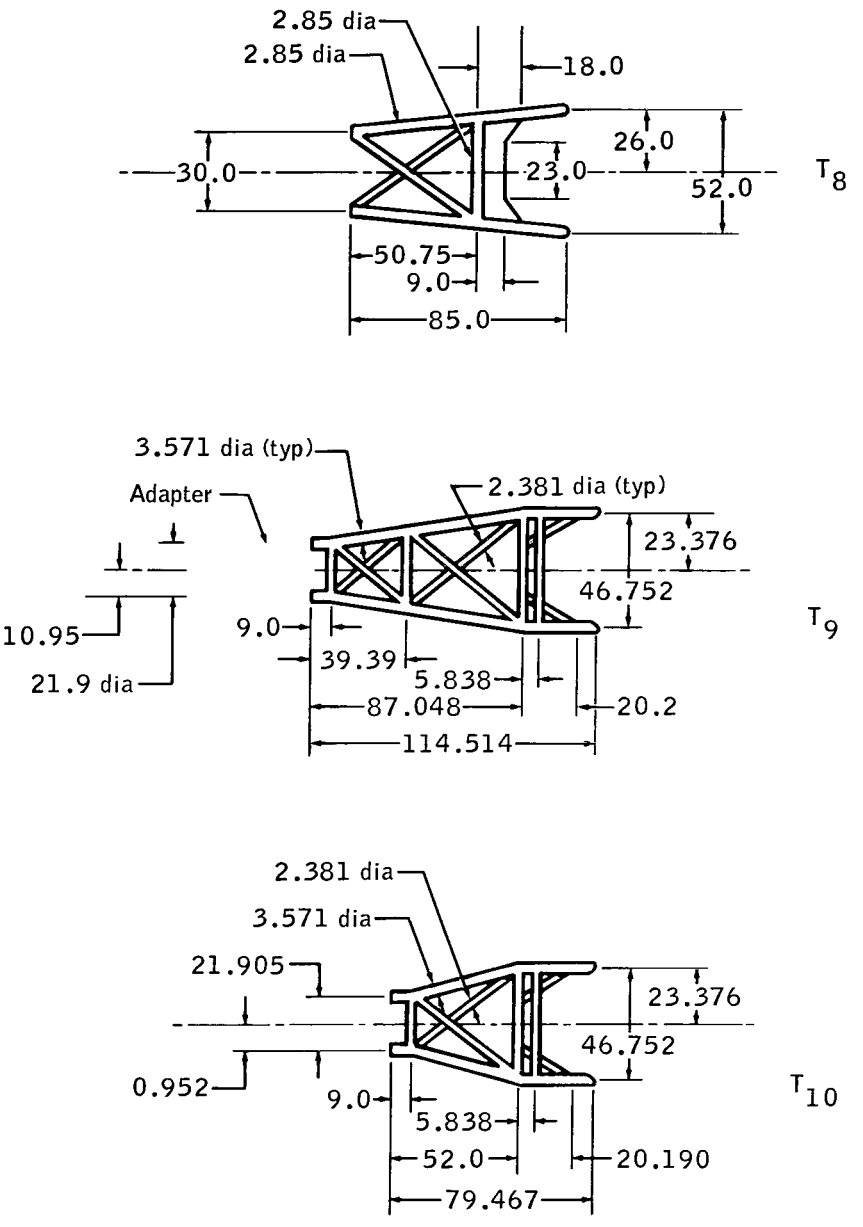

(d) Escape-tower structures T_8, T_9, and T_{10} showing full-scale dimensions in inches (drawings not to scale).

Figure 2. - Continued.

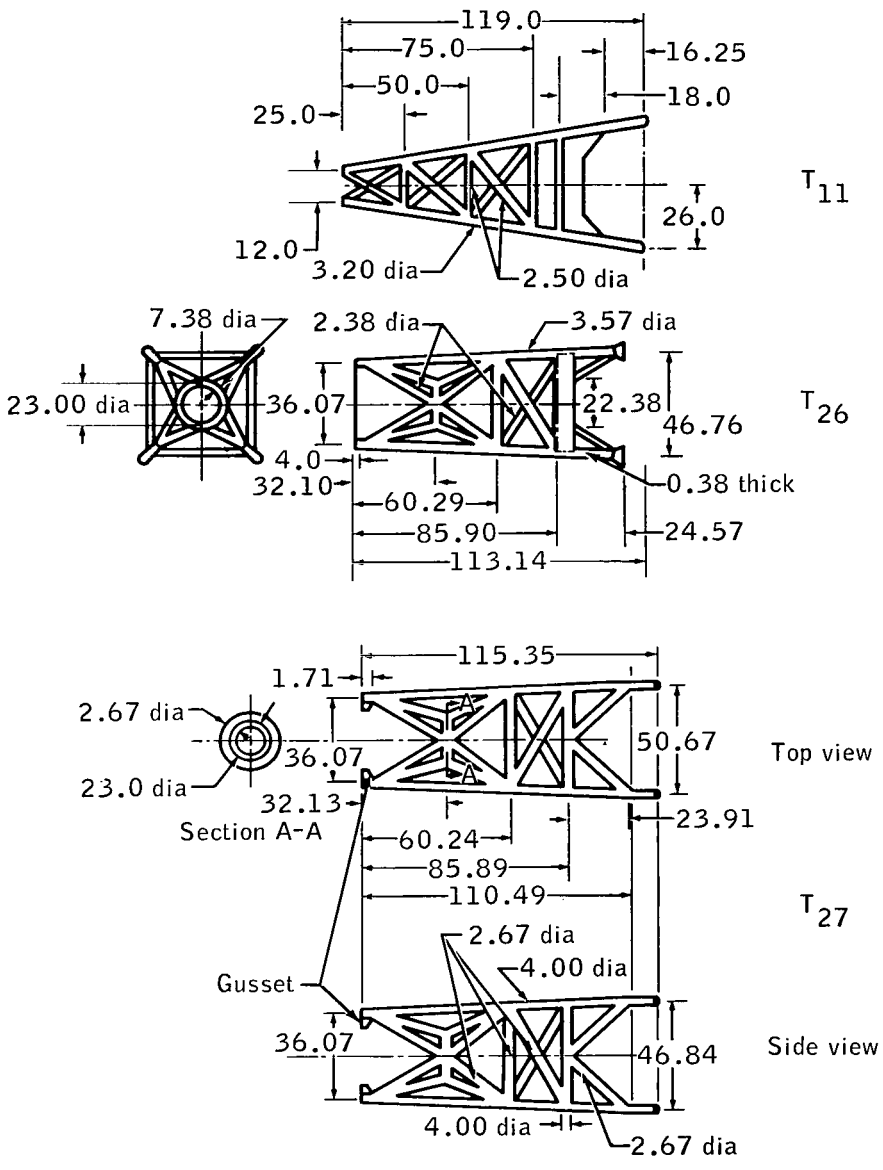

(e) Escape-tower structures T_{11}, T_{26}, and T_{27} showing full-scale dimensions in inches (drawings not to scale).

Figure 2. - Continued.

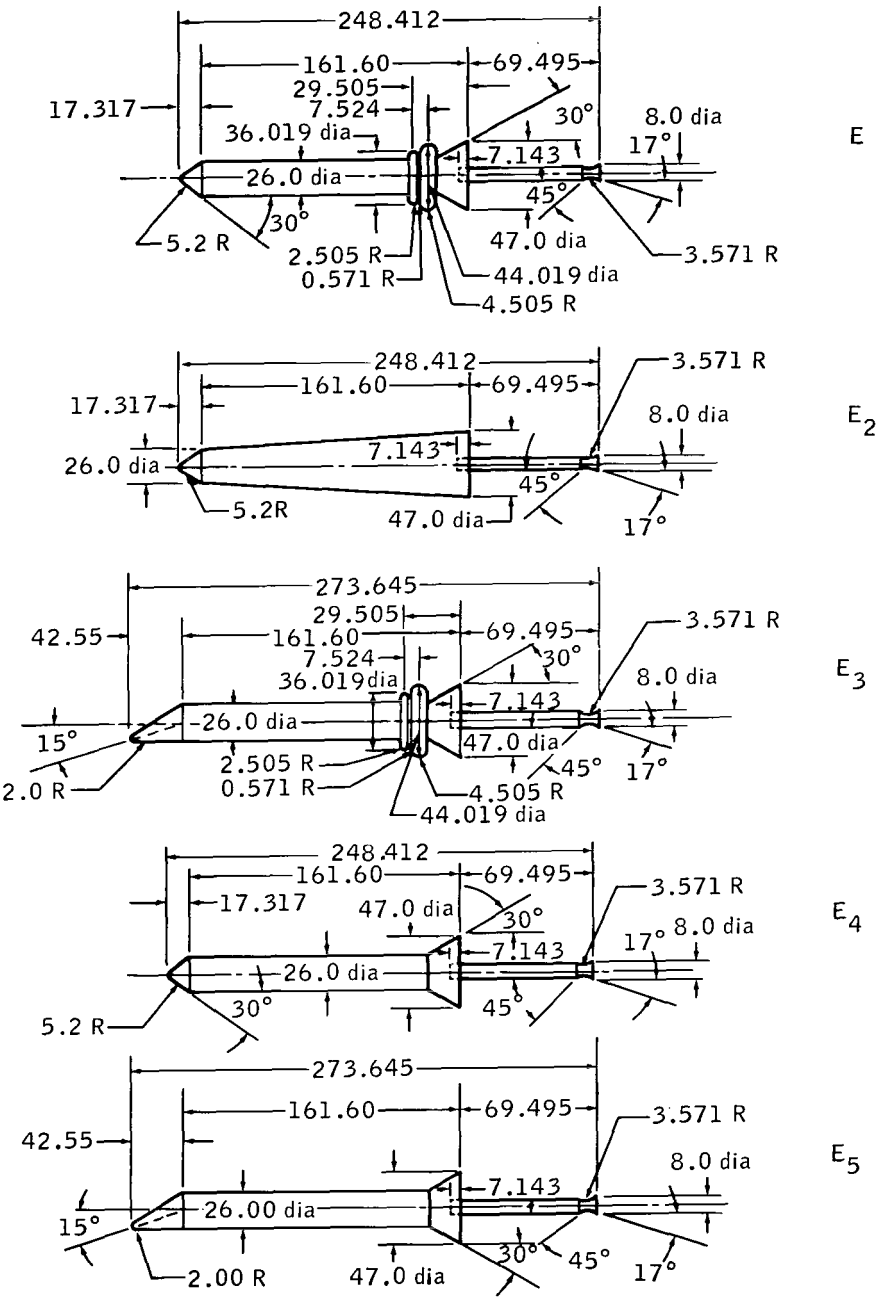

(f) Escape rockets E, E_2, E_3, E_4, and E_5 showing full-scale dimensions in inches (drawings not to scale).

Figure 2. - Continued.

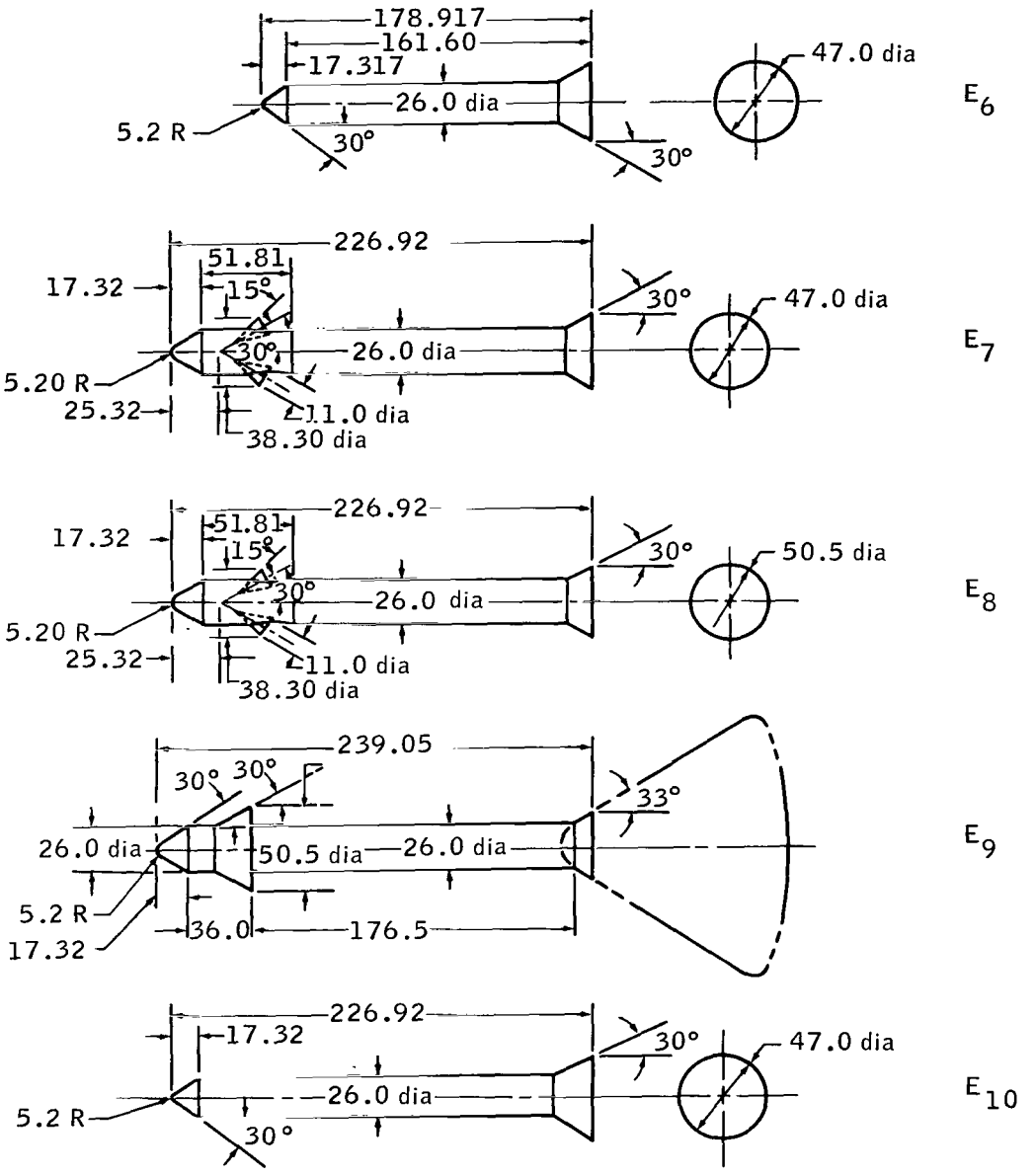

(g) Escape rockets E_6, E_7, E_8, E_9, and E_{10} showing full-scale dimensions in inches (drawings not to scale).

Figure 2. - Continued.

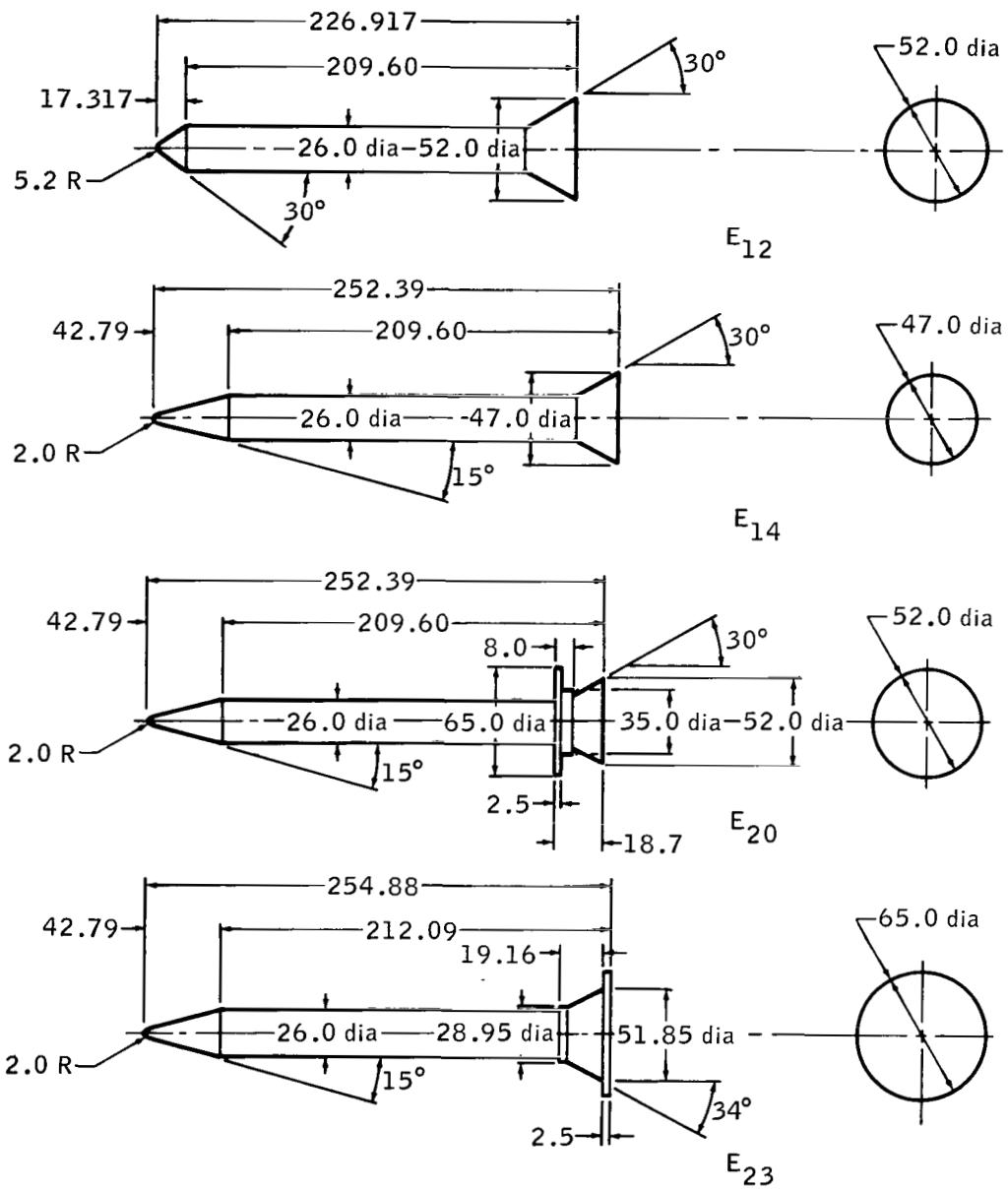

(h) Escape rockets E_{12}, E_{14}, E_{20}, and E_{23} showing full-scale dimensions in inches (drawings not to scale).

Figure 2. - Continued.

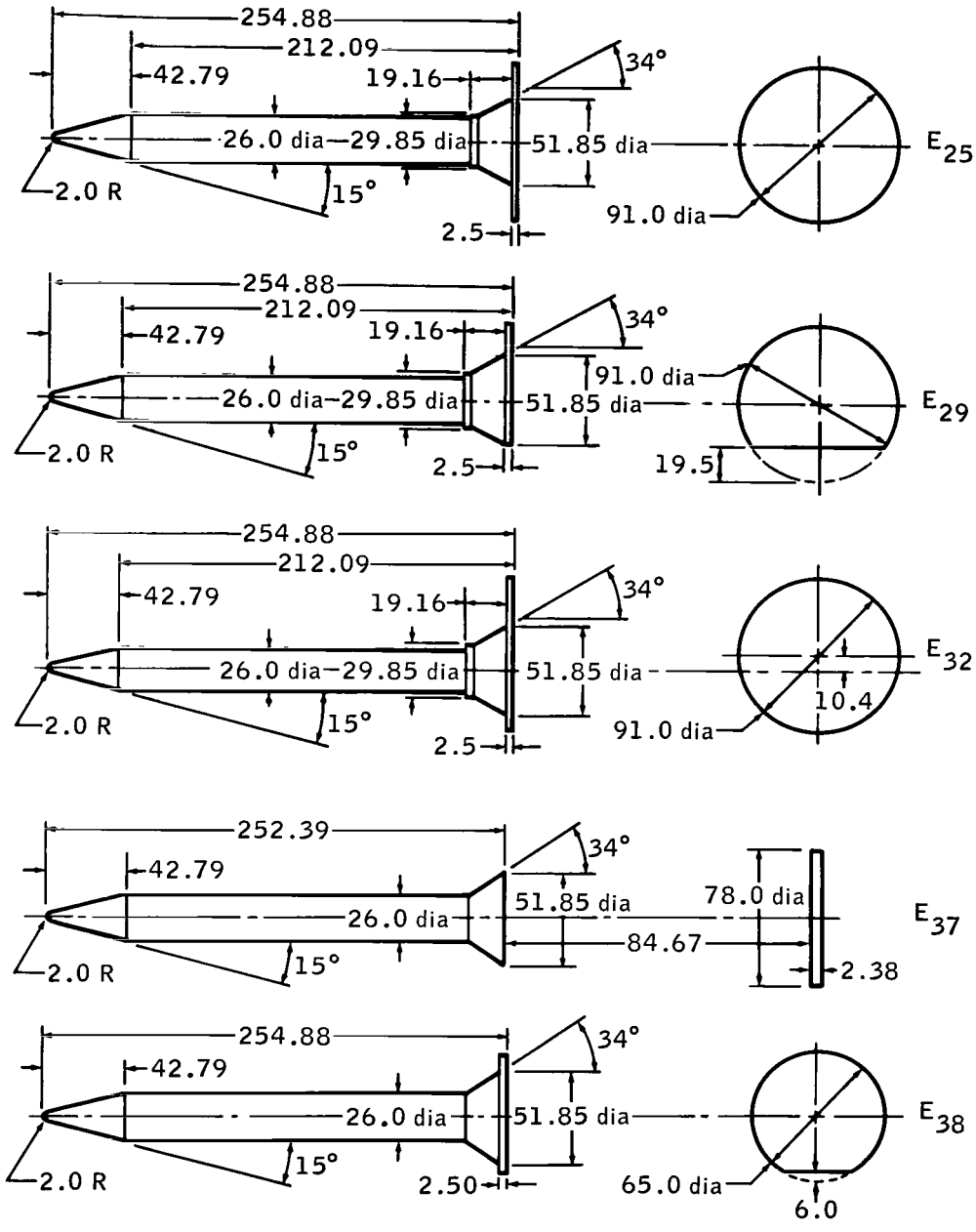

(i) Escape rockets E_{25}, E_{29}, E_{32}, E_{37}, and E_{38} showing full-scale dimensions in inches (drawings not to scale).

Figure 2. - Continued.

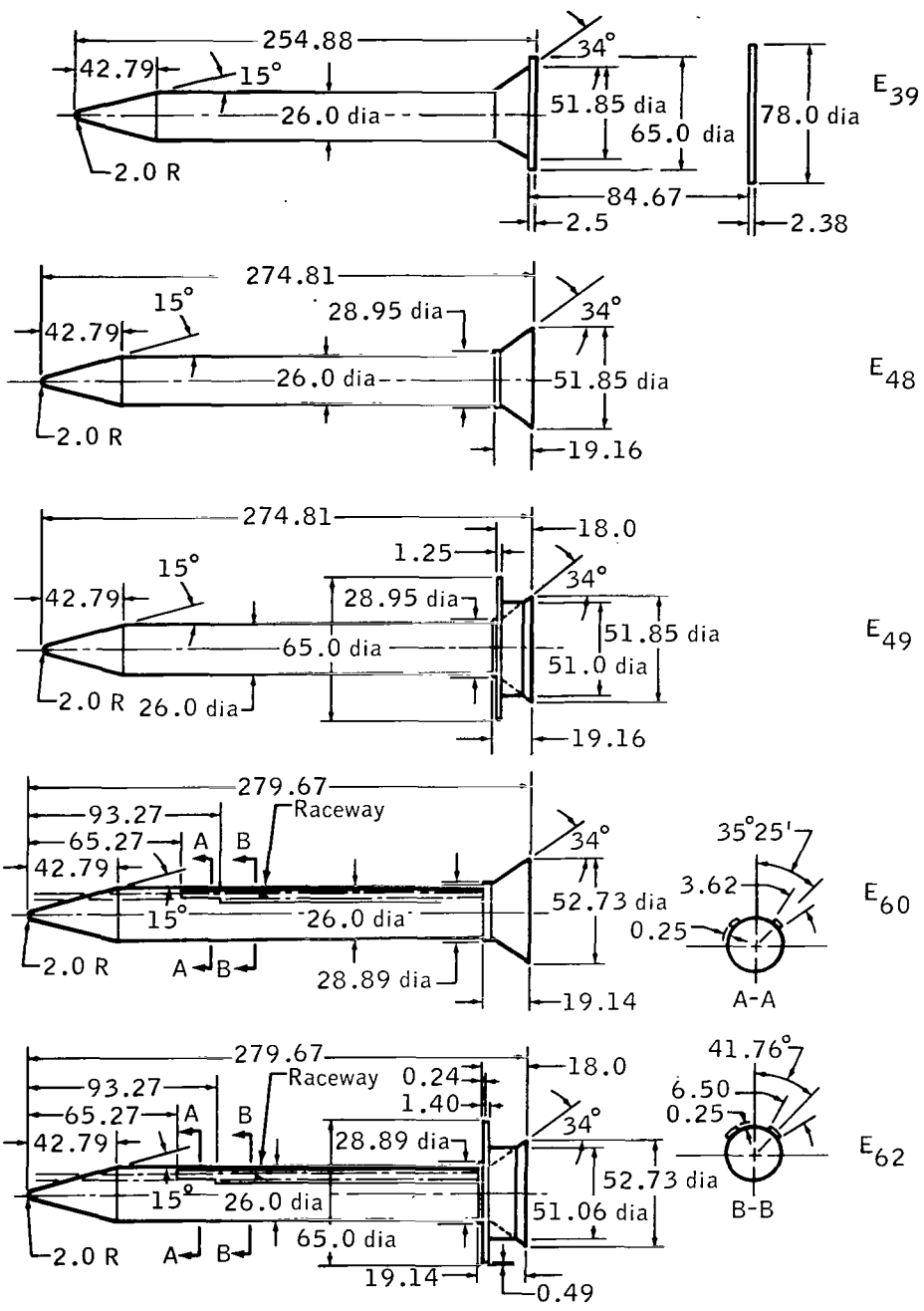

(j) Escape rockets E_{39}, E_{48}, E_{49}, E_{60}, and E_{62} showing full-scale dimensions in inches (drawings not to scale).

Figure 2. - Continued.

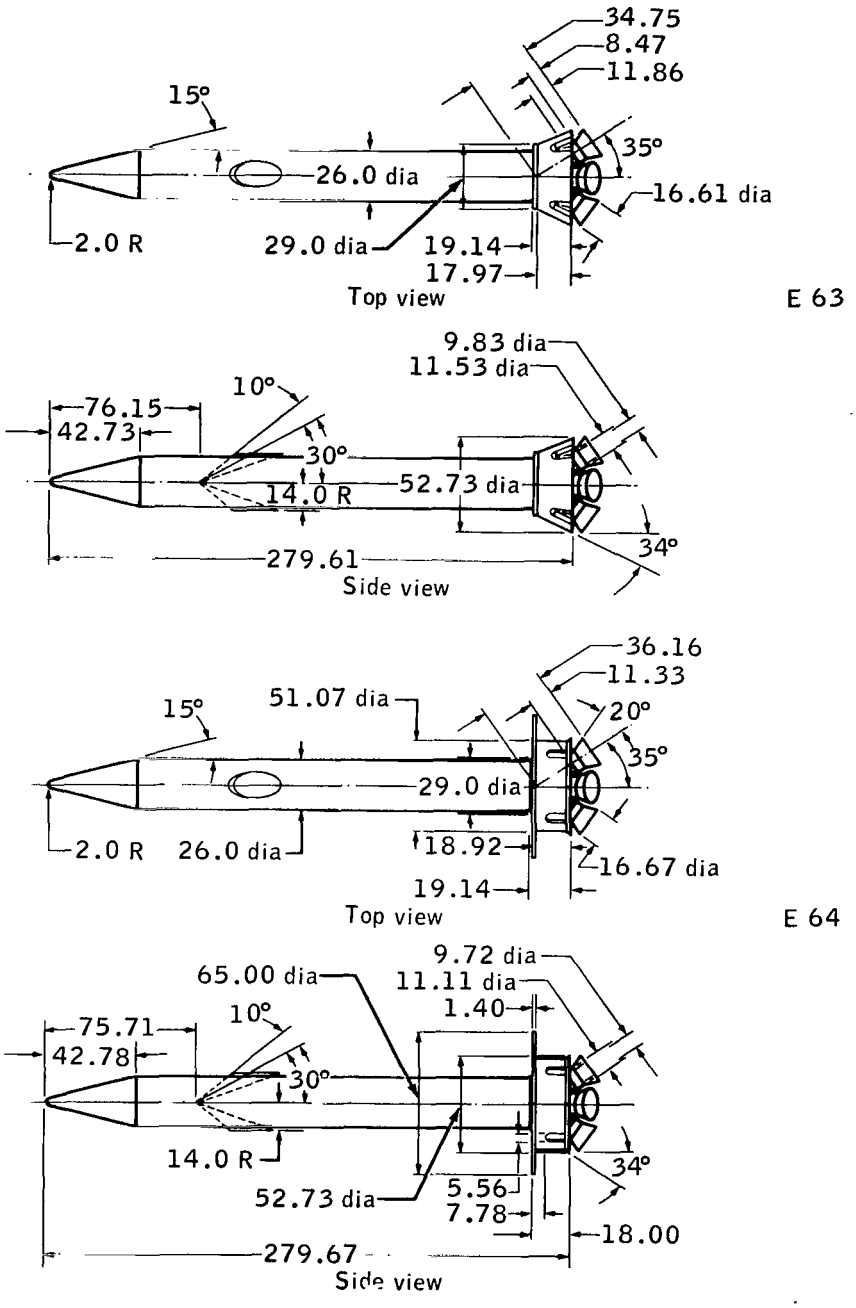

(k) Escape rockets E_{63} and E_{64} showing full-scale dimensions in inches (drawings not to scale).

Figure 2. - Concluded.

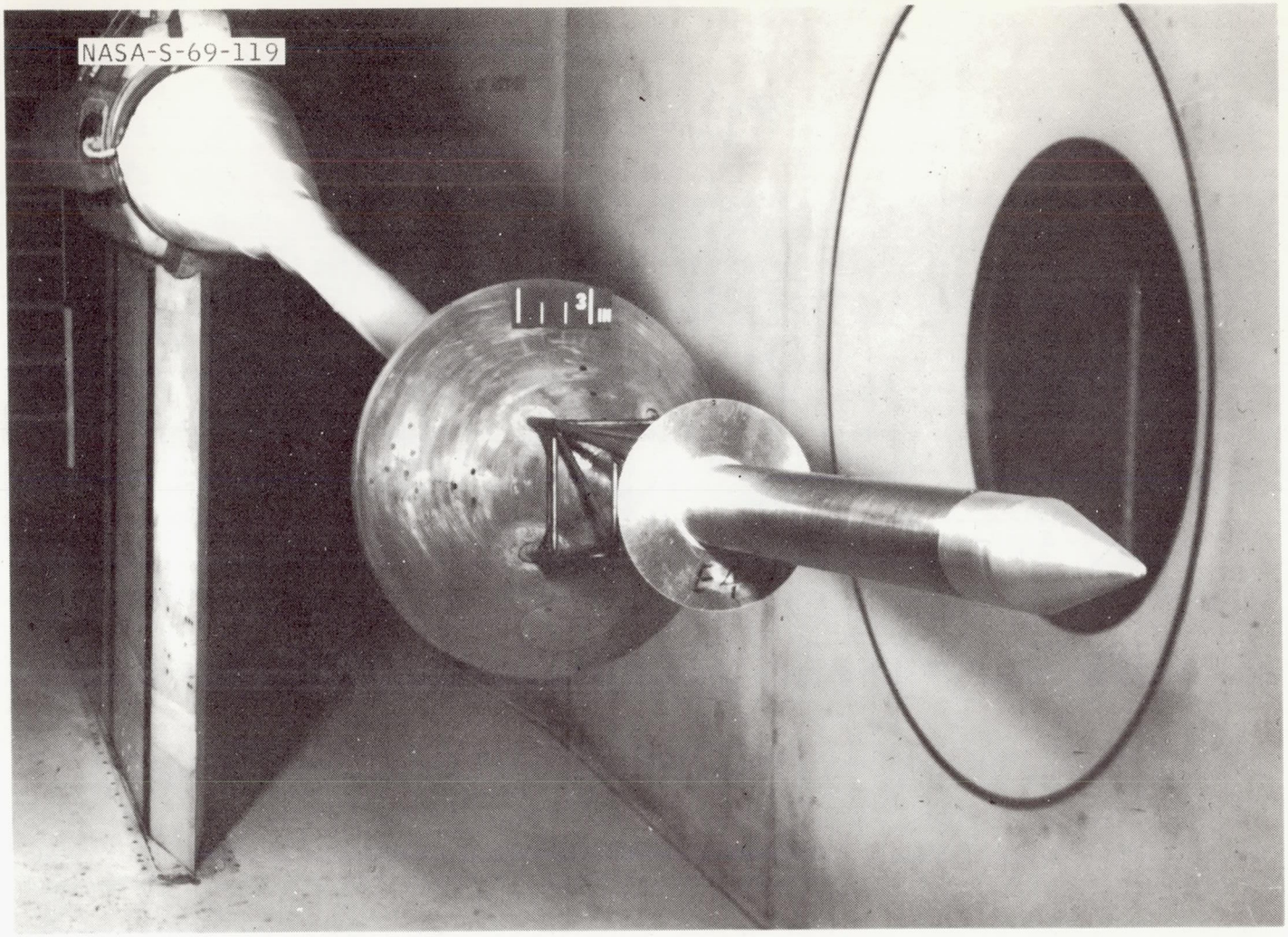

(a) Apollo LEV model installed in 8- by 7-foot test section of the Ames UPWT.

Figure 3. - Photographs of test models.

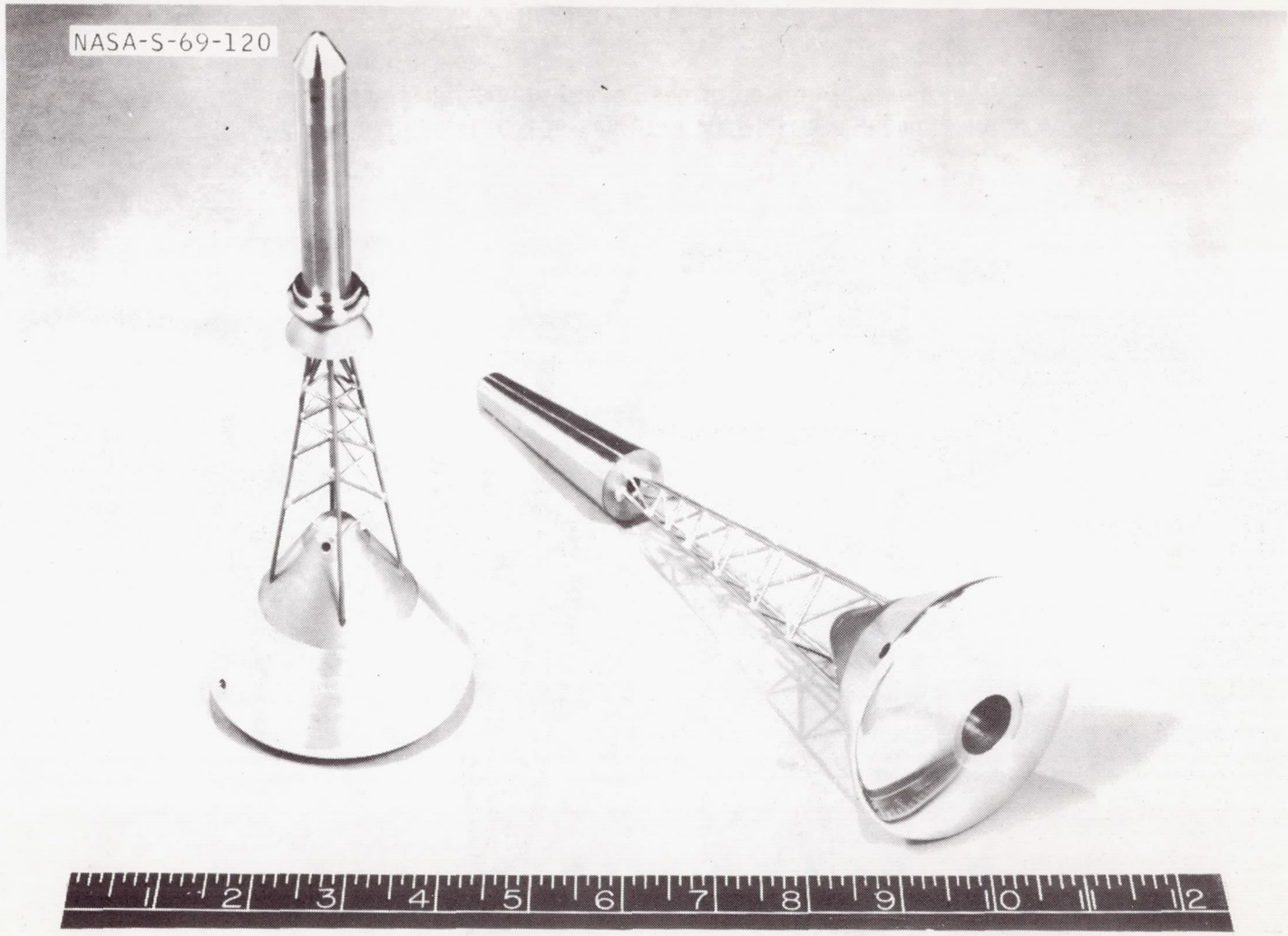

(b) The FS-1 models (0.02 scale) showing typical Apollo LEV configuration.

Figure 3. - Continued.

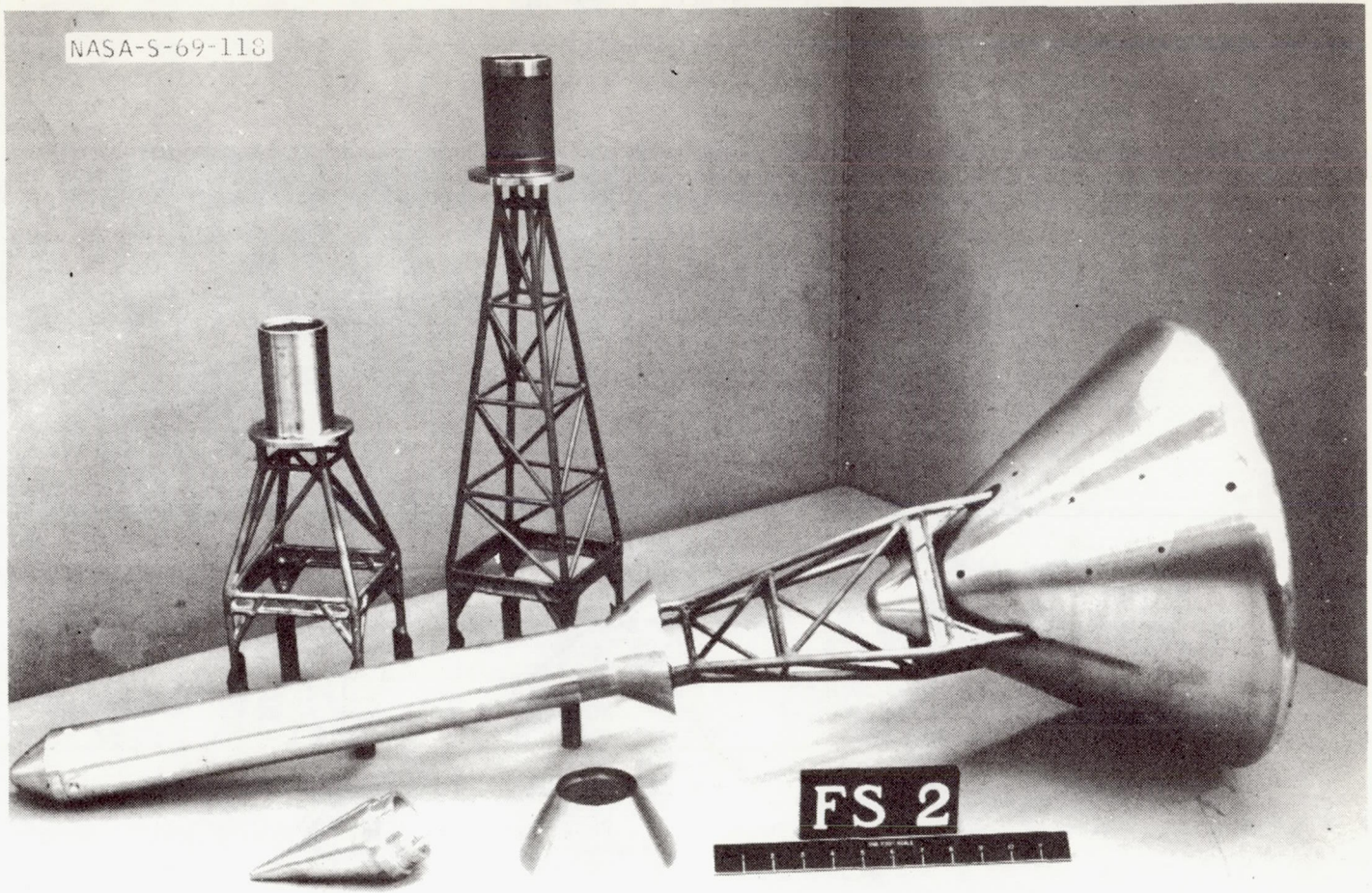

(c) The FS-2 model (0.105 scale) of Apollo LEV showing some of the interchangeable parts used in developing various configurations.

Figure 3. - Concluded.

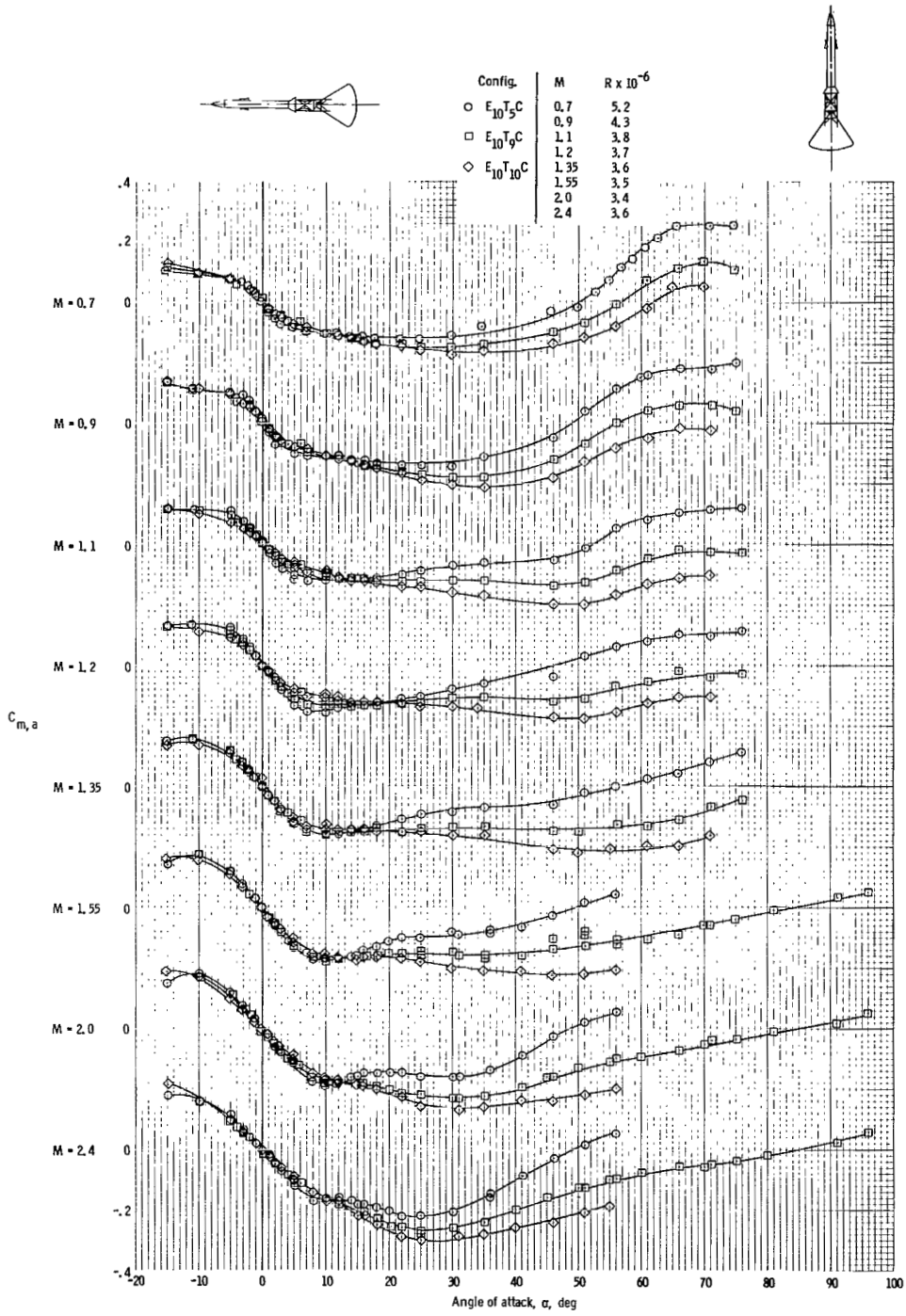

(a) Pitching-moment coefficient.

Figure 4. - Effect of tower-length variations on aerodynamic characteristics of Apollo LEV, M = 0.7 to 2.4.

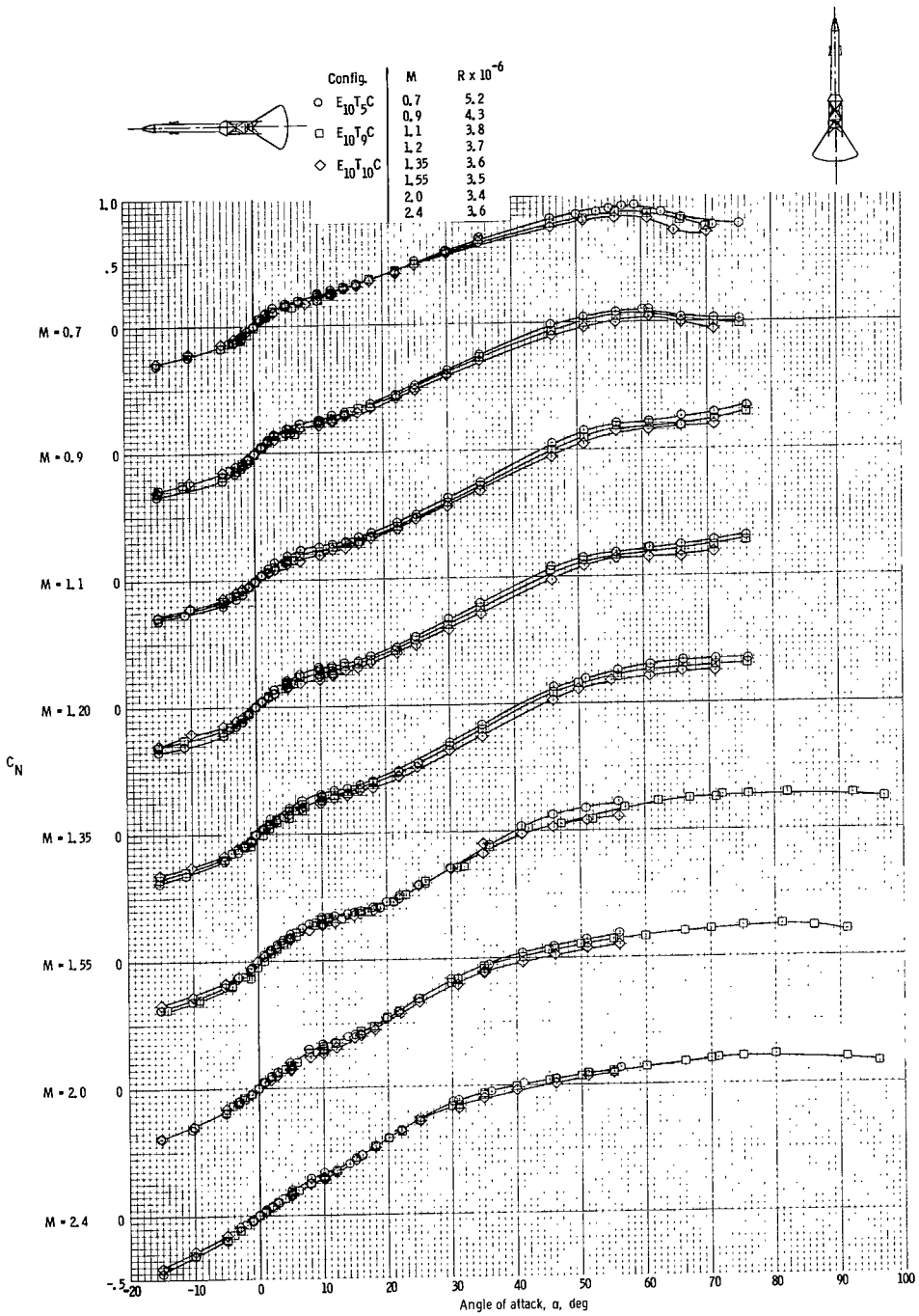

(b) Normal-force coefficient.

Figure 4. - Continued.

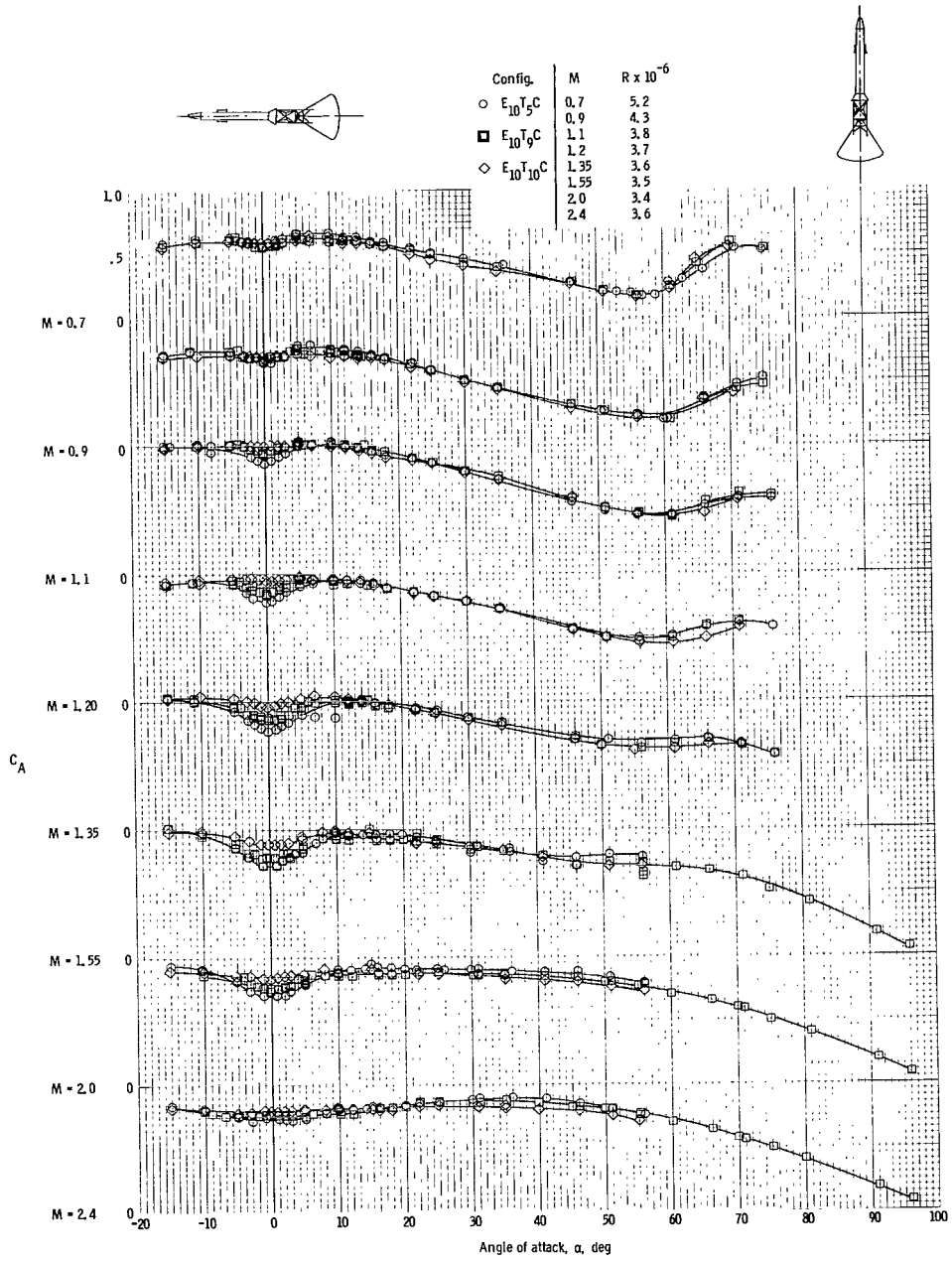

(c) Axial-force coefficient.

Figure 4. - Concluded.

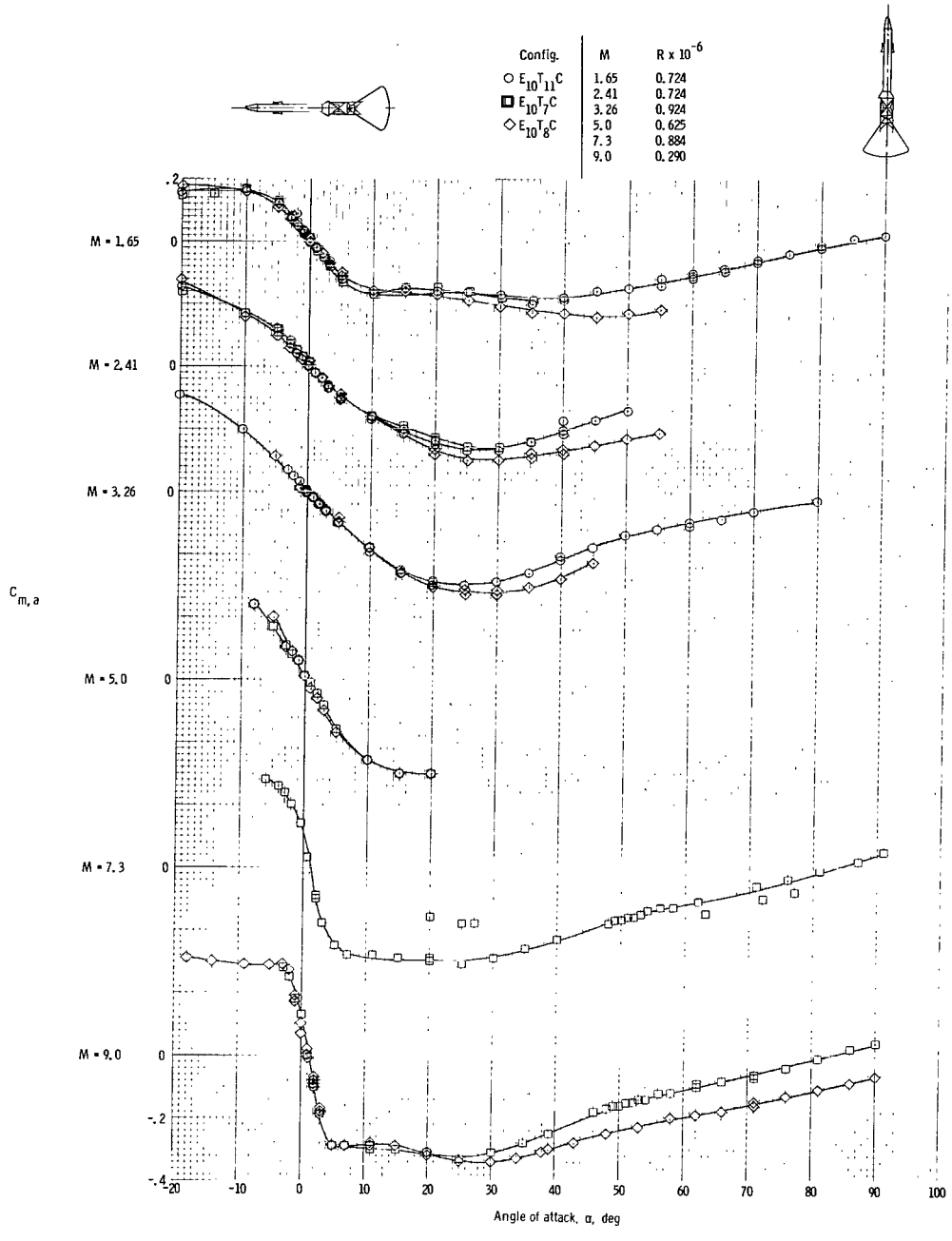

(a) Pitching-moment coefficient.

Figure 5. - Effect of tower-length variations on aerodynamic characteristics of Apollo LEV, M = 1.65 to 9.0.

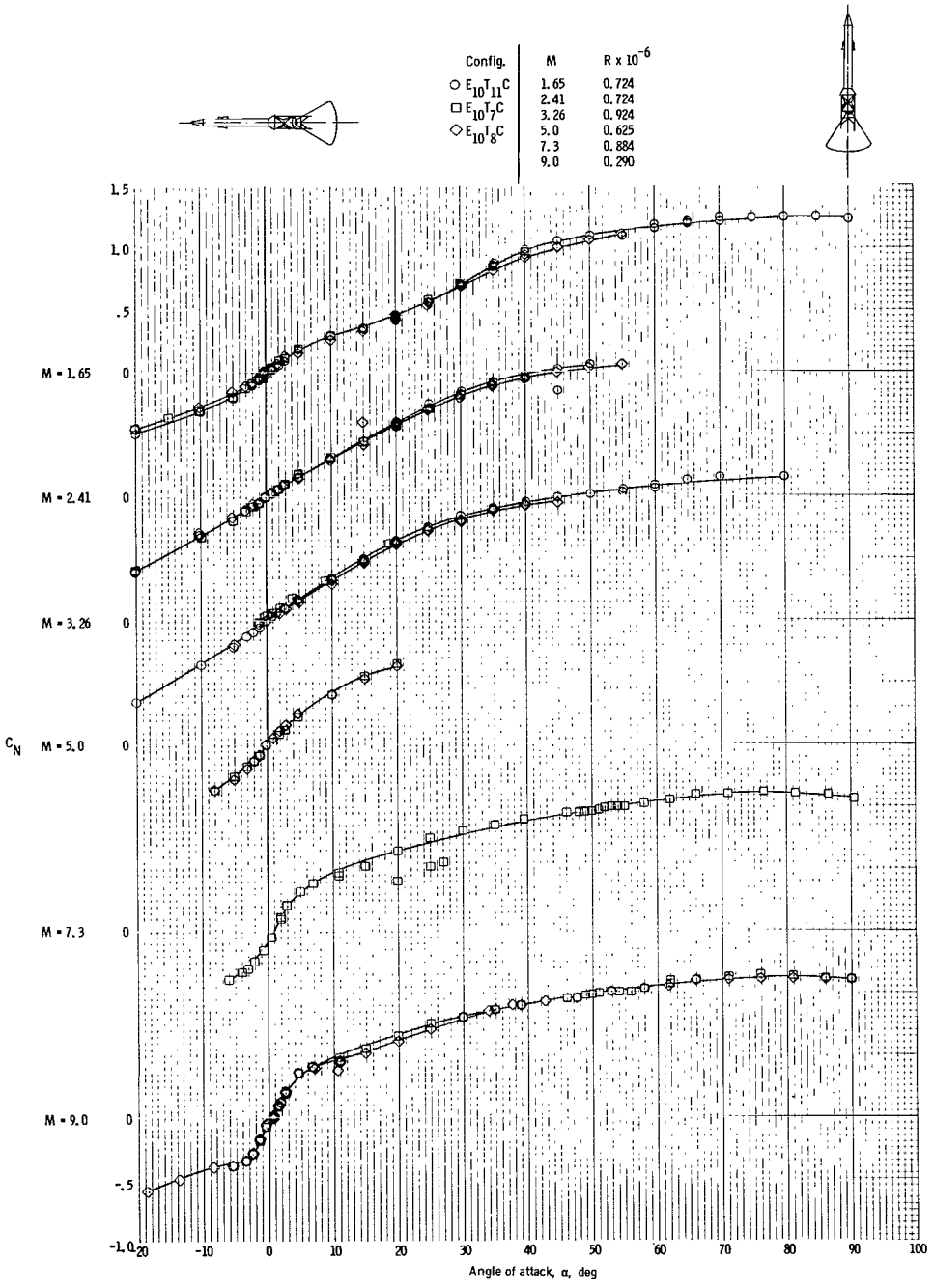

(b) Normal-force coefficient.

Figure 5. - Continued.

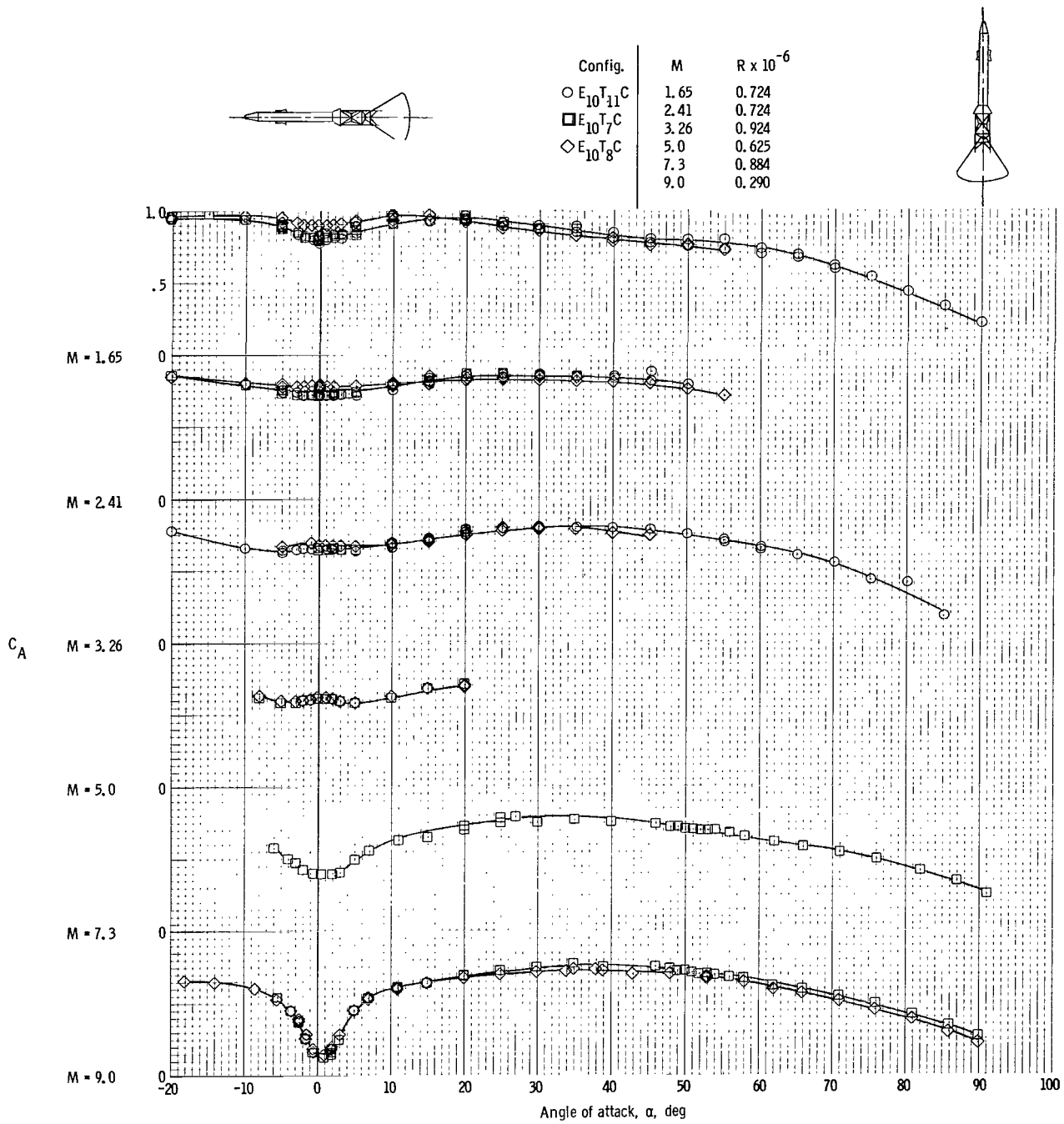

(c) Axial-force coefficient.

Figure 5. - Concluded.

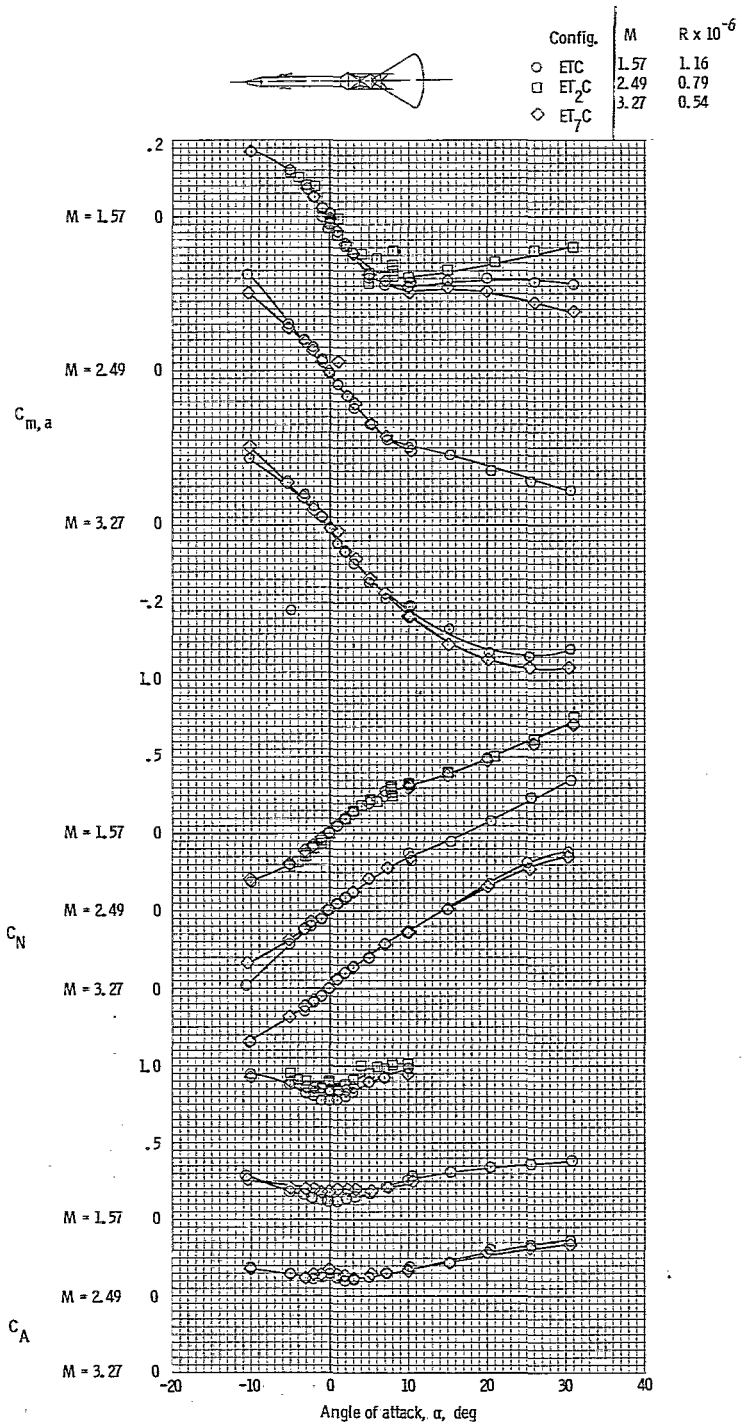

Figure 6. - Effect of tower-length variations on aerodynamic characteristics of Apollo LEV, M = 1.57, 2.49, and 3.27.

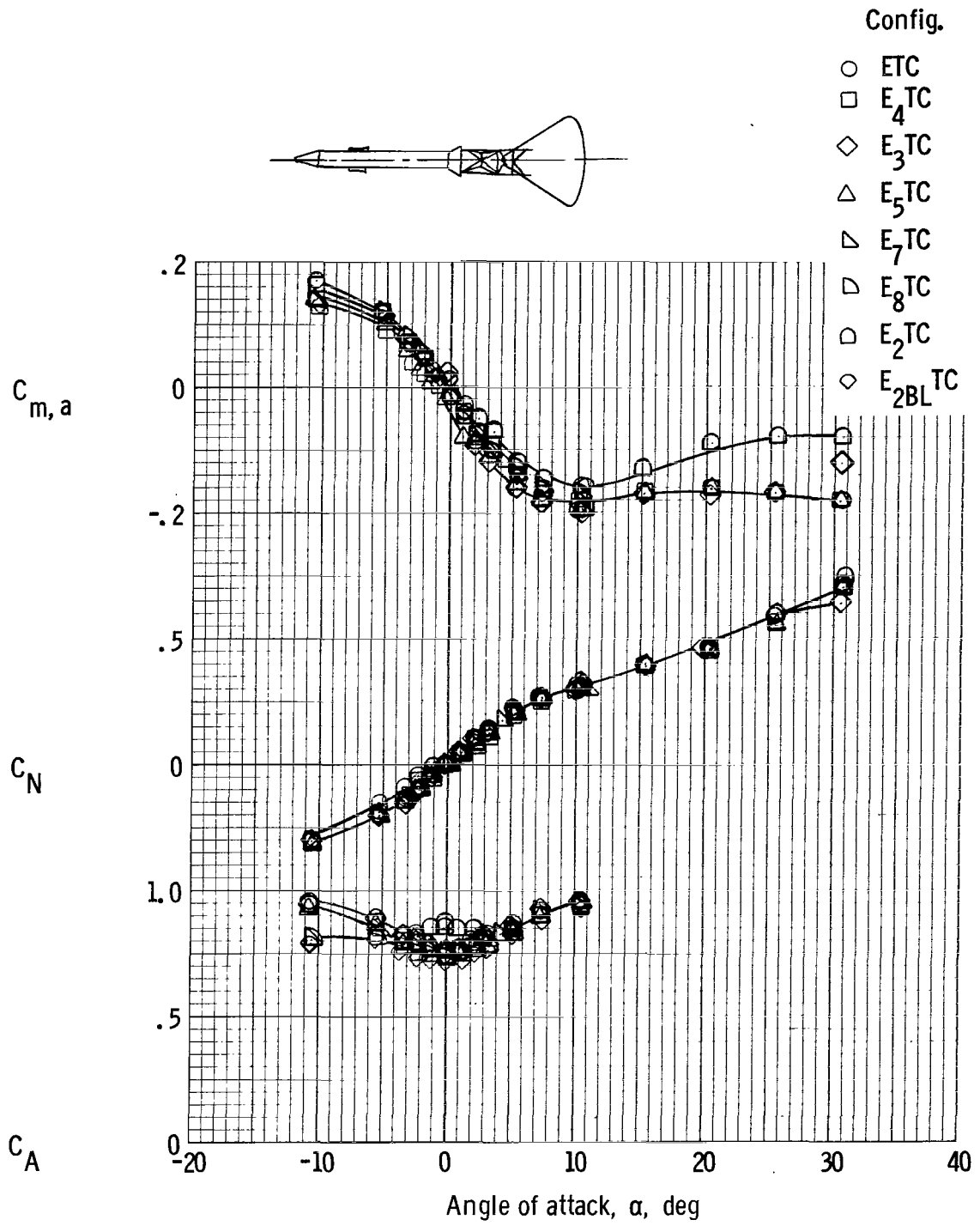

Figure 7. - Effect of variation in escape-rocket size and shape on aerodynamic characteristics of Apollo LEV, M = 1.57, escape-tower structure = T, command module = C, $R \times 10^{-6} = 1.16$.

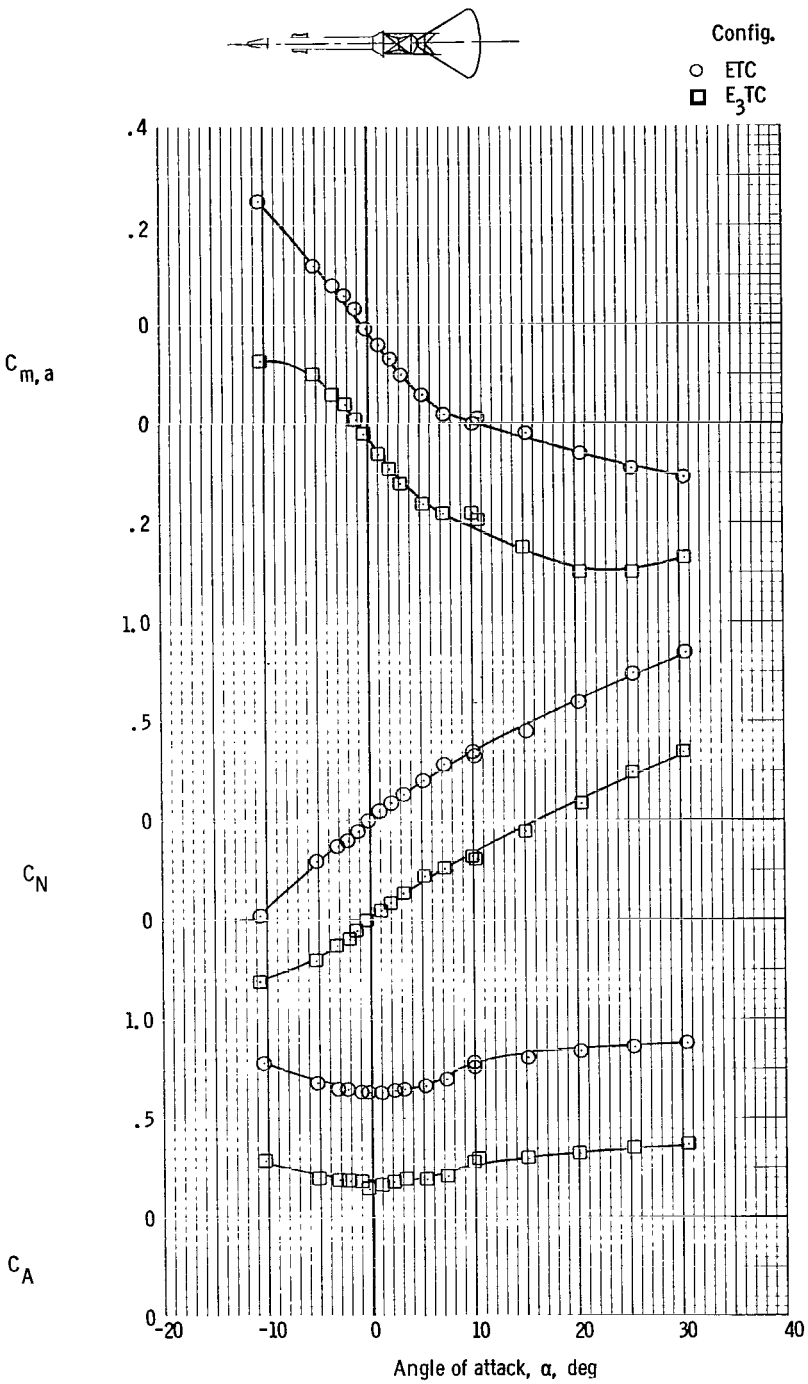

Figure 8. - Effect of variation in escape-rocket size and shape on aerodynamic characteristics of Apollo LEV, M = 2.49, escape-tower structure = T, command module = C, $R \times 10^{-6} = 0.79$.

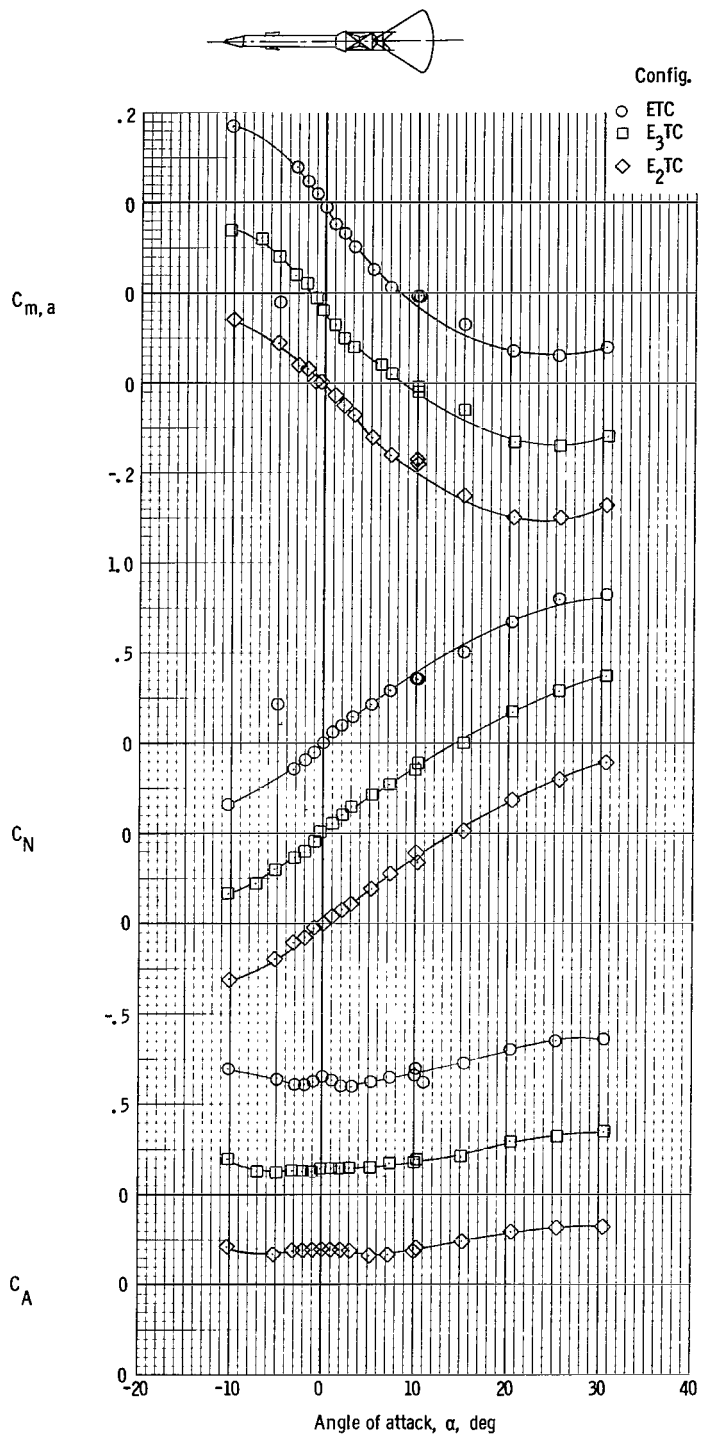

Figure 9. - Effect of variation in escape-rocket size and shape on aerodynamic characteristics of Apollo LEV, M = 3.27, escape-tower structure = T, command module = C, $R \times 10^{-6} = 0.54$.

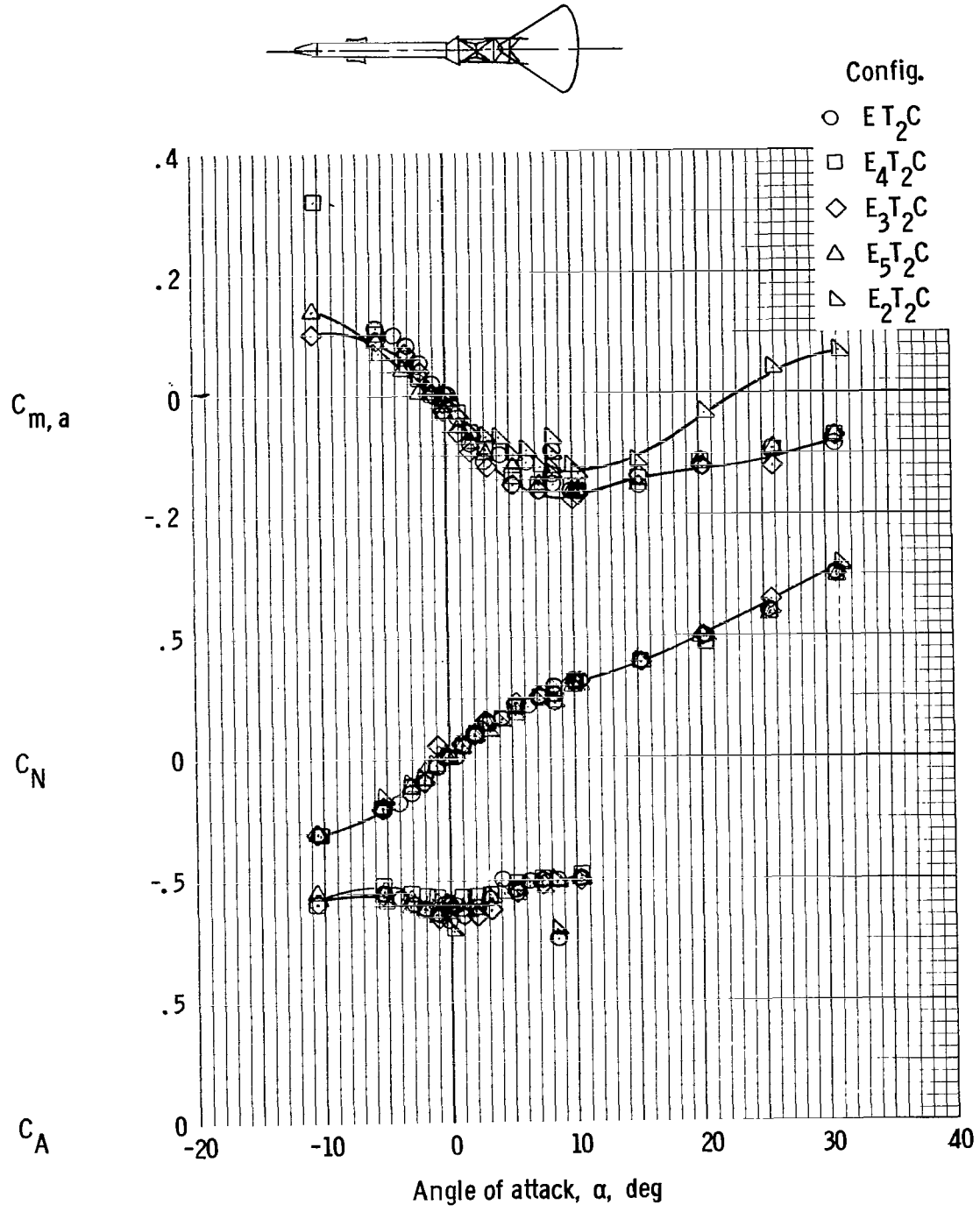

(a) Configurations ET_2C, E_4T_2C, E_3T_2C, E_5T_2C, and E_2T_2C.

Figure 10. - Effect of variation in escape-rocket size and shape on aerodynamic characteristics of Apollo LEV, M = 1.57, assorted escape-tower structures, command module = C, $R \times 10^{-6} = 1.16$.

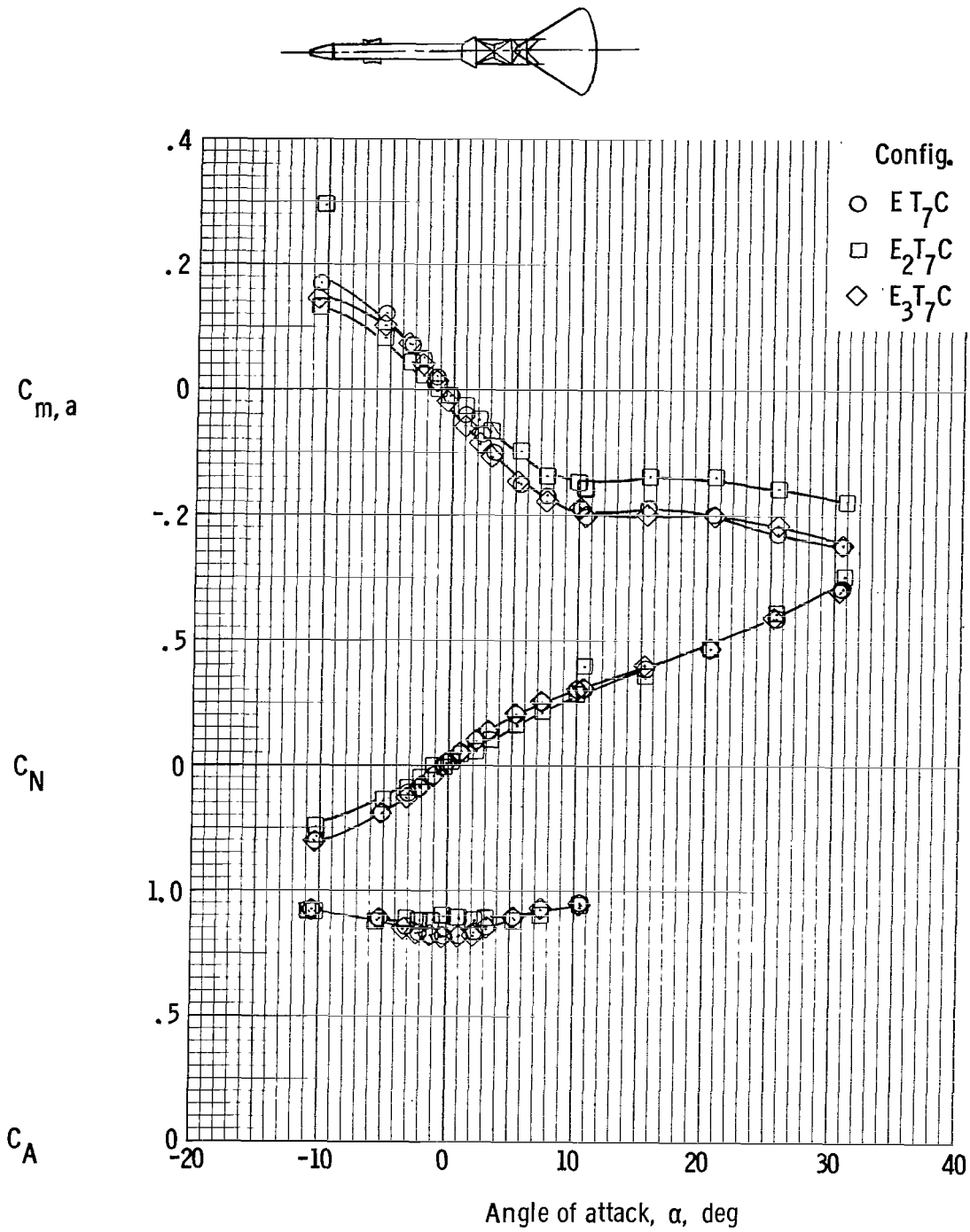

(b) Configurations ET_7C, E_2T_7C, and E_3T_7C.

Figure 10. - Continued.

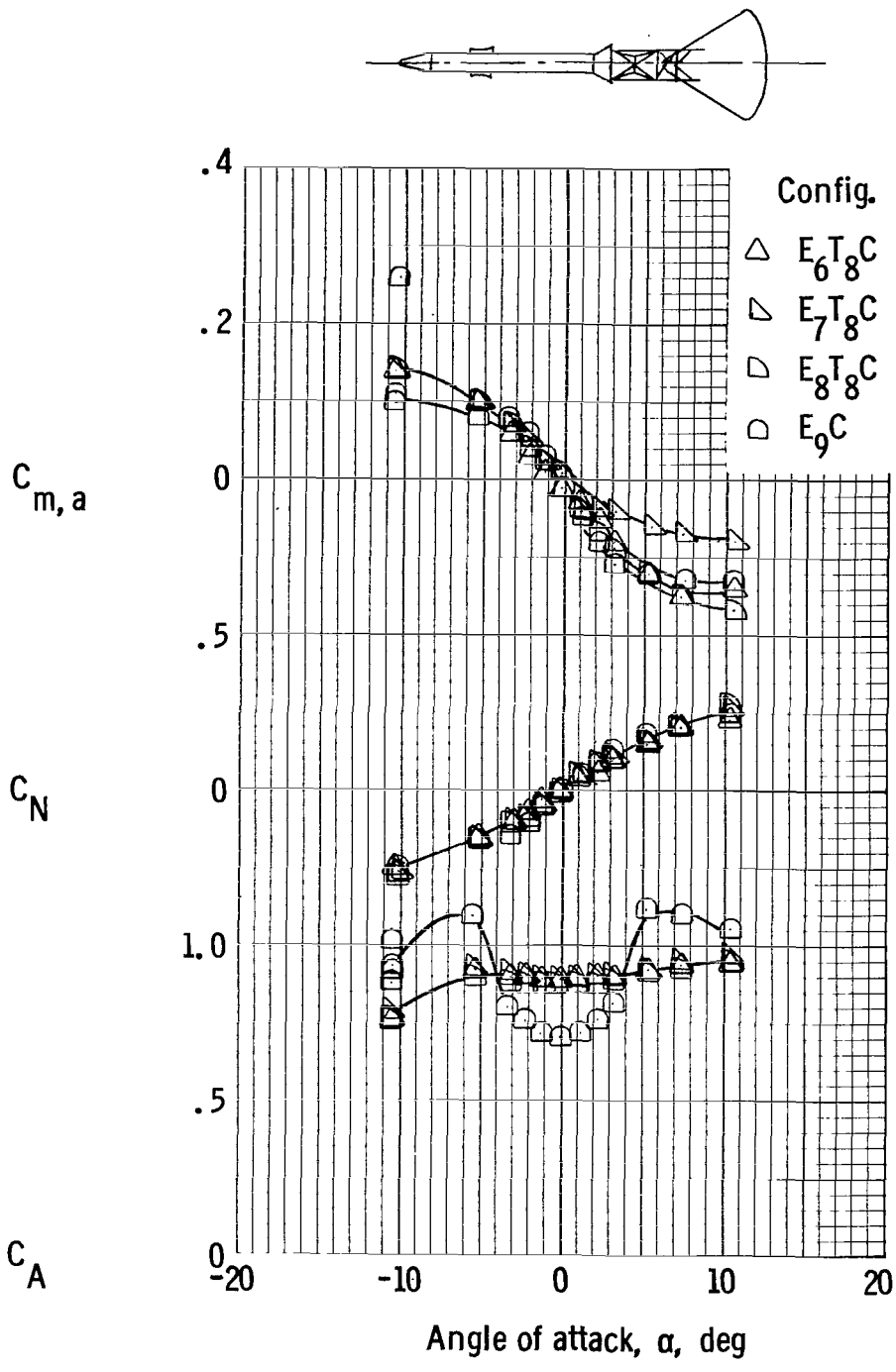

(c) Configurations E_6T_8C, E_7T_8C, E_8T_8C, and E_9C.

Figure 10. - Concluded.

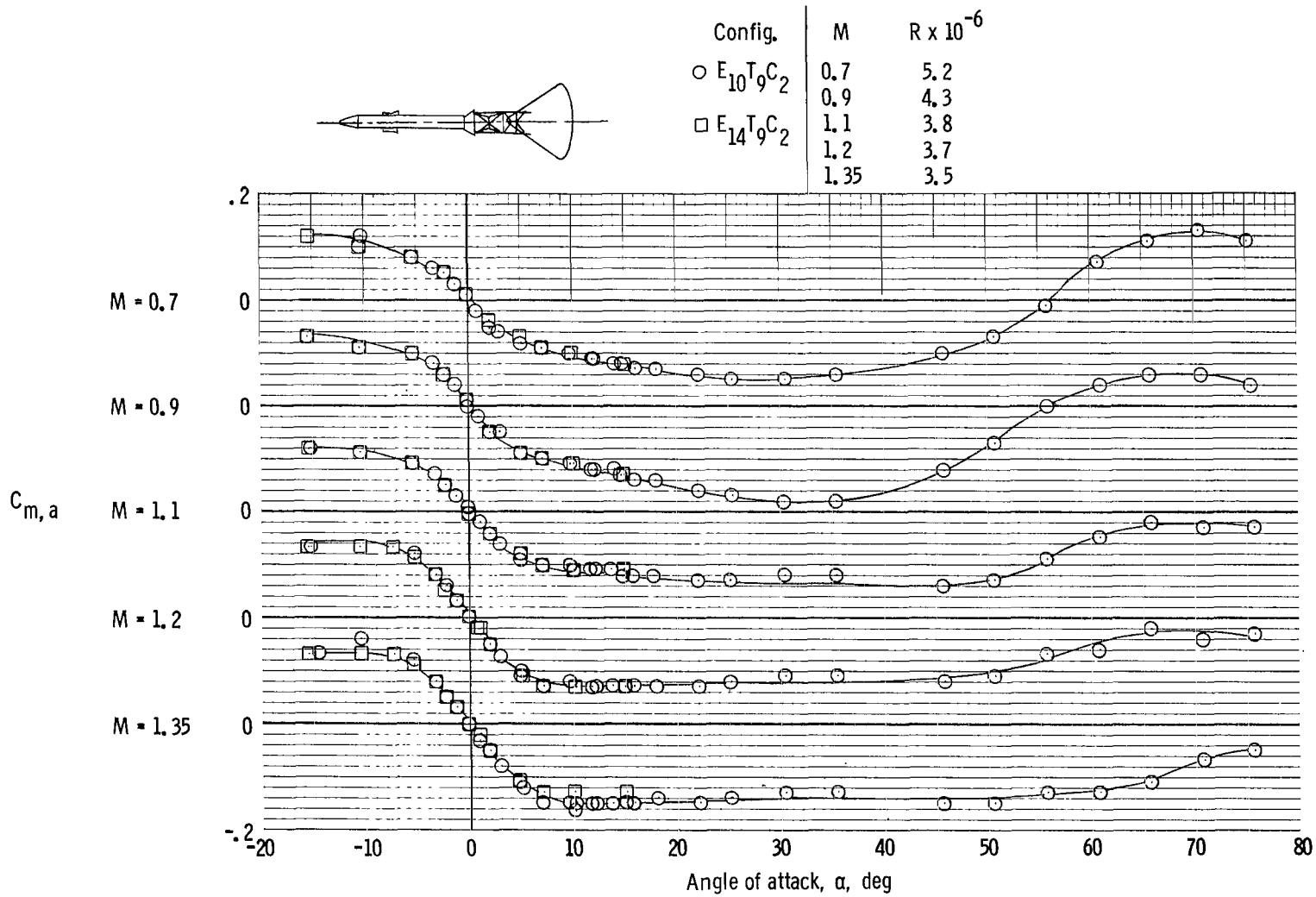

(a) Pitching-moment coefficient.

Figure 11. - Effects of escape-rocket nose-angle variations on aerodynamic characteristics of Apollo LEV, M = 0.7 to 1.35.

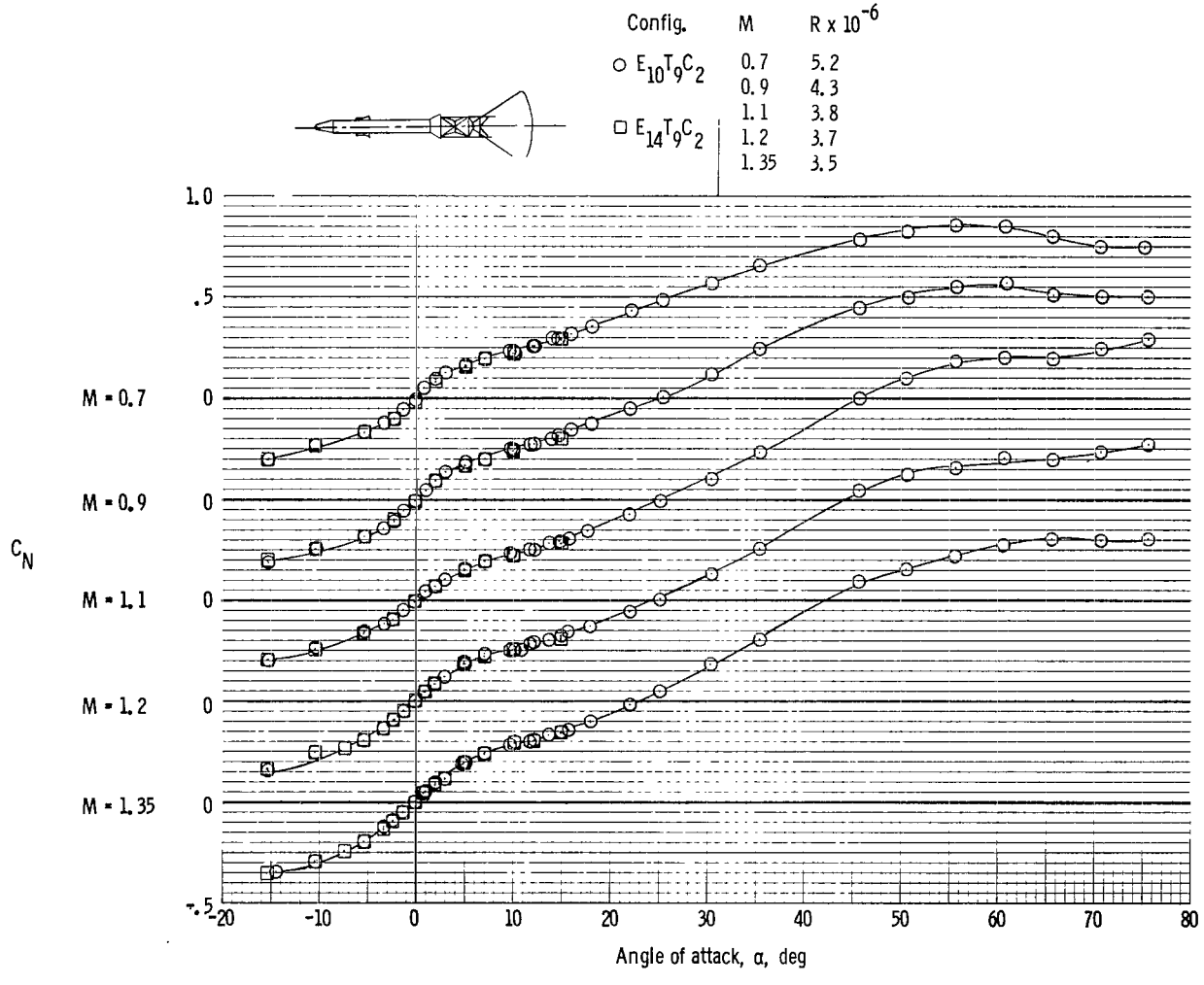

(b) Normal-force coefficient.

Figure 11. - Continued.

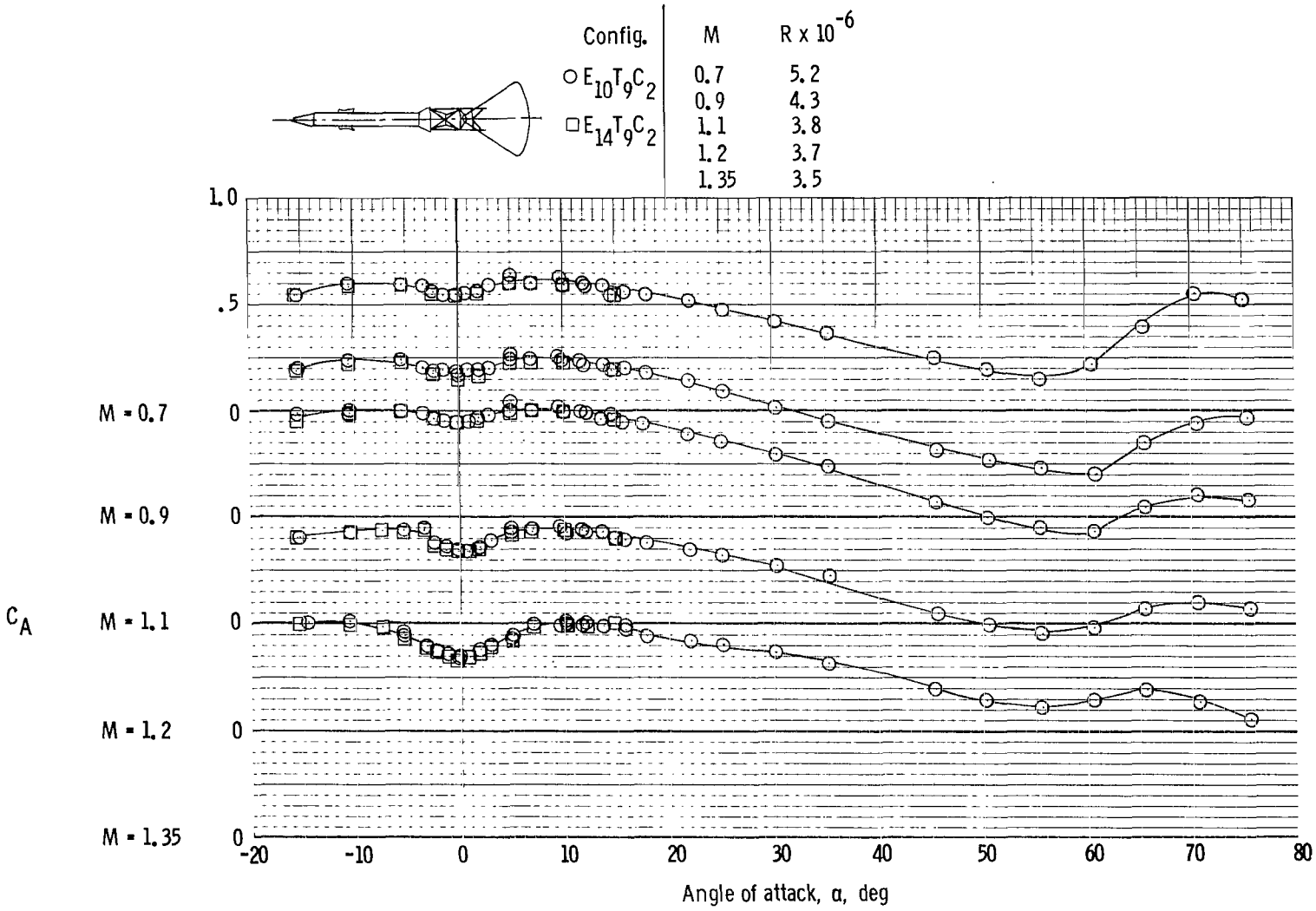

(c) Axial-force coefficient.

Figure 11. - Concluded.

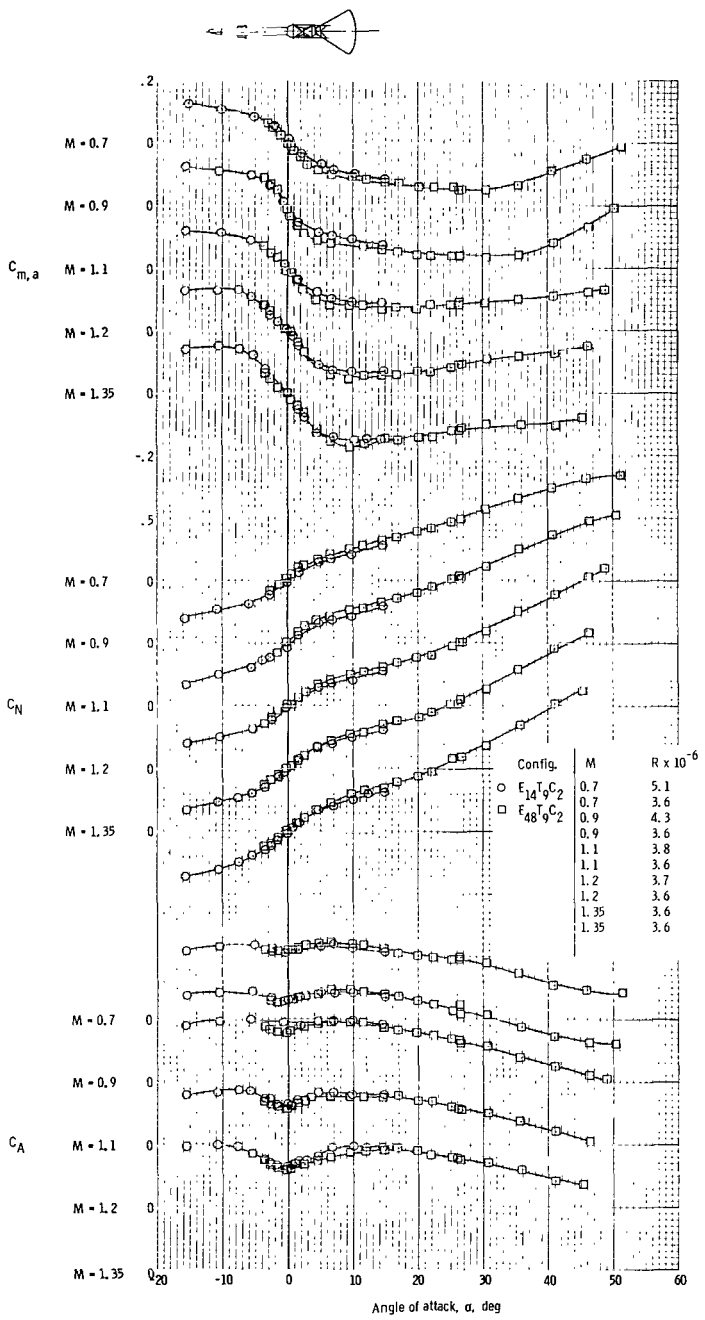

Figure 12. - Effect of variations in escape-rocket size and shape on aerodynamic characteristics of Apollo LEV, M = 0.7 to 1.35, escape-tower structure = T_9, command module = C_2.

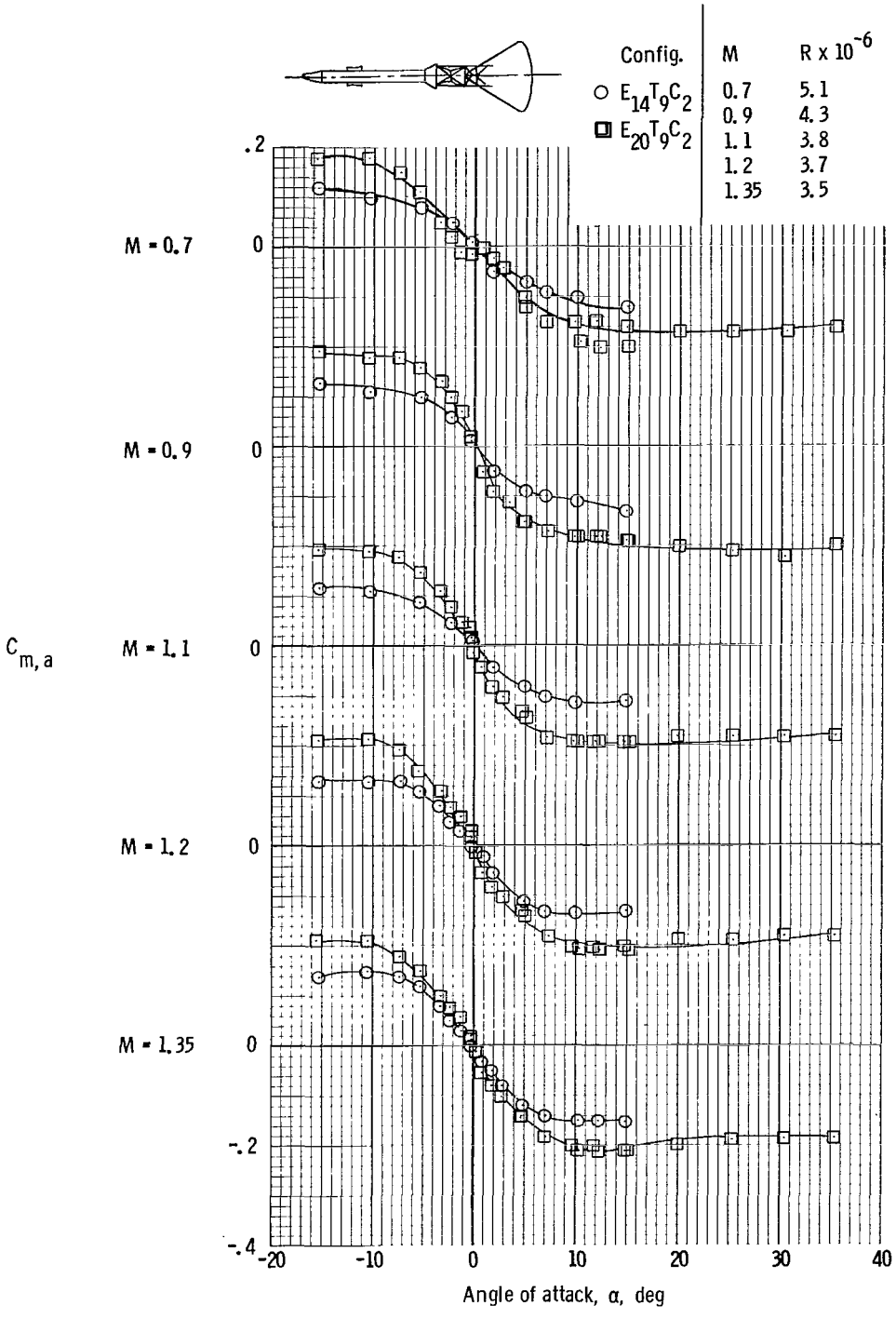

(a) Pitching-moment coefficient.

Figure 13. - Effects of adding disk ahead of escape-rocket skirt on aerodynamic characteristics of Apollo LEV, M = 0.7 to 1.35.

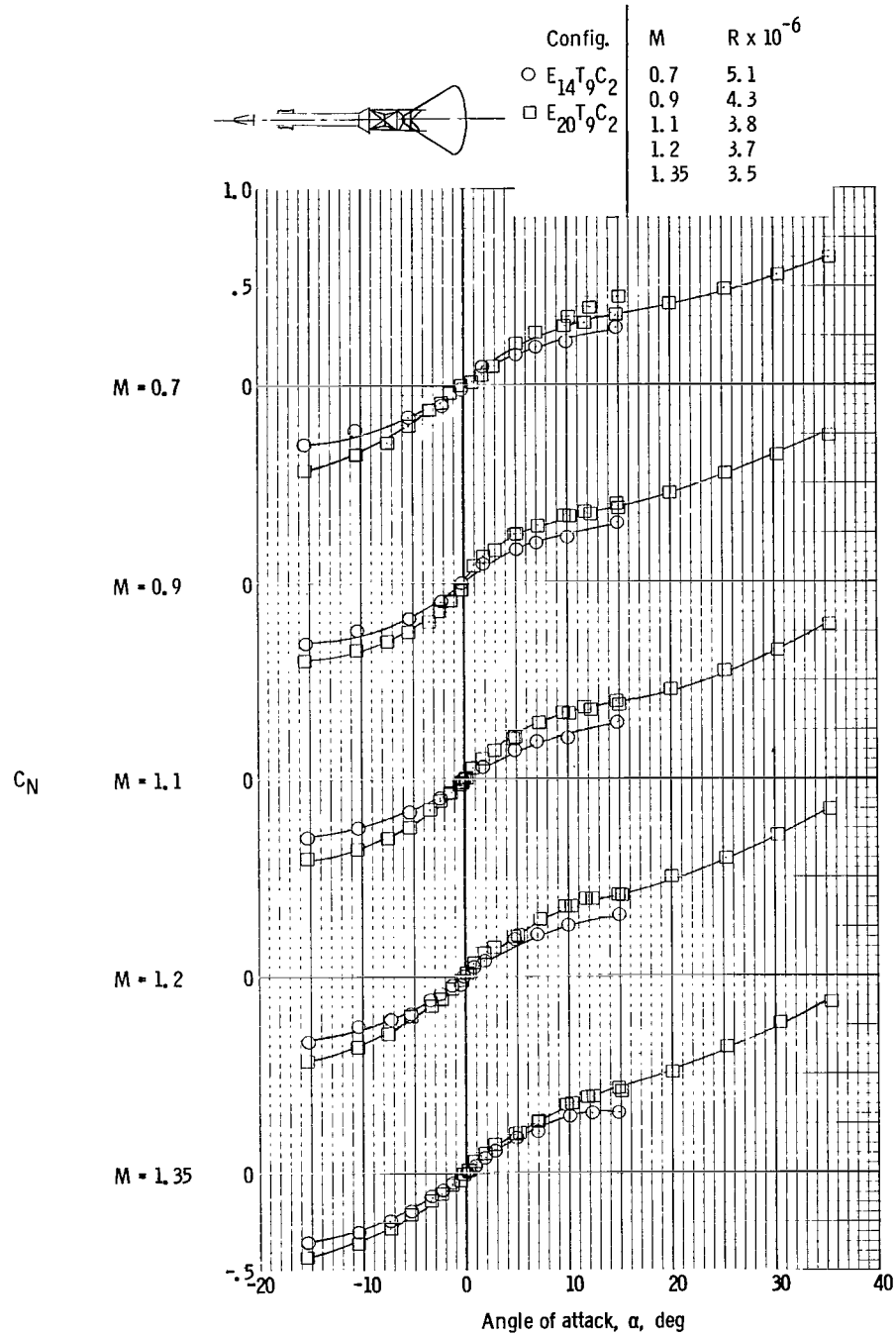

(b) Normal-force coefficient.

Figure 13. - Continued.

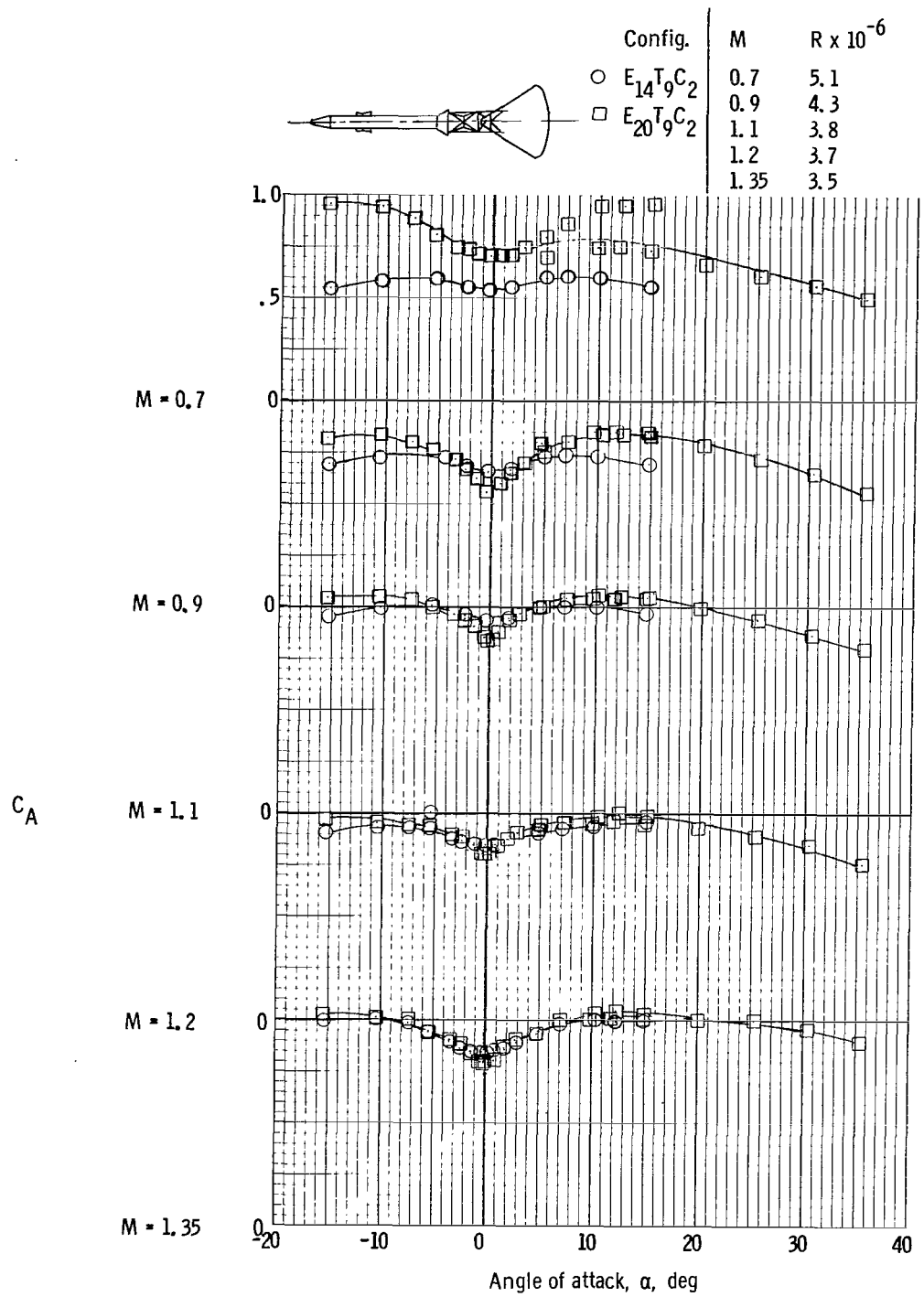

(c) Axial-force coefficient.

Figure 13. - Concluded.

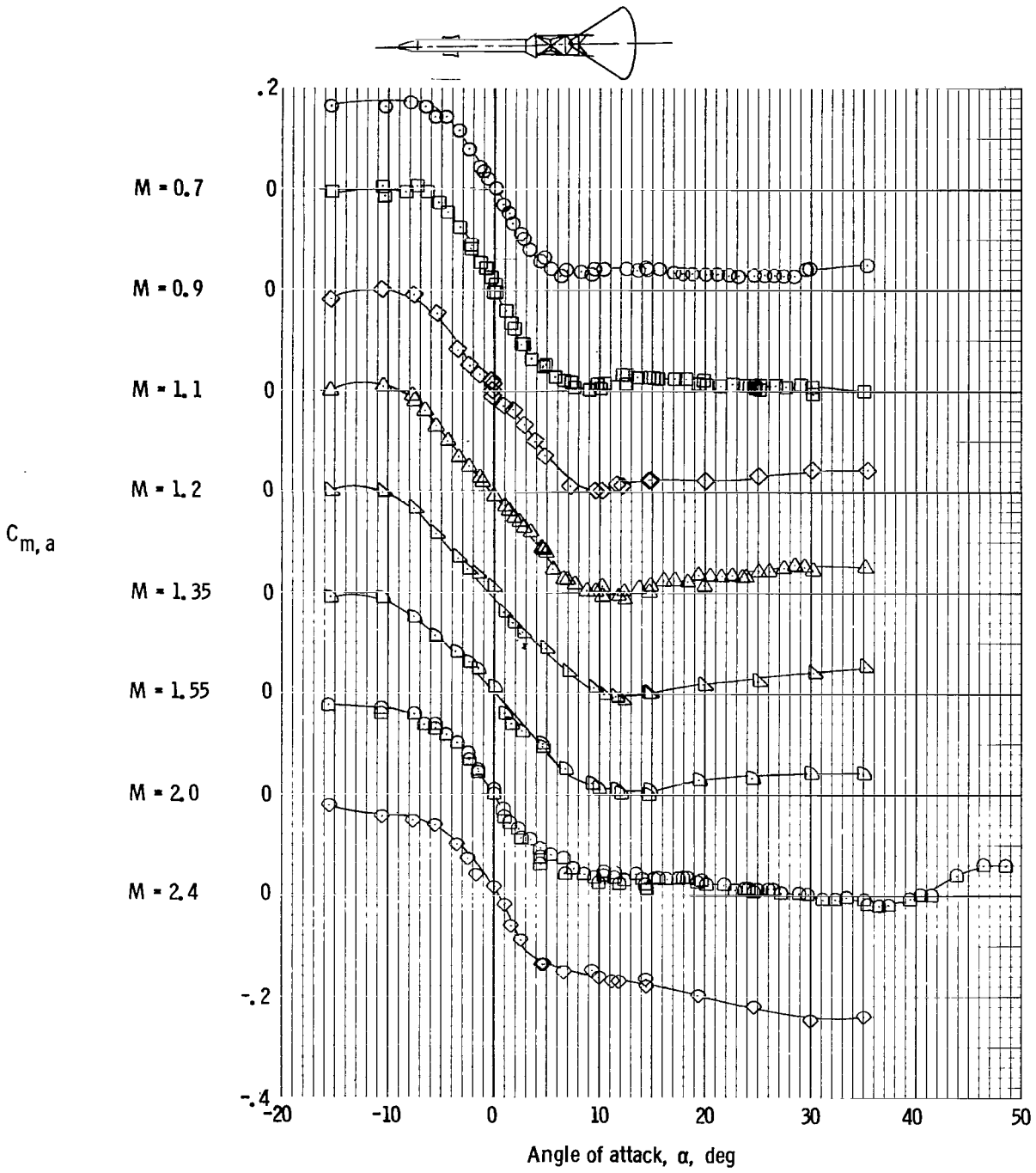

(a) Pitching-moment coefficient.

Figure 14. - Aerodynamic characteristics of Apollo LEV with disk at base of escape-rocket skirt, M = 0.7 to 2.4, escape rocket = E_{23}, escape-tower structure = T_9, command module = C_2.

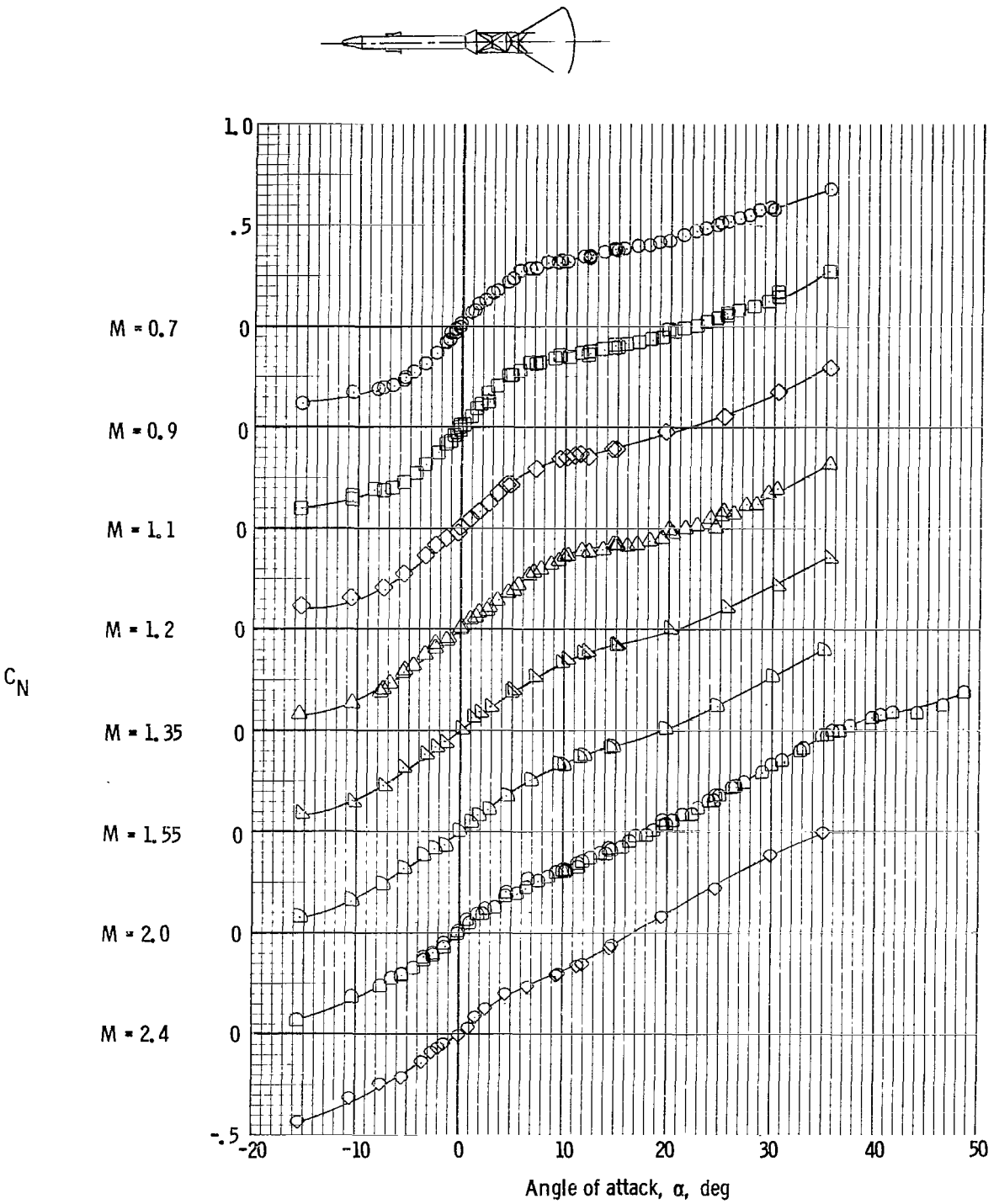

(b) Normal-force coefficient.

Figure 14. - Continued.

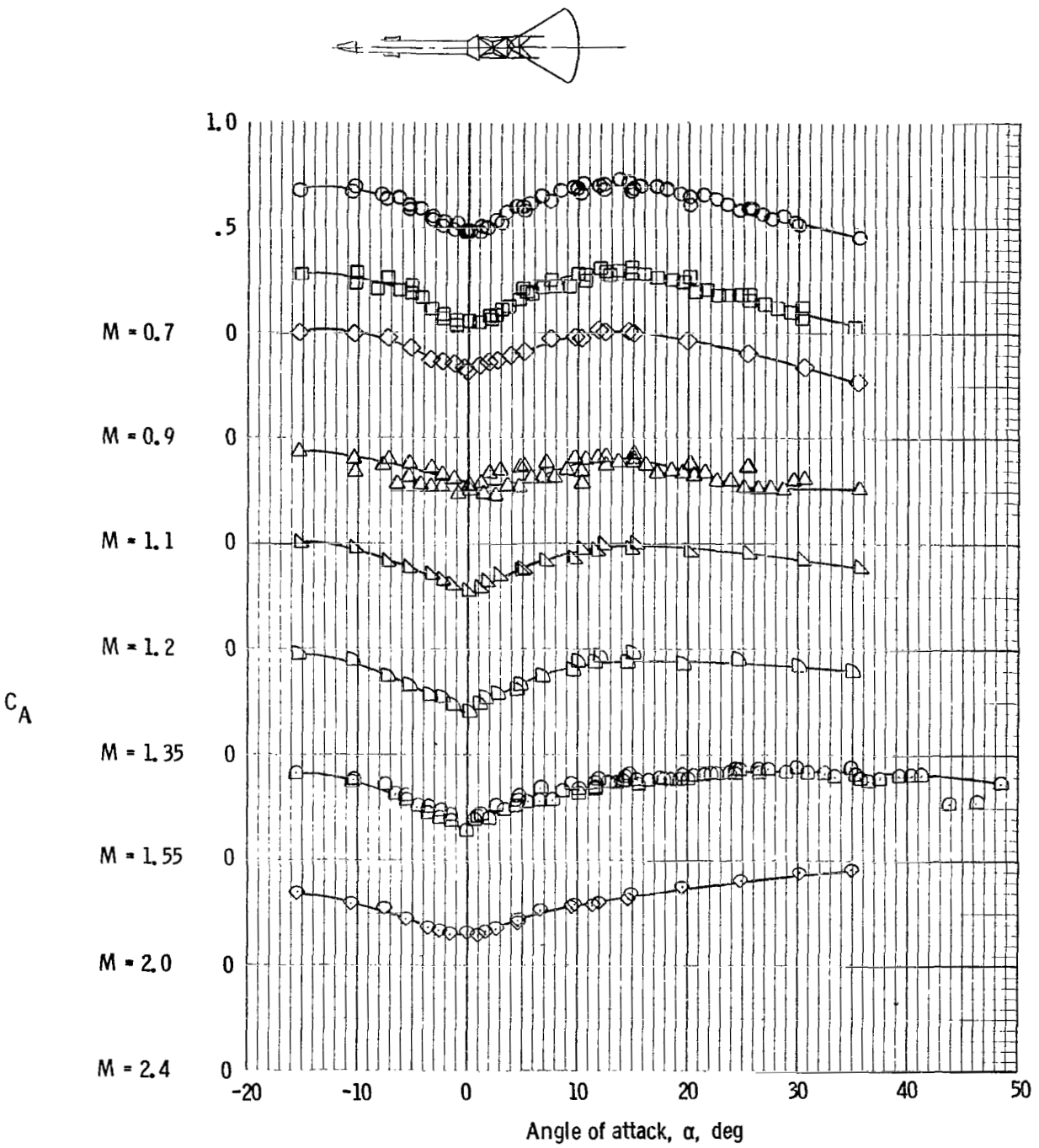

(c) Axial-force coefficient.

Figure 14. - Concluded.

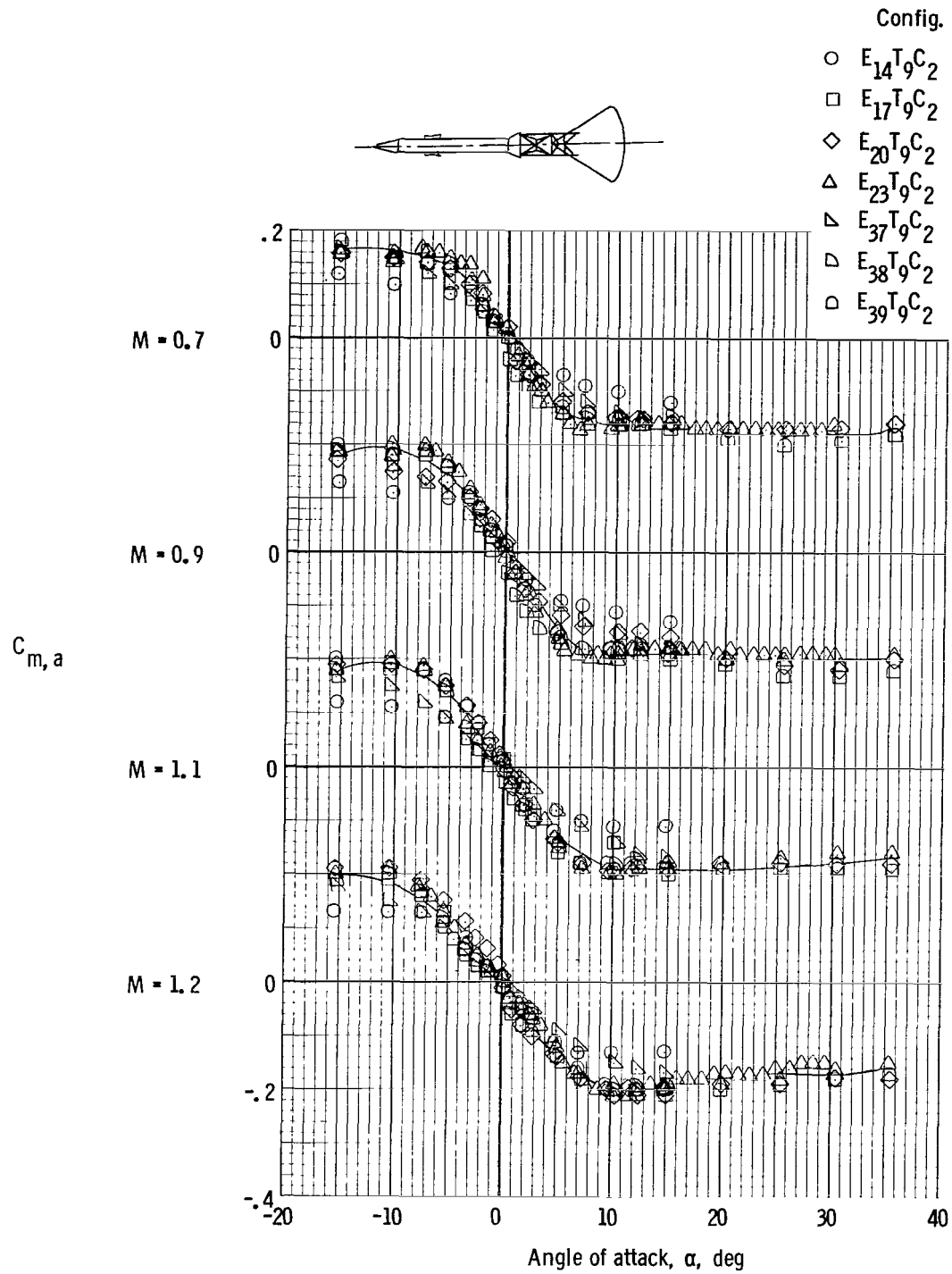

(a) Pitching-moment coefficient (M = 0.7 to 1.2).

Figure 15. - Effects of variations in size, placement, and shape of disk on aerodynamic characteristics of Apollo LEV, M = 0.7 to 2.4.

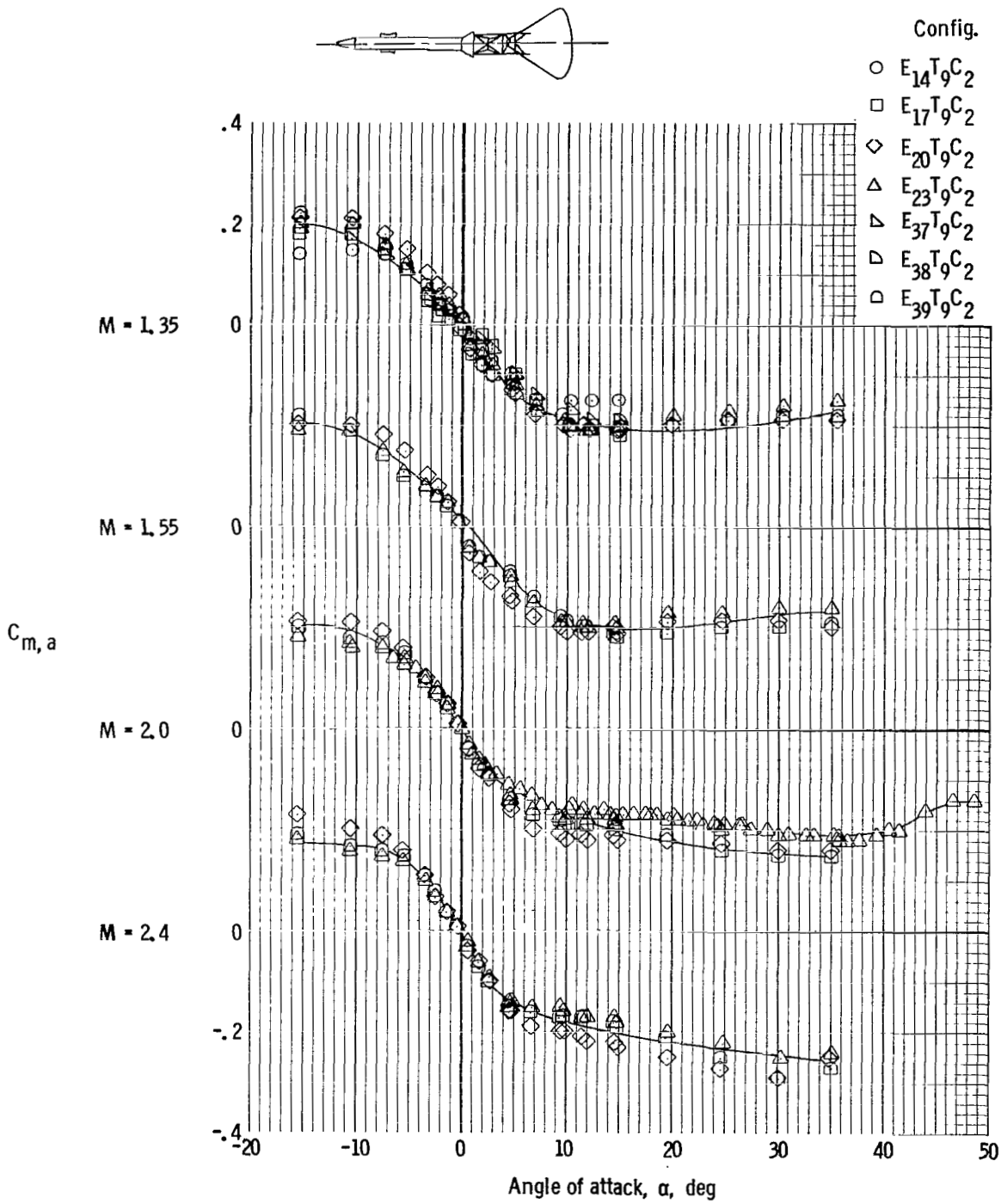

(b) Pitching-moment coefficient (M = 1.35 to 2.4).

Figure 15. - Continued.

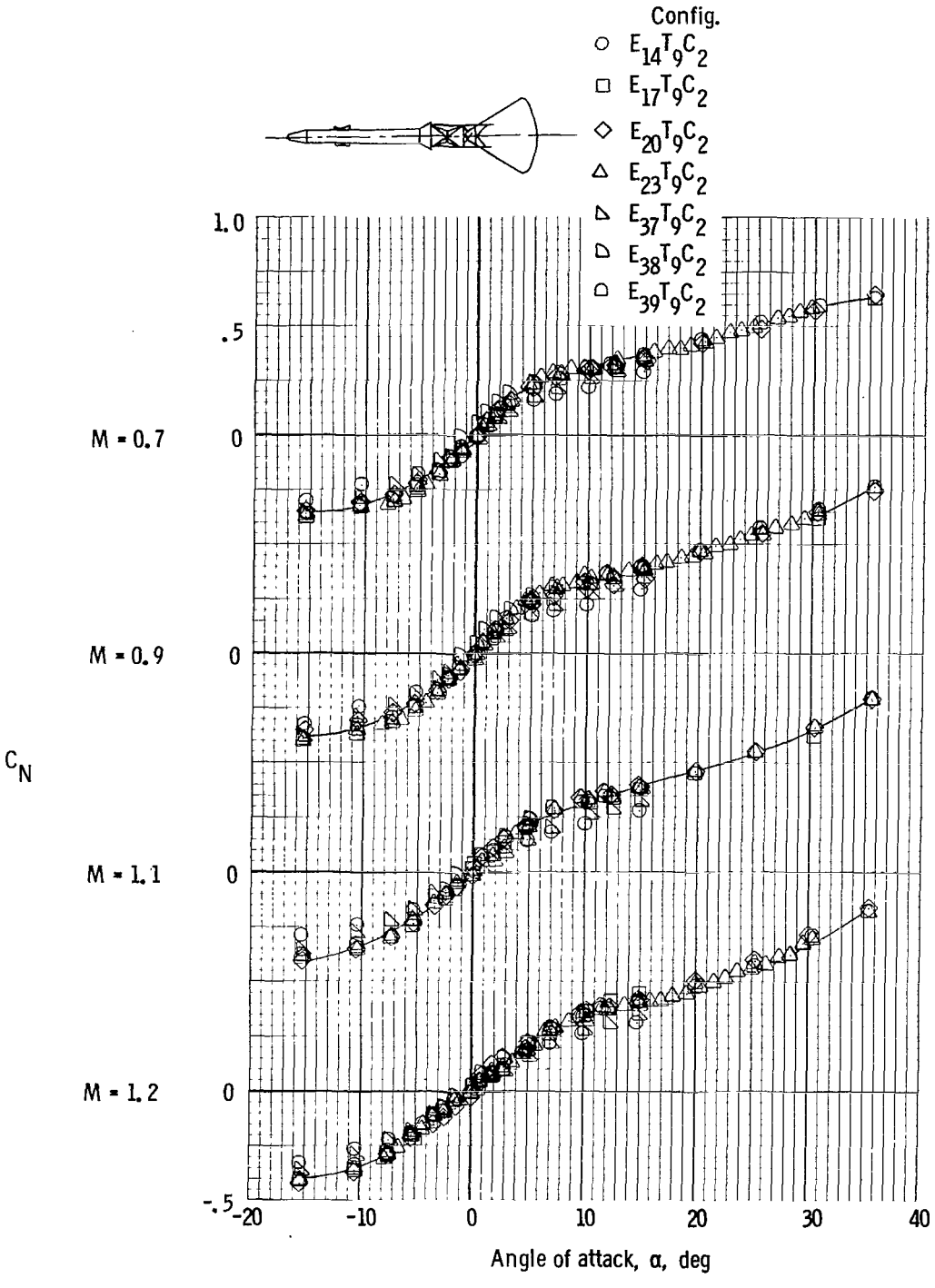

(c) Normal-force coefficient (M = 0.7 to 1.2).

Figure 15. - Continued.

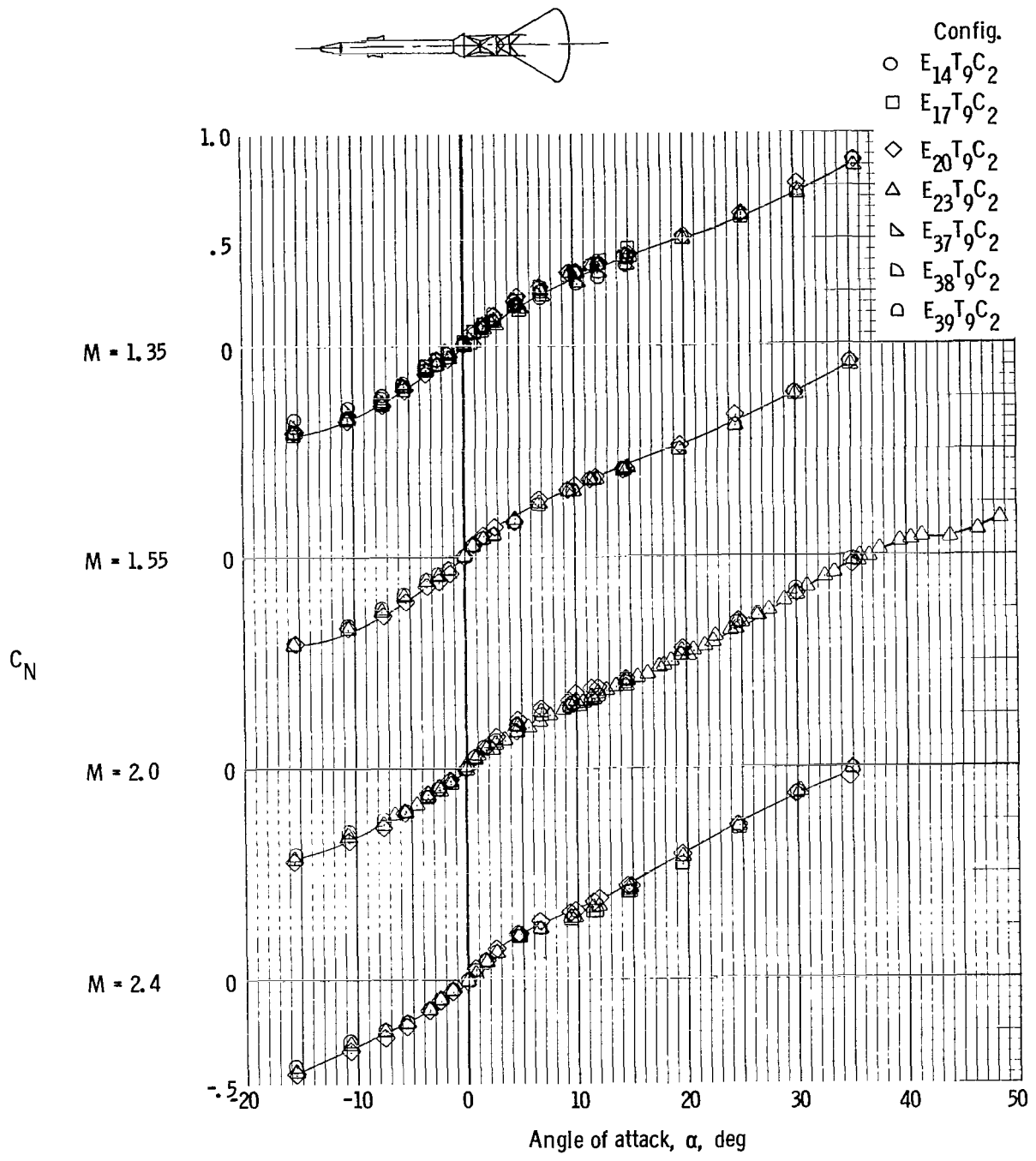

(d) Normal-force coefficient (M = 1.35 to 2.4).

Figure 15. - Continued.

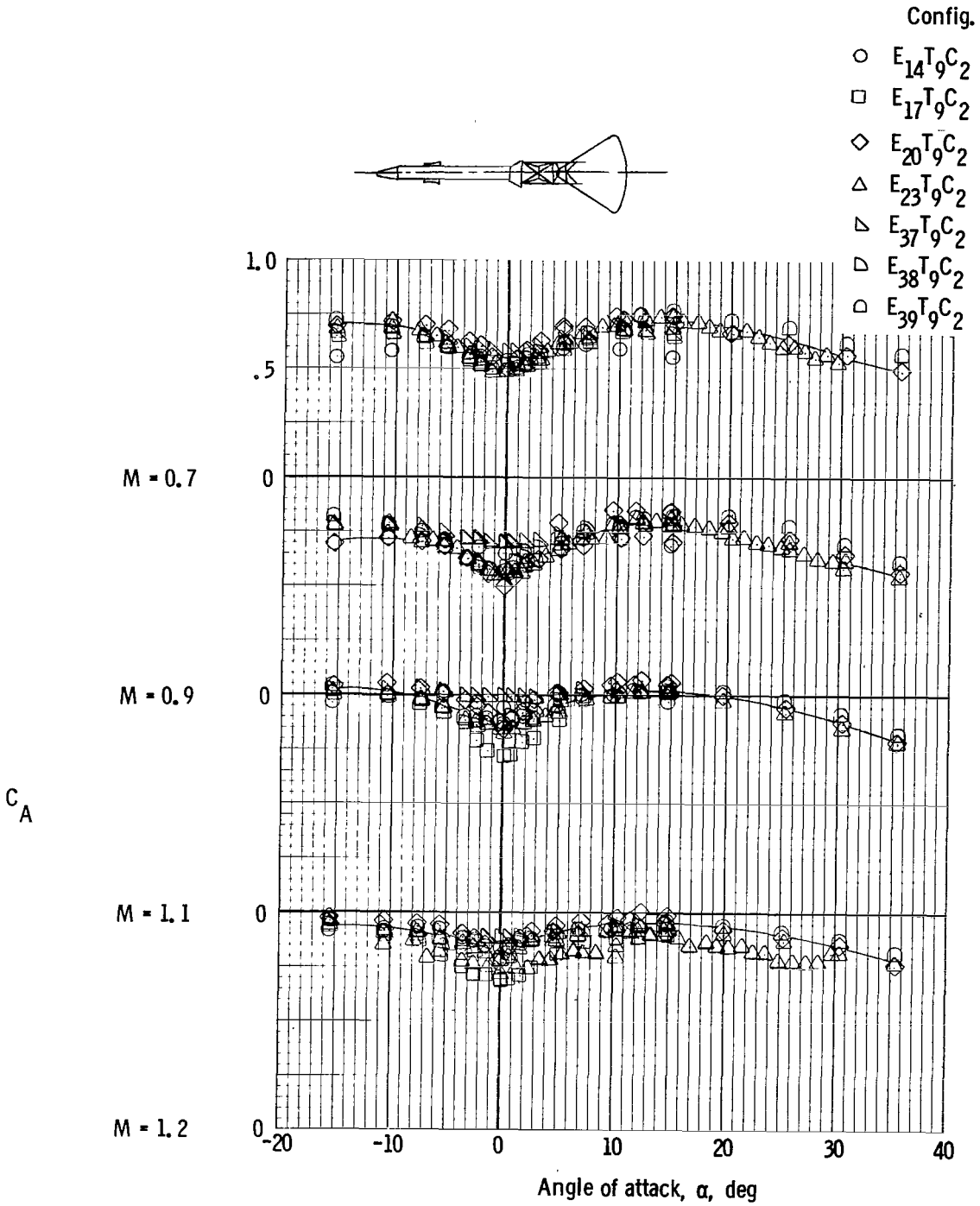

(e) Axial-force coefficient (M = 0.7 to 1.2).

Figure 15. - Continued.

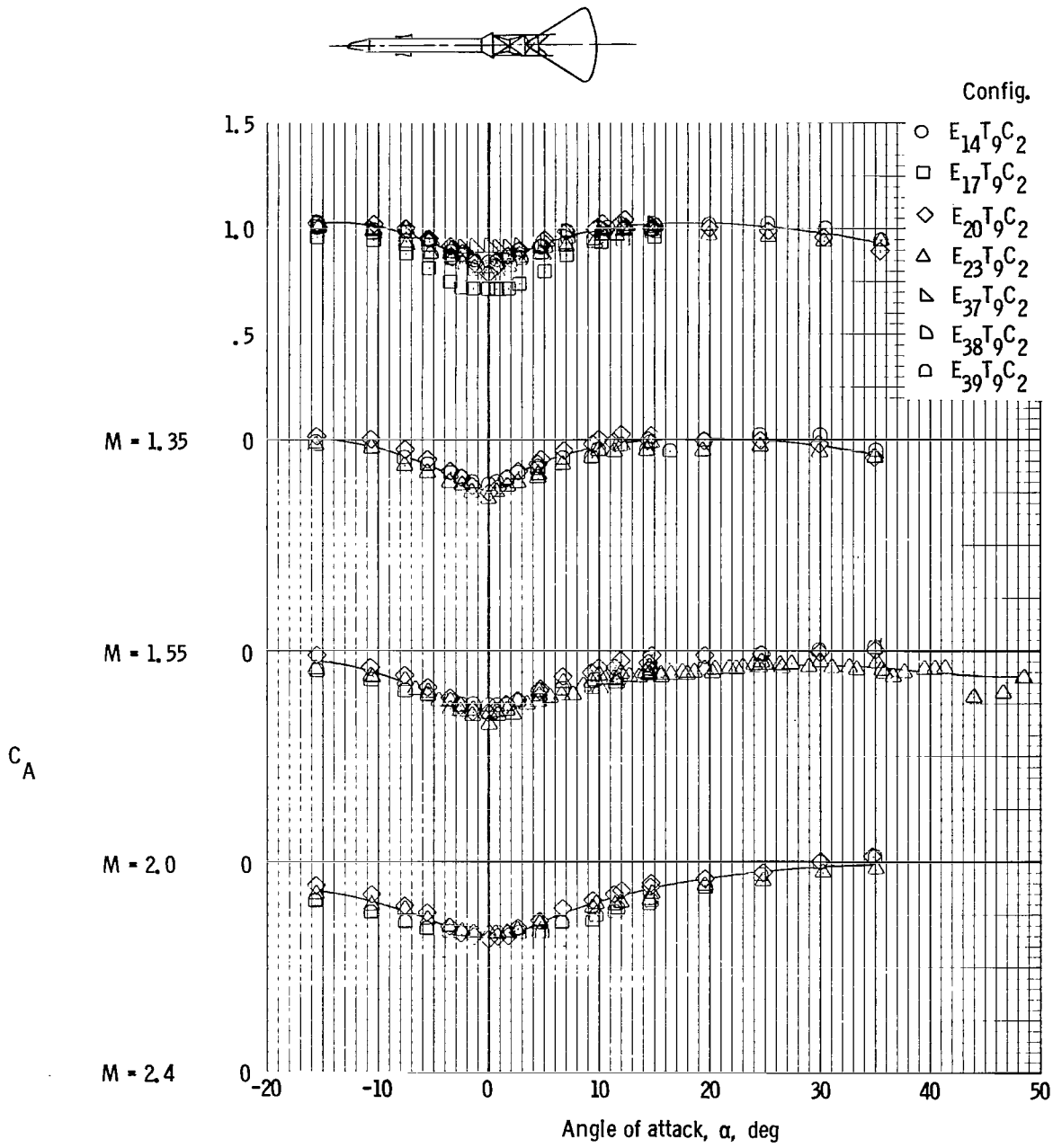

(f) Axial-force coefficient (M = 1.35 to 2.4).

Figure 15. - Concluded.

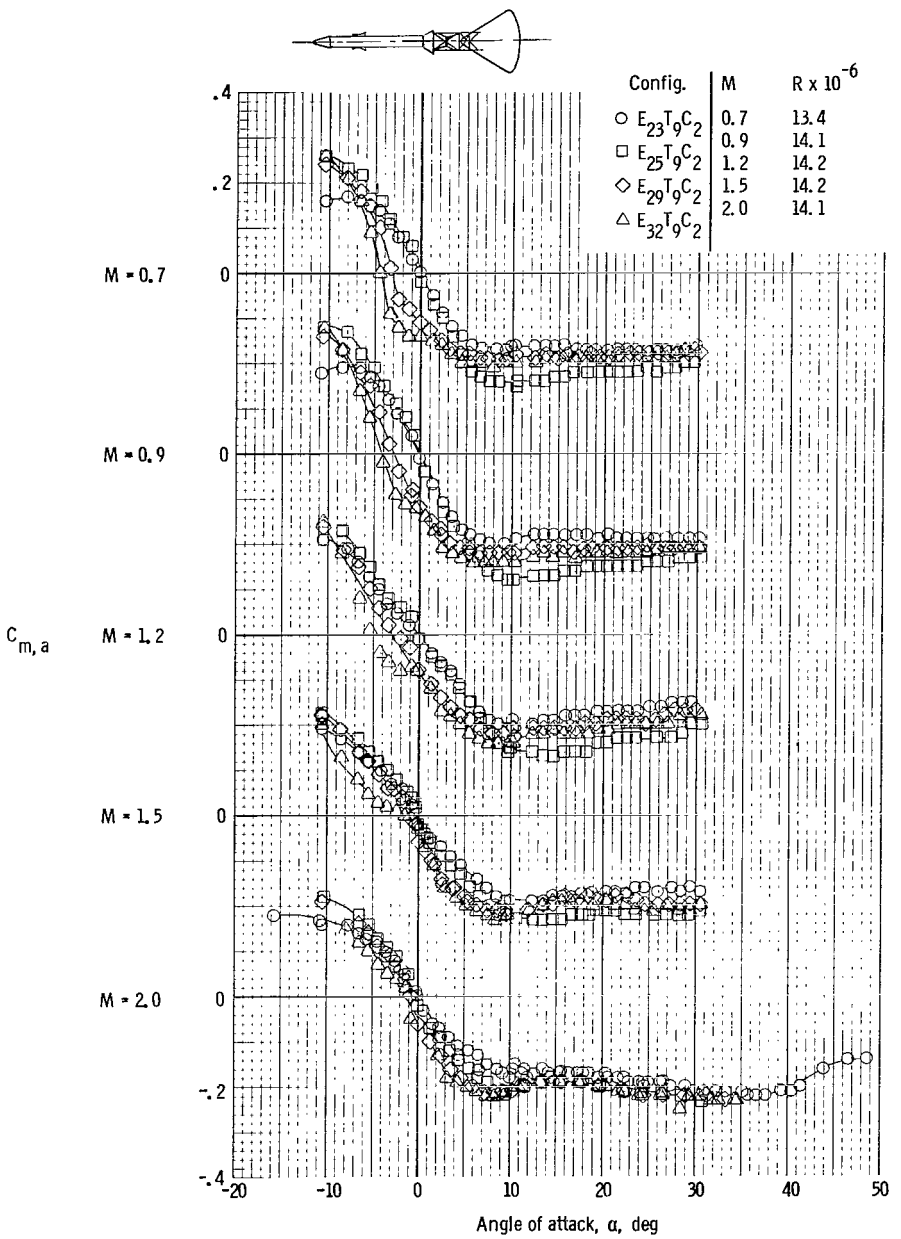

(a) Pitching-moment coefficient.

Figure 16. - Effects of variations in size and shape of disk located at base of escape-rocket skirt on aerodynamic characteristics of Apollo LEV, M = 0.7 to 2.0.

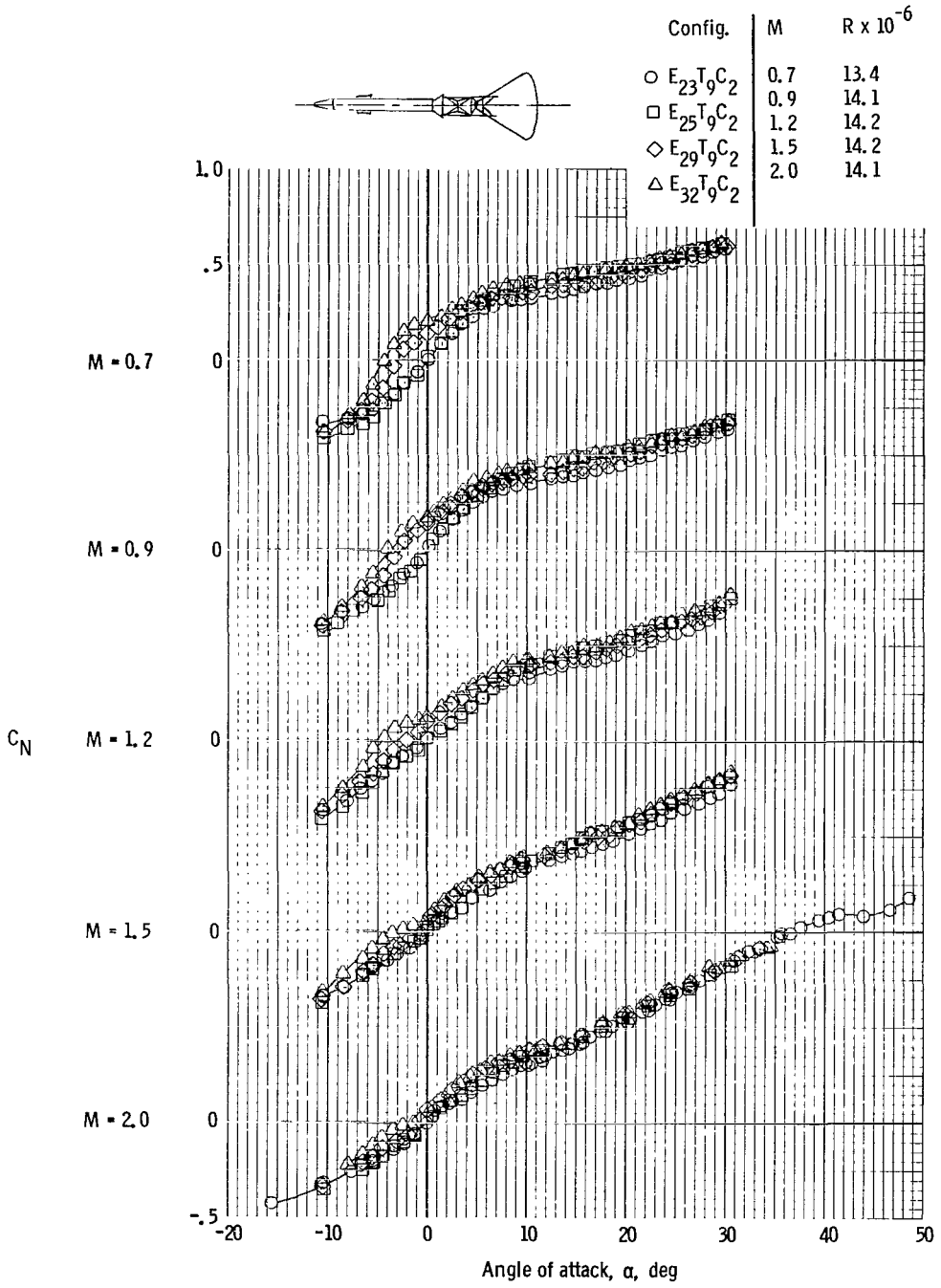

(b) Normal-force coefficient.

Figure 16. - Continued.

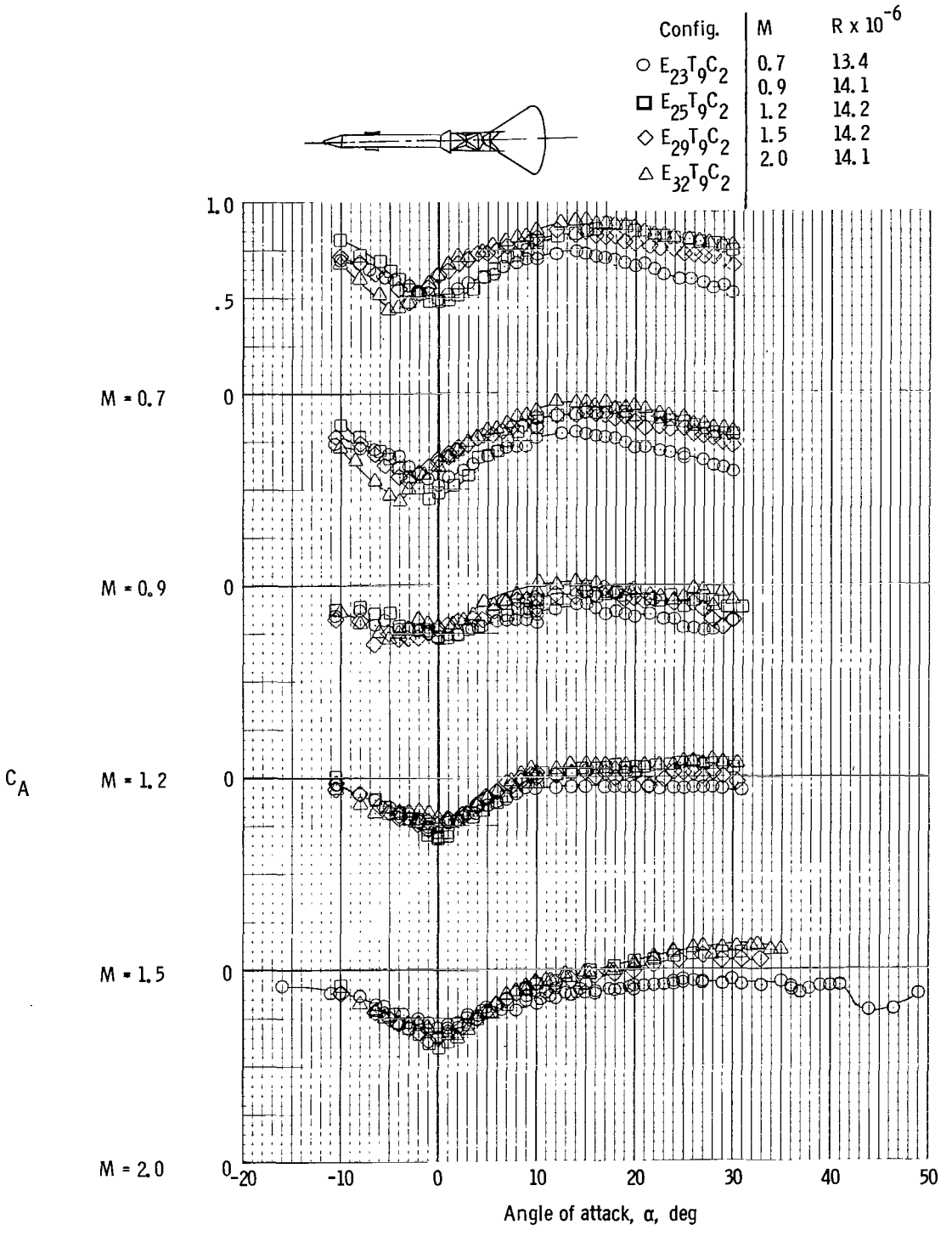

(c) Axial-force coefficient.

Figure 16. - Concluded.

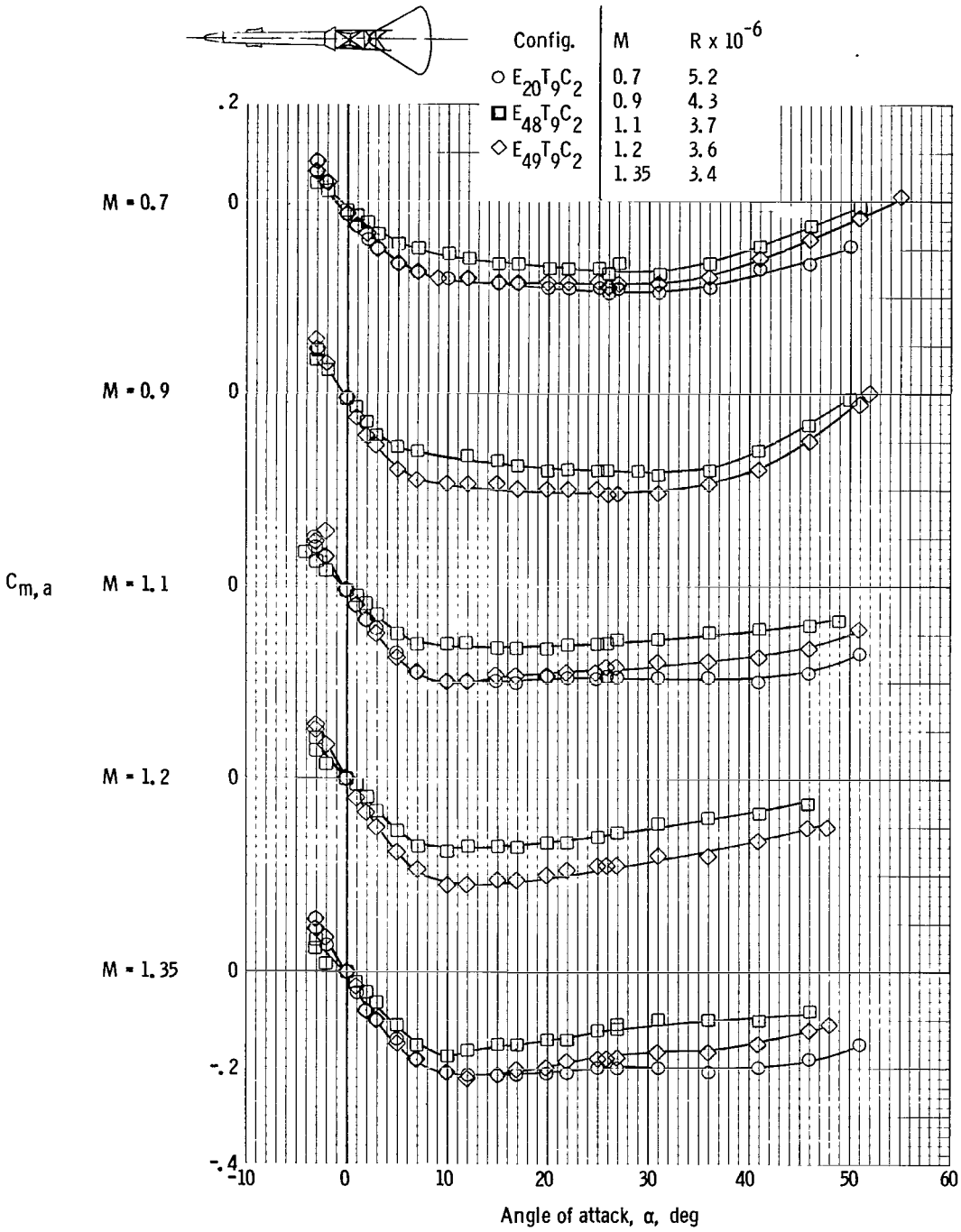

(a) Pitching-moment coefficient (M = 0. 7 to 1. 35).

Figure 17. - Aerodynamic characteristics of Apollo LEV with and without flow separator.

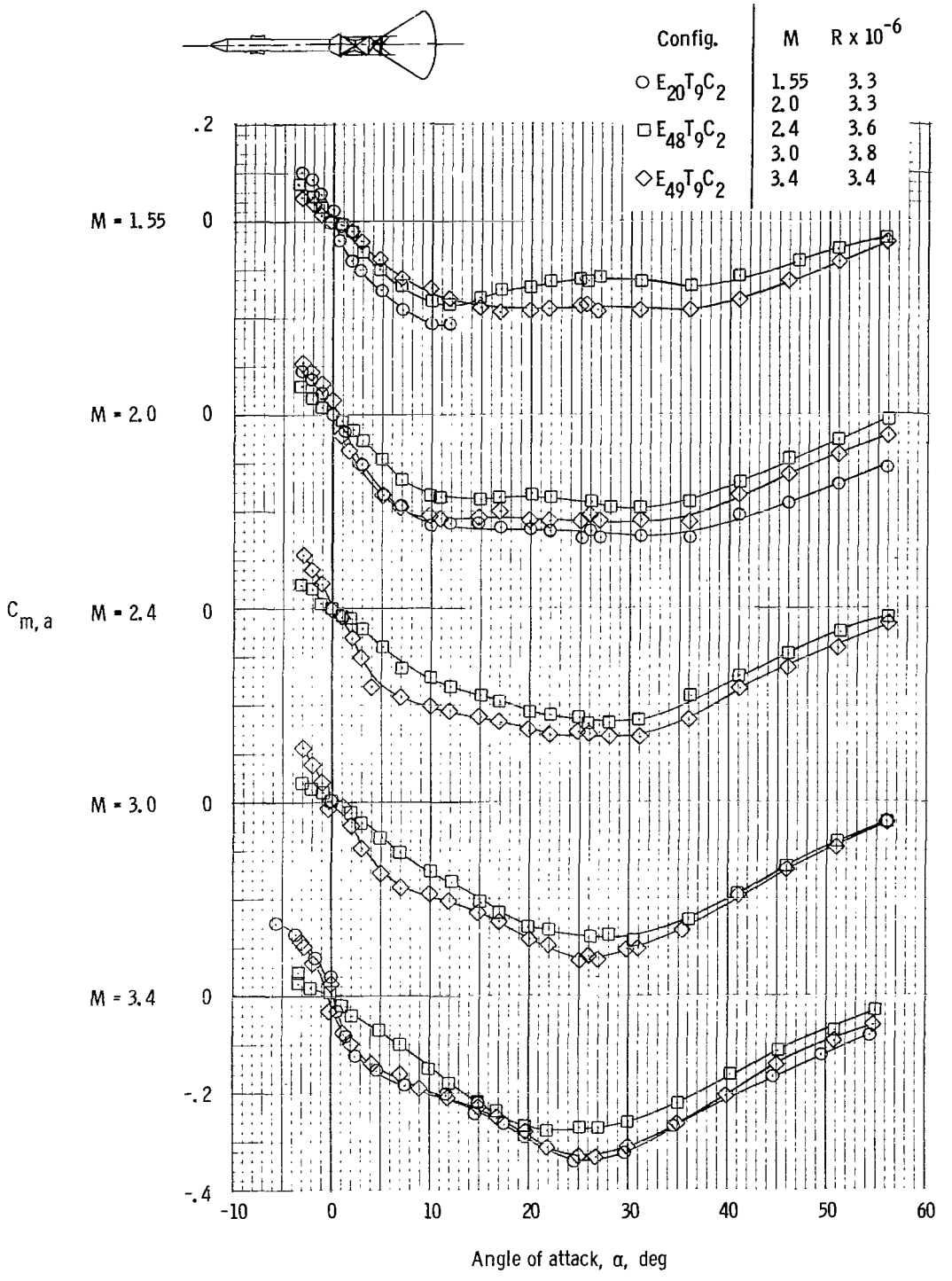

(b) Pitching-moment coefficient (M = 1.55 to 3.4).

Figure 17. - Continued.

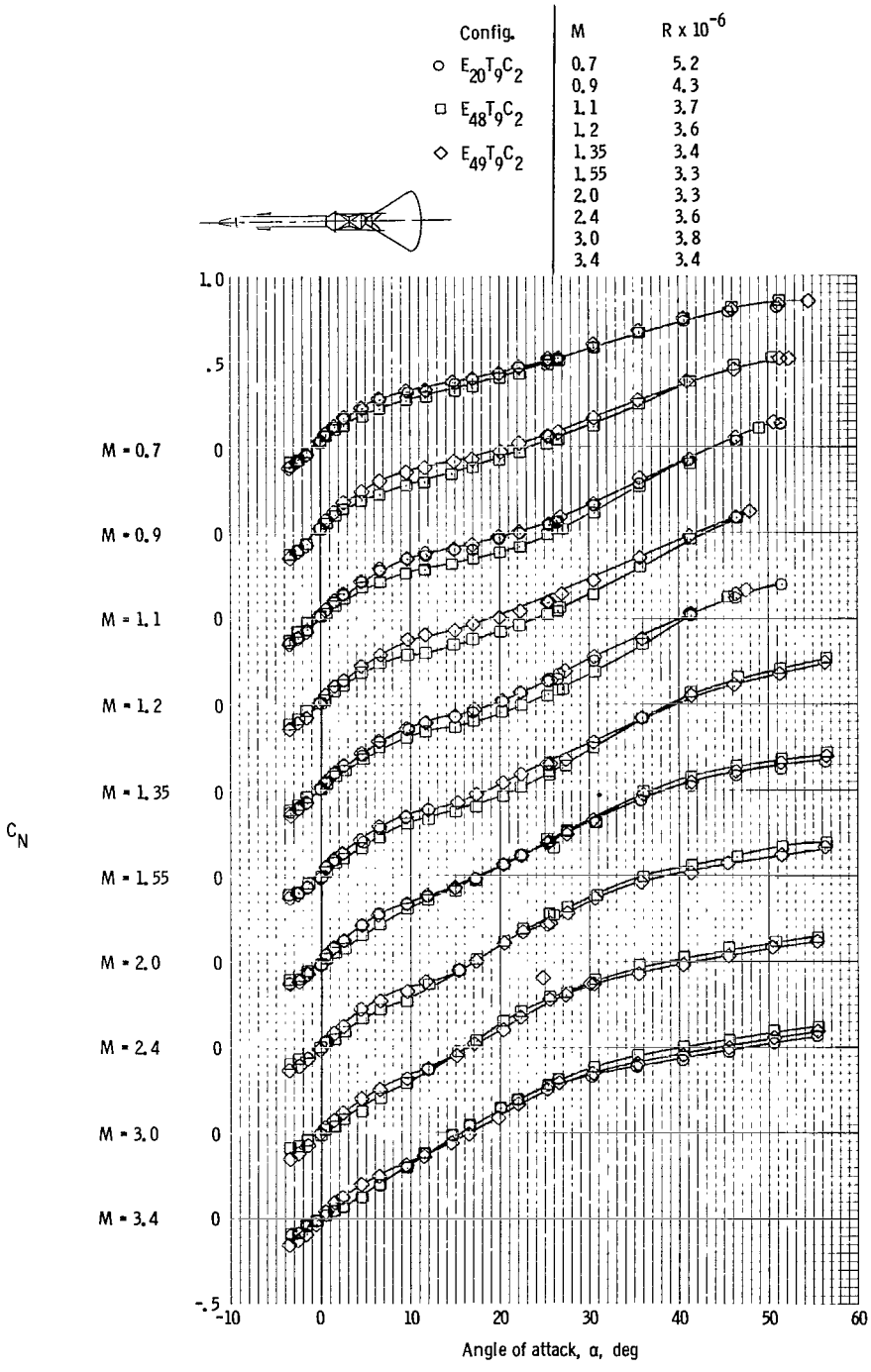

(c) Normal-force coefficient (M = 0.7 to 3.4).

Figure 17. - Continued.

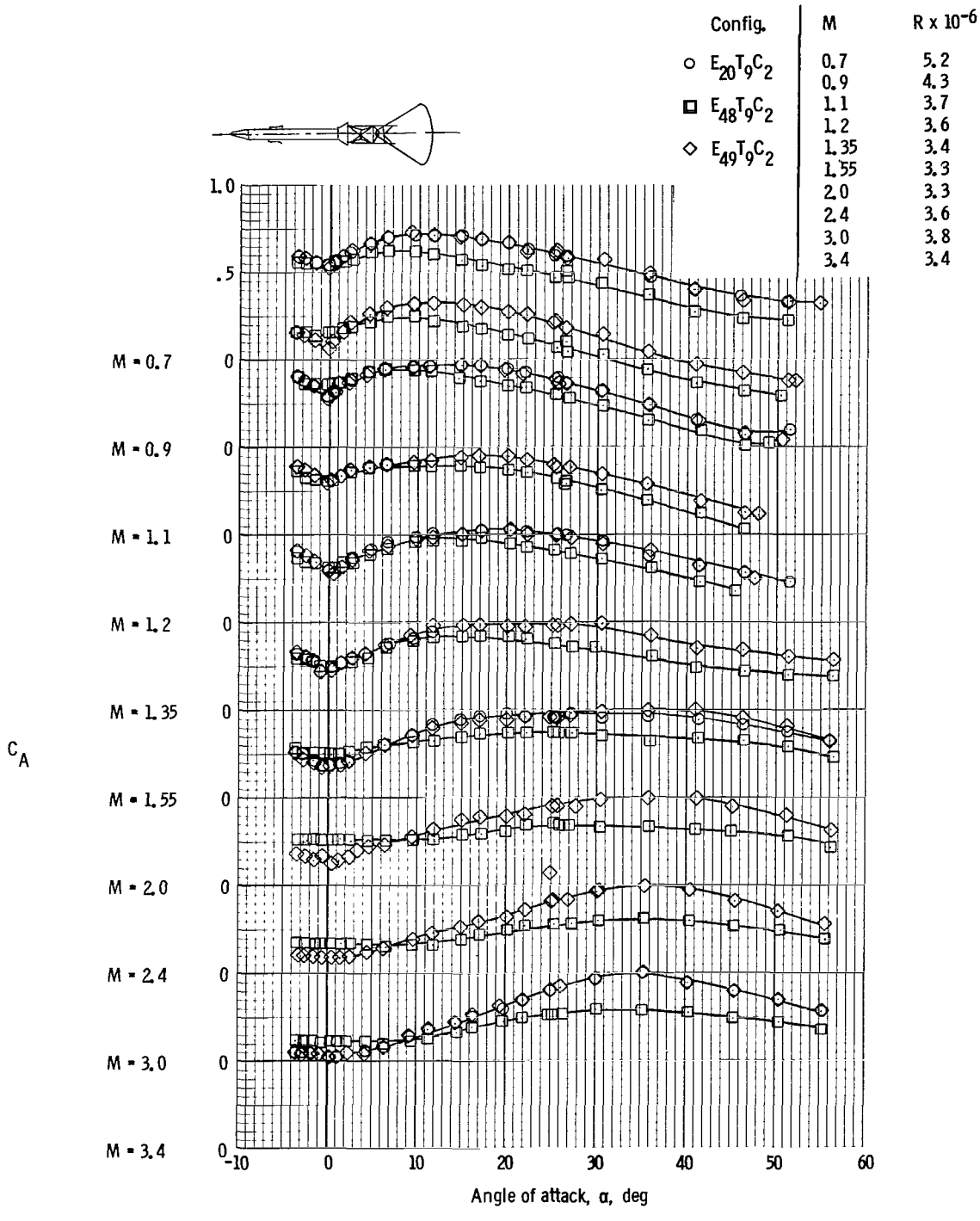

(d) Axial-force coefficient (M = 0.7 to 3.4).

Figure 17. - Concluded.

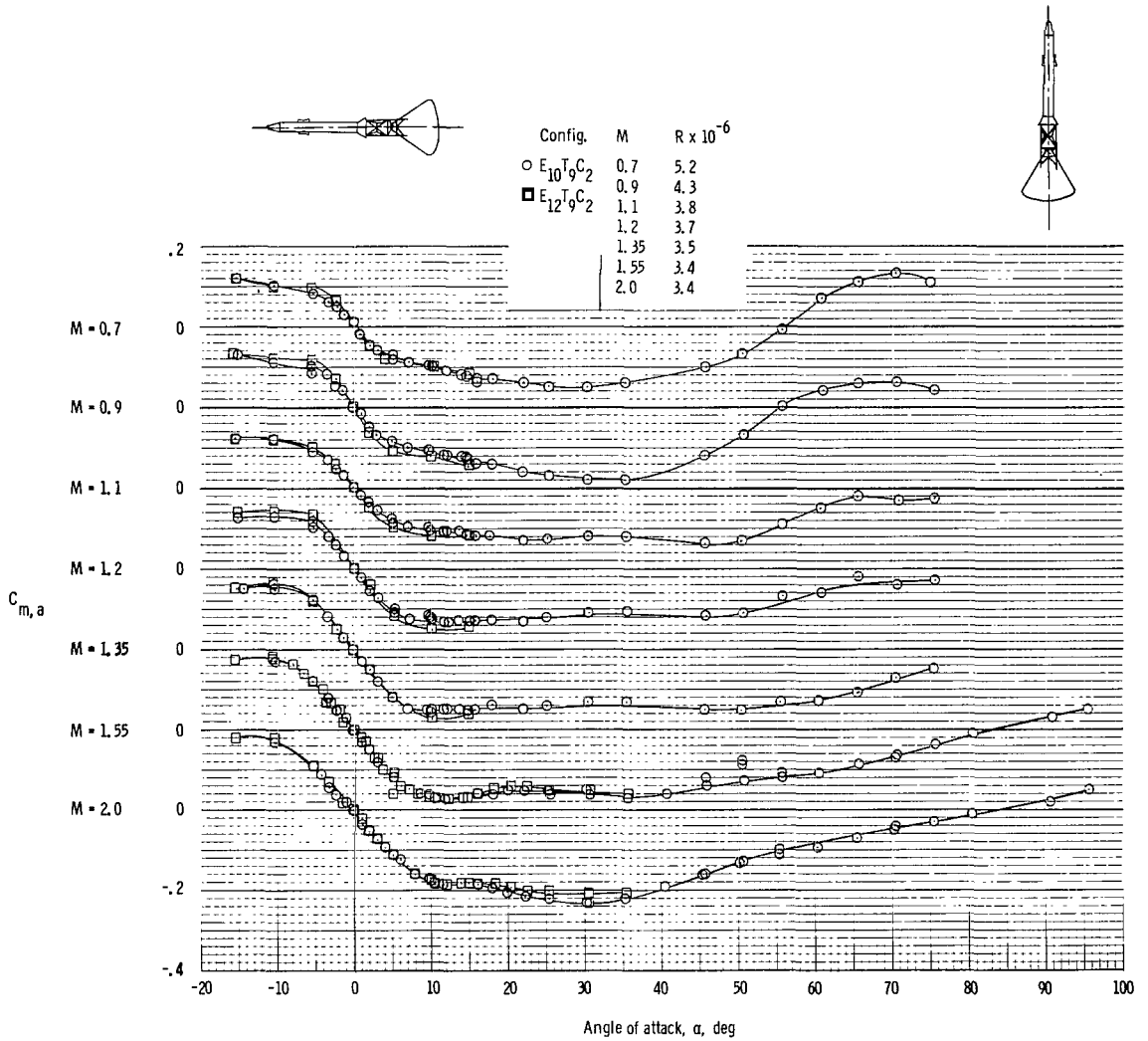

(a) Pitching-moment coefficient.

Figure 18. - Effects of varying skirt-base diameter on aerodynamic characteristics of Apollo LEV, M = 0.7 to 2.0.

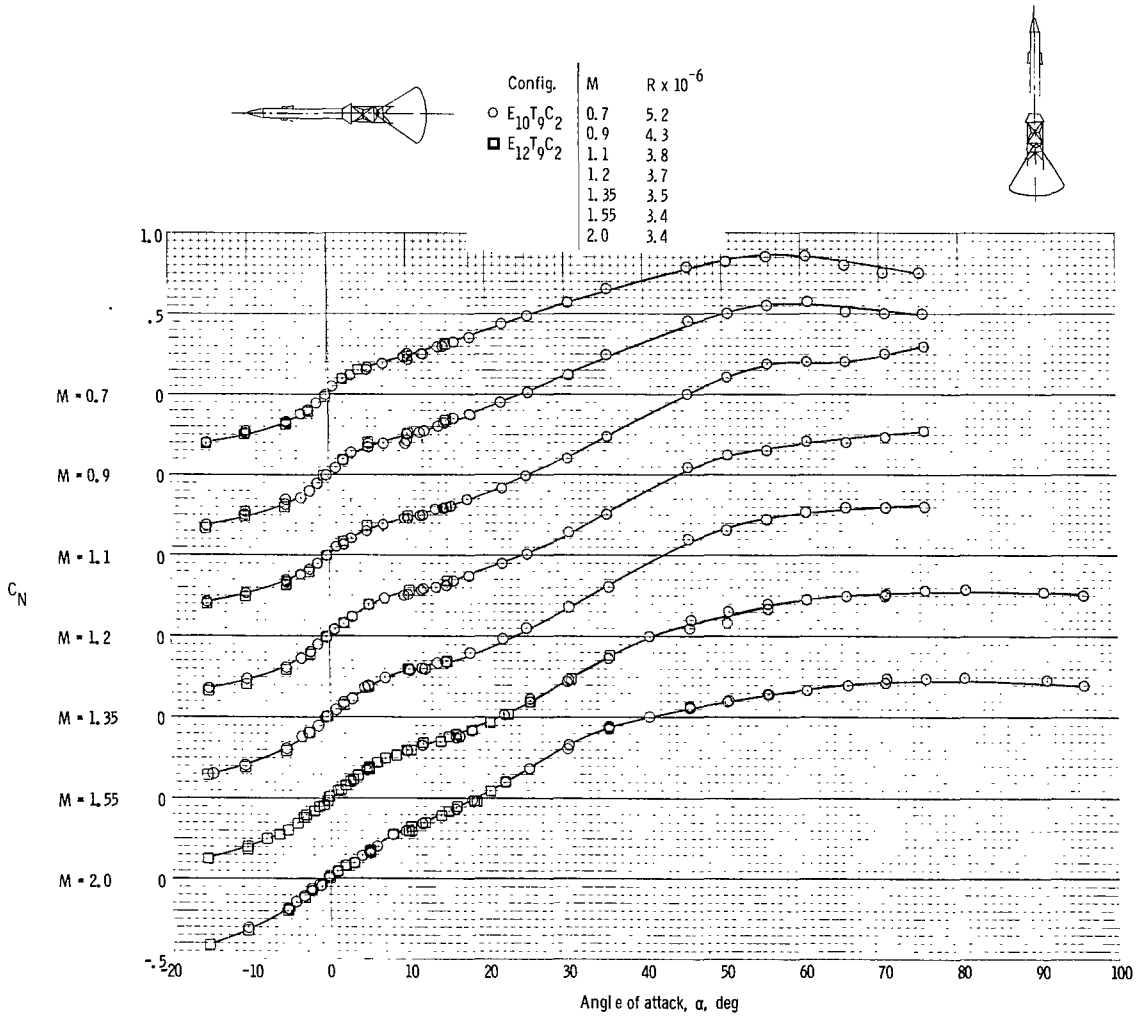

(b) Normal-force coefficient.

Figure 18. - Continued.

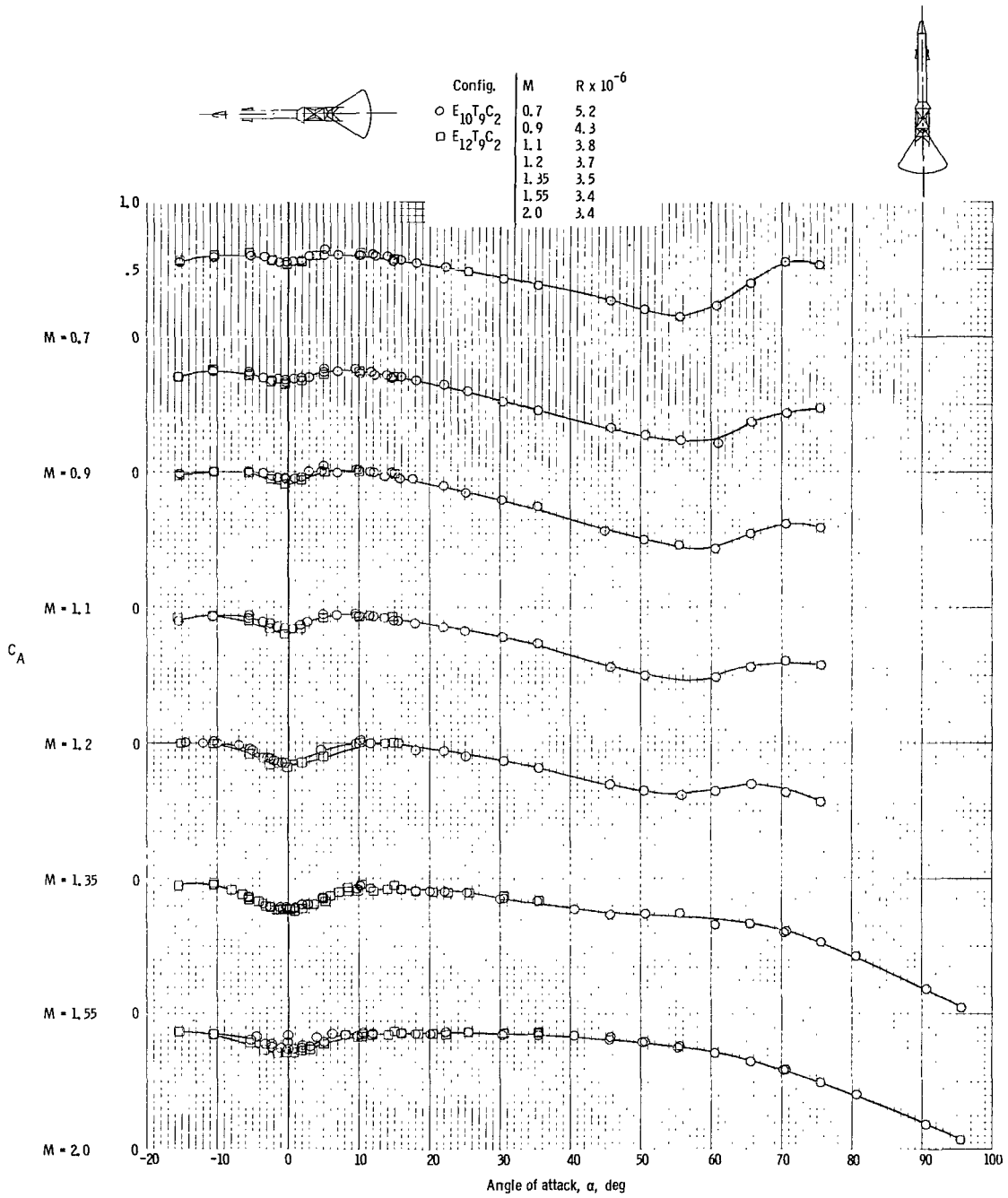

(c) Axial-force coefficient.

Figure 18. - Concluded.

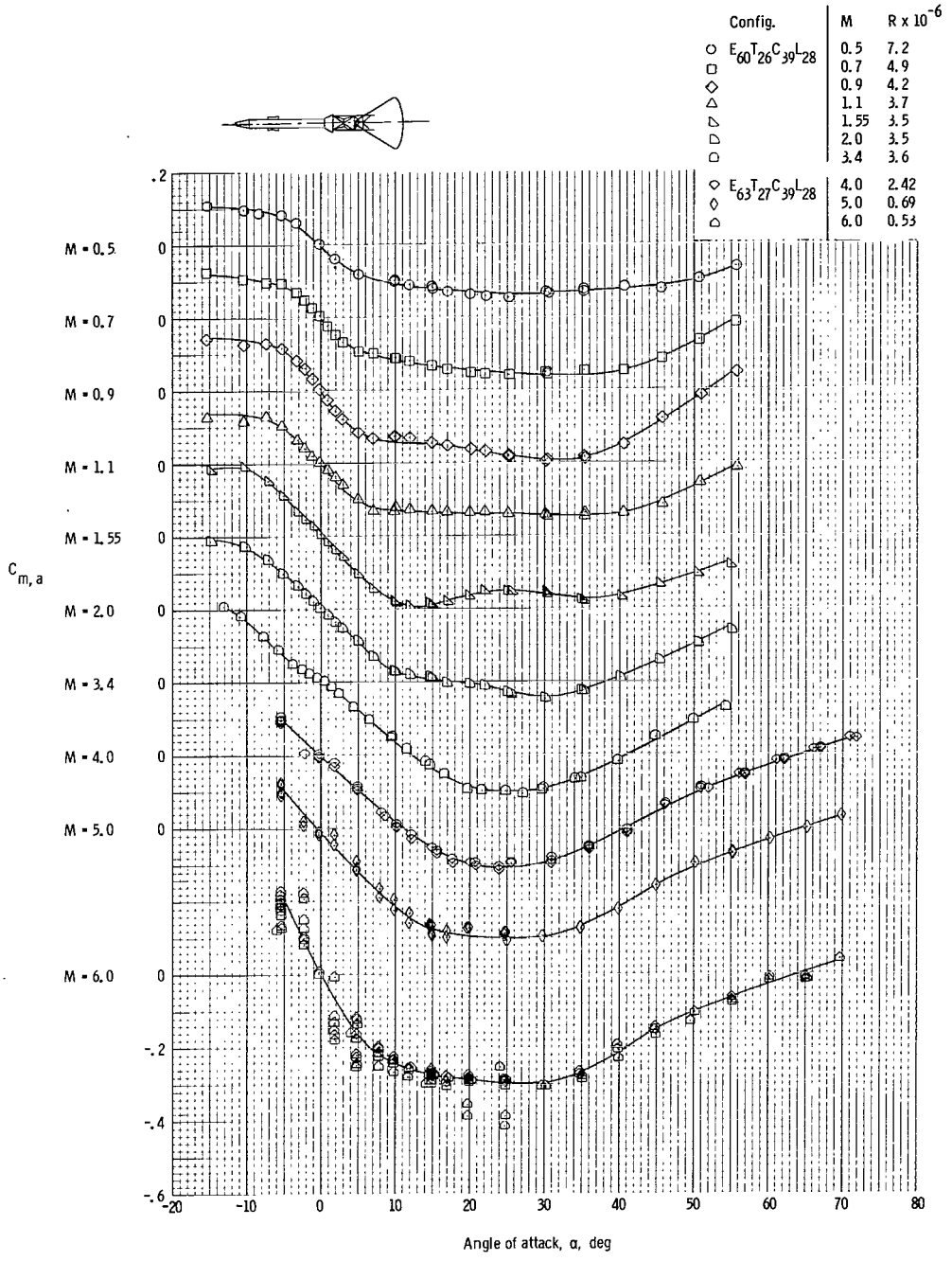

(a) Pitching-moment coefficient.

Figure 19. - Aerodynamic characteristics of Apollo LEV with strakes, M = 0.5 to 6.0.

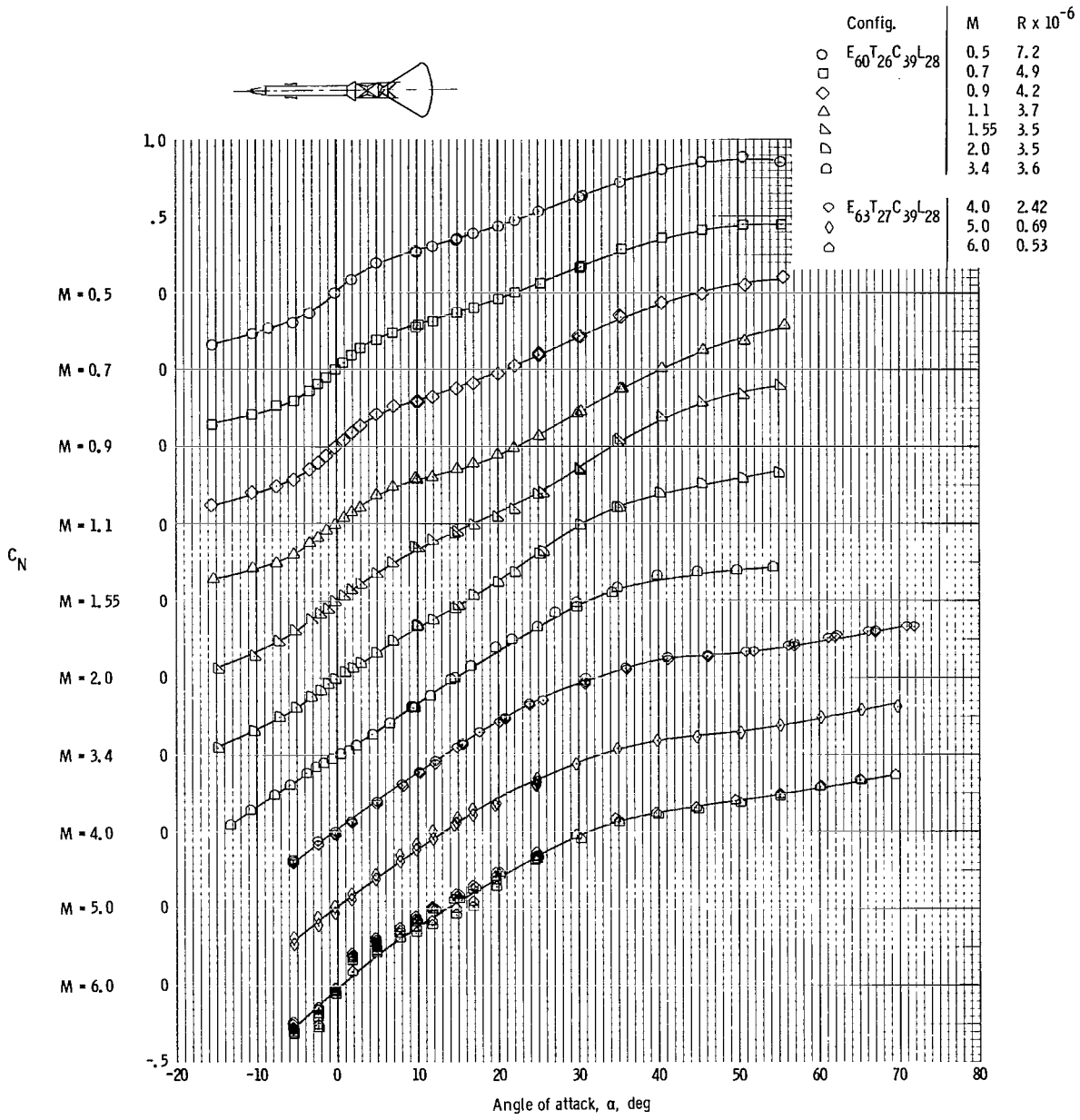

(b) Normal-force coefficient.

Figure 19. - Continued.

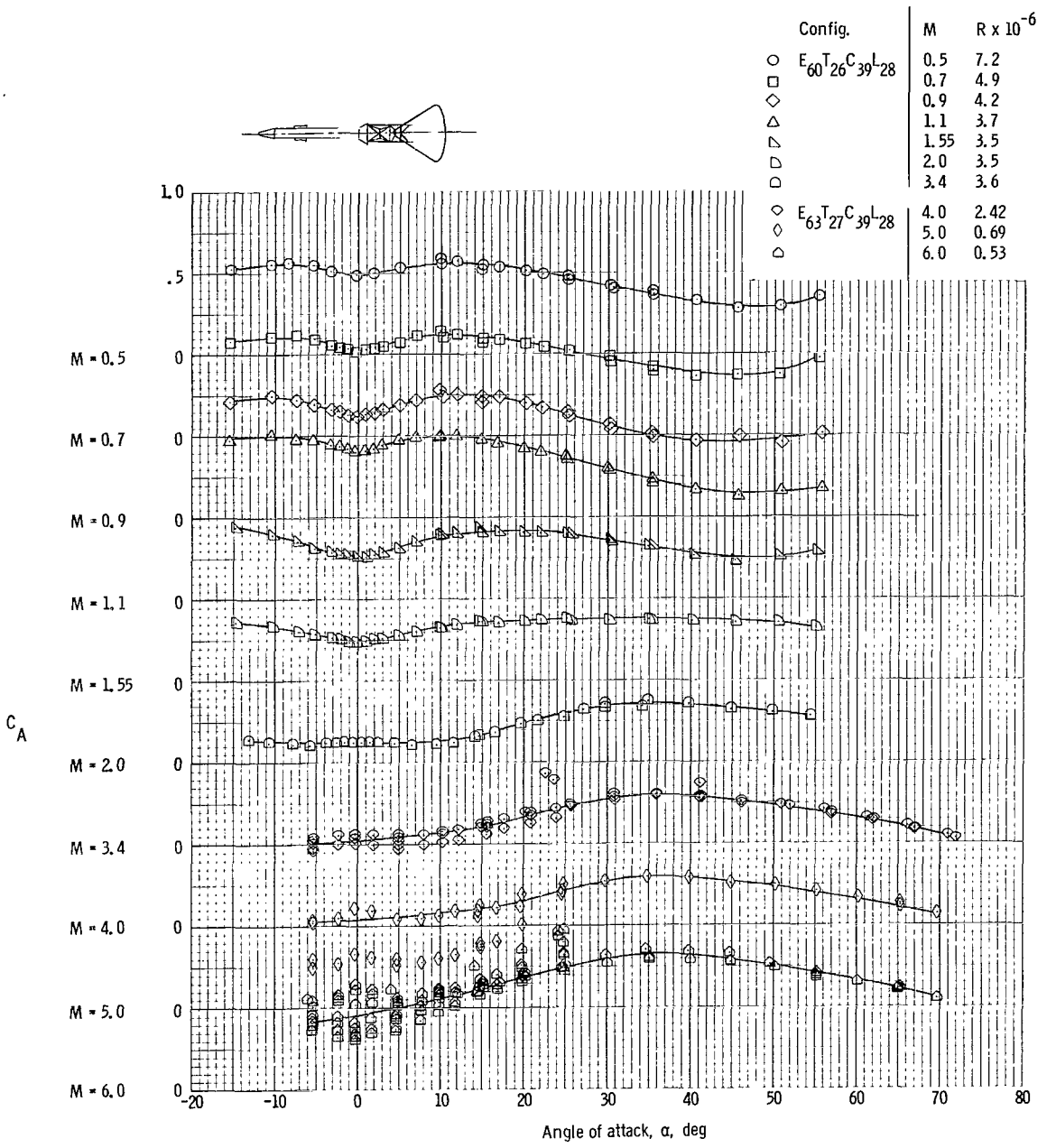

(c) Axial-force coefficient.

Figure 19. - Concluded.

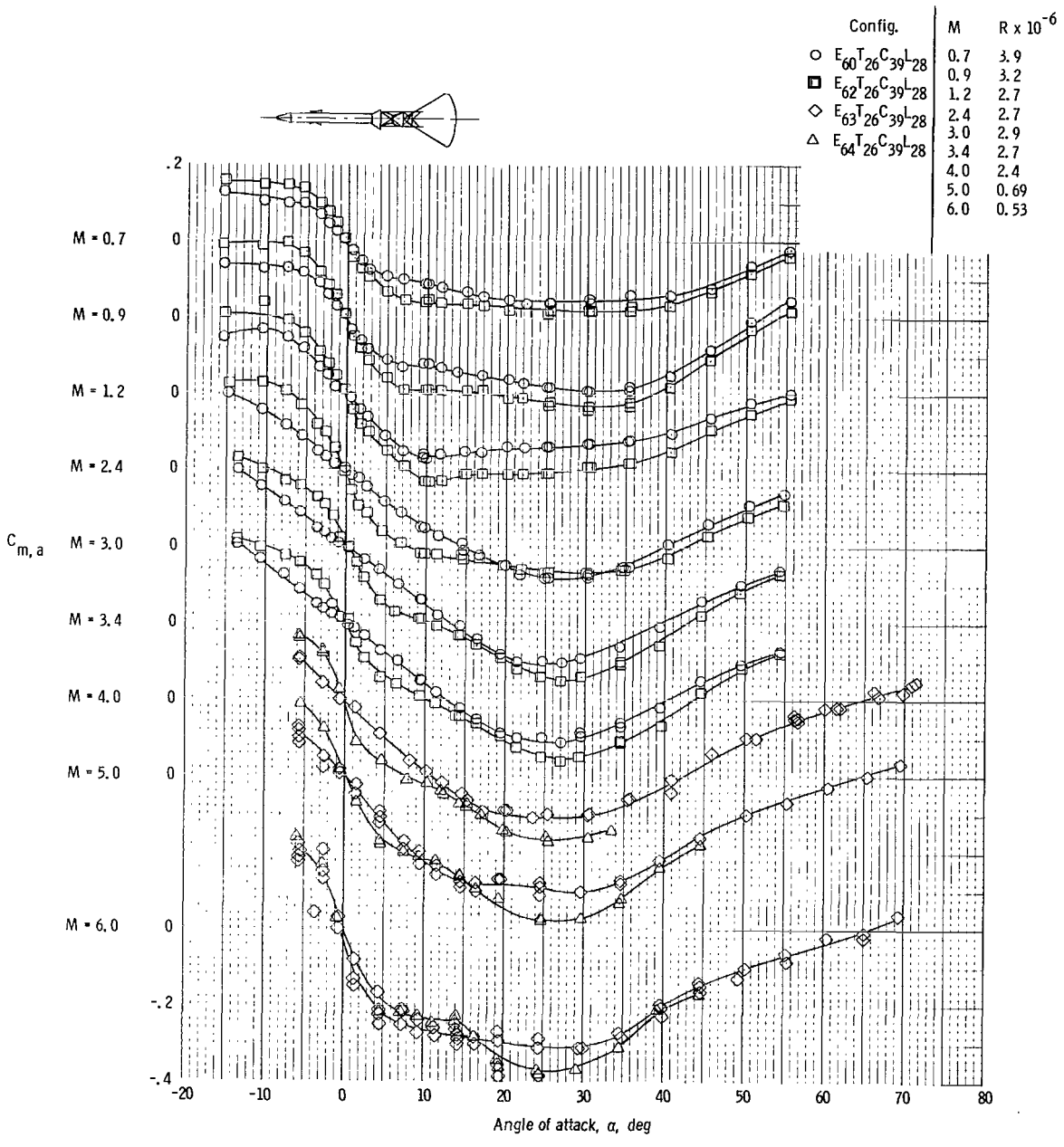

(a) Pitching-moment coefficient.

Figure 20. - Aerodynamic characteristics of Apollo LEV with strakes, M = 0.7 to 6.0.

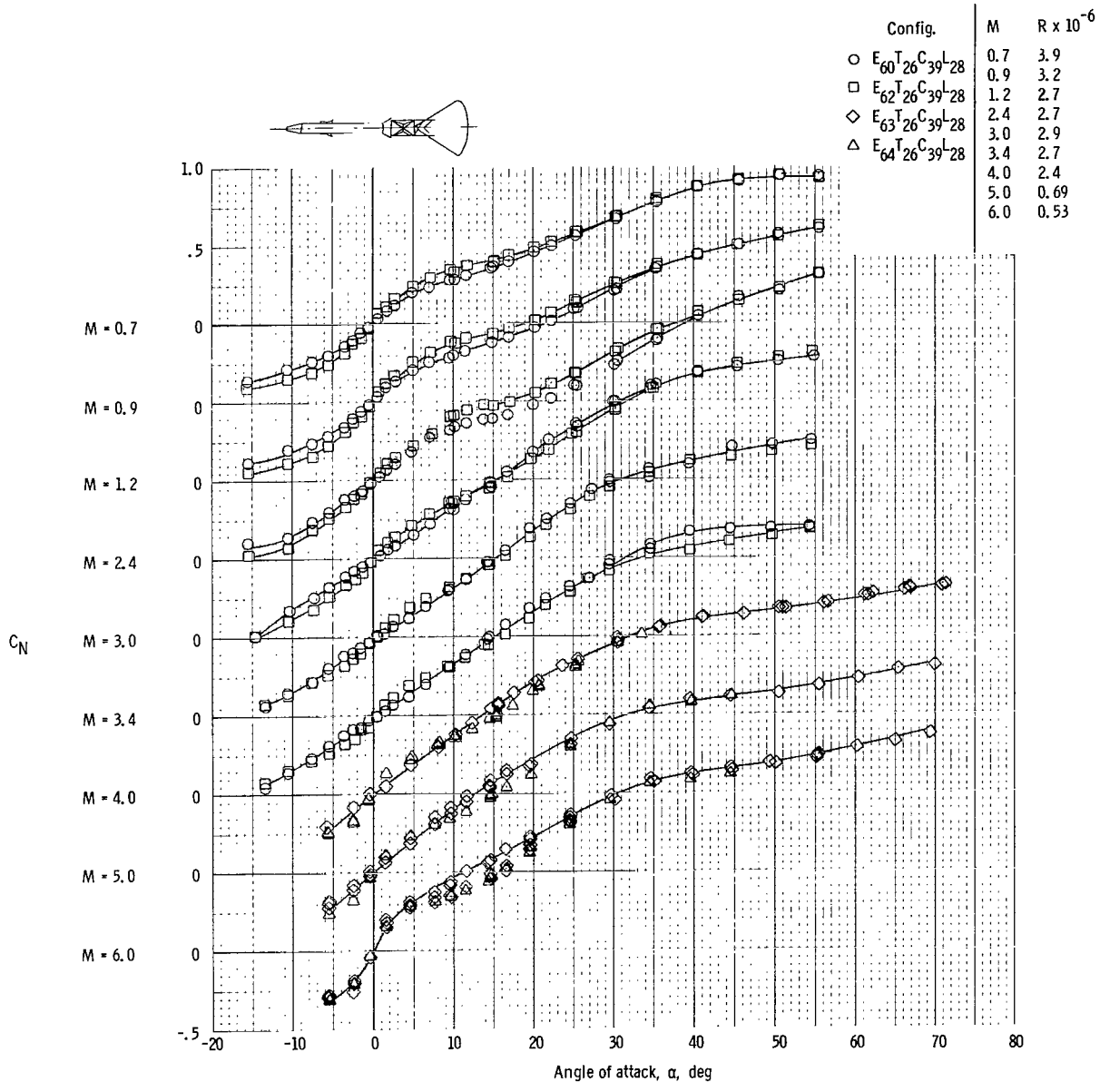

(b) Normal-force coefficient.

Figure 20. - Continued.

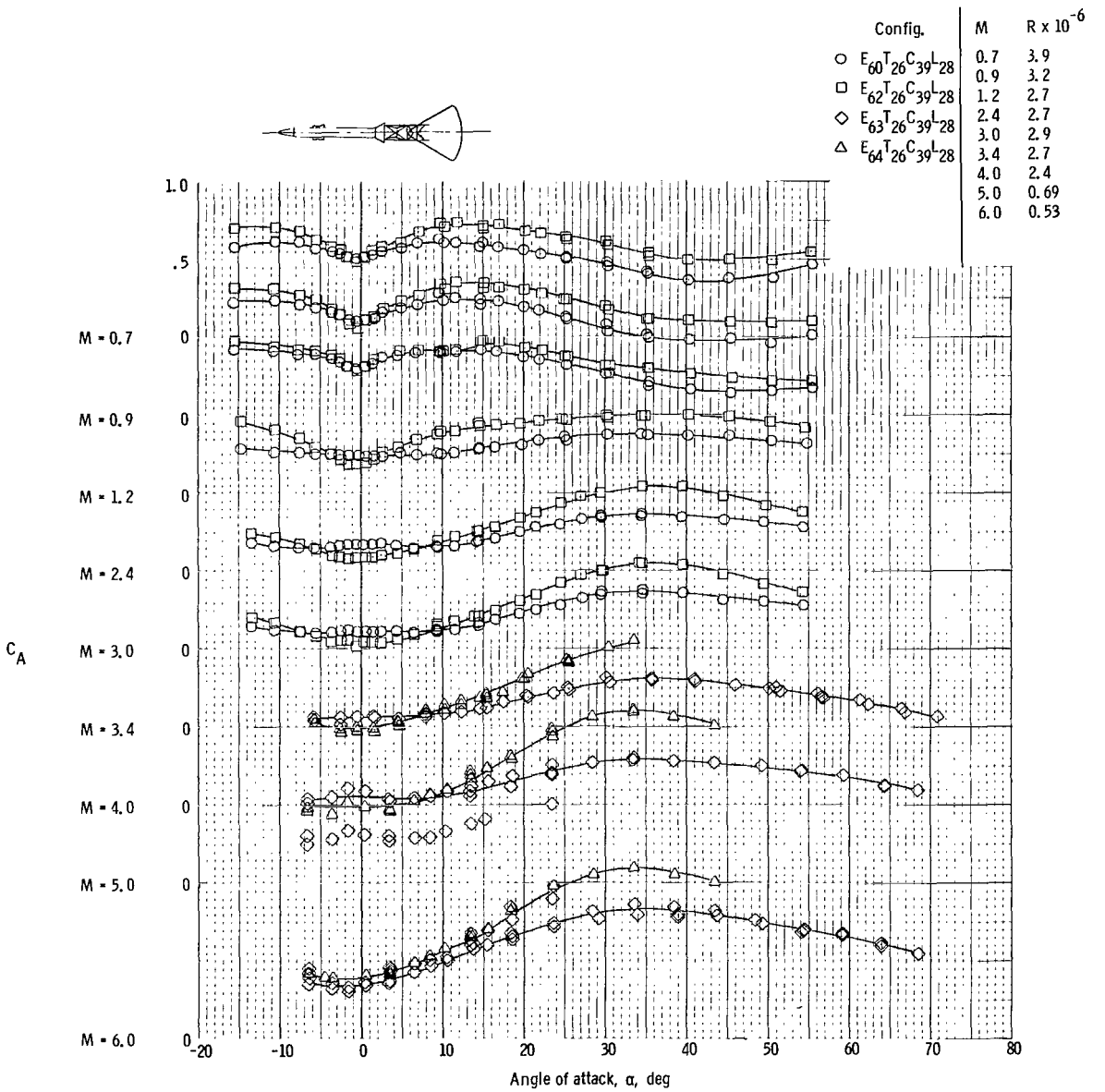

(c) Axial-force coefficient.

Figure 20. - Concluded.

NATIONAL AERONAUTICS AND SPACE ADMINISTRATION
WASHINGTON, D. C. 20546

OFFICIAL BUSINESS

FIRST CLASS MAIL

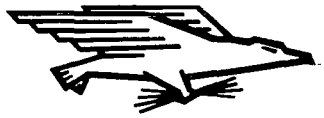

POSTAGE AND FEES PAID
NATIONAL AERONAUTICS AND
SPACE ADMINISTRATION

POSTMASTER: If Undeliverable (Section 158 Postal Manual) Do Not Return

"The aeronautical and space activities of the United States shall be conducted so as to contribute . . . to the expansion of human knowledge of phenomena in the atmosphere and space. The Administration shall provide for the widest practicable and appropriate dissemination of information concerning its activities and the results thereof."

—NATIONAL AERONAUTICS AND SPACE ACT OF 1958

NASA SCIENTIFIC AND TECHNICAL PUBLICATIONS

TECHNICAL REPORTS: Scientific and technical information considered important, complete, and a lasting contribution to existing knowledge.

TECHNICAL NOTES: Information less broad in scope but nevertheless of importance as a contribution to existing knowledge.

TECHNICAL MEMORANDUMS: Information receiving limited distribution because of preliminary data, security classification, or other reasons.

CONTRACTOR REPORTS: Scientific and technical information generated under a NASA contract or grant and considered an important contribution to existing knowledge.

TECHNICAL TRANSLATIONS: Information published in a foreign language considered to merit NASA distribution in English.

SPECIAL PUBLICATIONS: Information derived from or of value to NASA activities. Publications include conference proceedings, monographs, data compilations, handbooks, sourcebooks, and special bibliographies.

TECHNOLOGY UTILIZATION PUBLICATIONS: Information on technology used by NASA that may be of particular interest in commercial and other non-aerospace applications. Publications include Tech Briefs, Technology Utilization Reports and Notes, and Technology Surveys.

Details on the availability of these publications may be obtained from:

SCIENTIFIC AND TECHNICAL INFORMATION DIVISION

NATIONAL AERONAUTICS AND SPACE ADMINISTRATION

Washington, D.C. 20546